INFORMATION TO USERS

This manuscript has been reproduced from the microfilm master. UMI films the text directly from the original or copy submitted. Thus, some thesis and dissertation copies are in typewriter face, while others may be from any type of computer printer.

The quality of this reproduction is dependent upon the quality of the copy submitted. Broken or indistinct print, colored or poor quality illustrations and photographs, print bleedthrough, substandard margins, and improper alignment can adversely affect reproduction.

In the unlikely event that the author did not send UMI a complete manuscript and there are missing pages, these will be noted. Also, if unauthorized copyright material had to be removed, a note will indicate the deletion.

Oversize materials (e.g., maps, drawings, charts) are reproduced by sectioning the original, beginning at the upper left-hand corner and continuing from left to right in equal sections with small overlaps. Each original is also photographed in one exposure and is included in reduced form at the back of the book.

Photographs included in the original manuscript have been reproduced xerographically in this copy. Higher quality 6" x 9" black and white photographic prints are available for any photographs or illustrations appearing in this copy for an additional charge. Contact UMI directly to order.

U·M·I

University Microfilms International
A Bell & Howell Information Company
300 North Zeeb Road, Ann Arbor, MI 48106-1346 USA
313/761-4700 800/521-0600

Order Number 9224867

The study of pathological changes in the islets of Langerhans in hamsters infected with the 139H strain of scrapie

Ye, Xuemin, Ph.D.

City University of New York, 1992

U·M·I
300 N. Zeeb Rd.
Ann Arbor, MI 48106

A

THE STUDY OF PATHOLOGICAL CHANGES IN THE ISLETS OF LANGERHANS IN HAMSTERS INFECTED WITH THE 139H STRAIN OF SCRAPIE

By

XUEMIN YE

A dissertation submitted to the Graduate Faculty in Biology in partial fulfillment of the requirements for the degree of Doctor of Philosophy, The City University of New York.

1992

This manuscript has been read and accepted for the Graduate Faculty in Biology in satisfaction of the dissertation requirement for the degree of Doctor of Philosophy.

4-21-92
date

Chairman of Examining Committee
Prof. D. Soifer, Institute for Basic Research

4/22/92
date

Executive Officer
Dr. Peter C. Chabora

Prof. R.I. Carp, Institute for Basic Research

Prof. R. Kasecak, Institute for Basic Research

Prof. Y. Ehrlich, College of Staten Island

Prof. S. Castells, SUNY Health Sciences Center at Brooklyn

Prof. J. Cara, SUNY Health Sciences Center at Brooklyn

Supervisory Committee

The City University of New York

ABSTRACT

THE STUDY OF PATHOLOGICAL CHANGES IN THE ISLETS OF LANGERHANS IN HAMSTERS INFECTED WITH THE 139H STRAIN OF SCRAPIE

By

XUEMIN YE

Adviser: Professor **Richard I. Carp**

The purpose of this study was to examine pathological changes in the islets of Langerhans in hamsters infected with the 139H strain of scrapie. In comparing 139H-infected and control hamsters, the following was found:

(1) The number and total area of islet profiles was greater in 139H-infected than in control animals.

(2) The ratio of B:A:D:F cells in islets was changed from 27:5:1:0.04 in controls to 122:7:1:0.04 in 139H-infected hamsters. The increase in B cells would account for the islet enlargement and the hypoglycemia-hyperinsulinemia previously observed in 139H-infected hamsters.

(3) The optical density of immunostained insulin containing cells was decreased, suggesting that the concentration of insulin in B granules or the number of B granules was decreased, or both.

(4) There were extensive histopathological changes in the islets and pituitary in 139H-infected hamsters. These changes included cellular hypertrophy, cellular atrophy, vacuolation,

nuclear swelling, pyknosis, karyorrhexis and karyolysis. Some of these changes were also seen in hamsters infected with the 263K strain of scrapie, but at a much reduced incidence.

(5) Abnormal structures which I termed blood vessel cores(BVCs) were seen in the islets of 139H-treated hamsters. I developed new terms to described pathological phenomena seen in 139H-infected hamsters, including the abnormal PAS-positive substance(PPS), the linkage-reaction, linkage-inflammatory cells, localized vacuolization(LV), diffuse vacuolization(DV), and pathological pattern synchronism. I also proposed the accordion effect concept to explain a function of the extracellular spaces in the islets.

(6) I observed that the pattern of positive cells immunostained with antibodies against several hormones was changed in the vacuolated areas of the pituitaries of 139H-infected hamsters.

(7) There was a significant increase in the number of corticotropin-releasing factor(CRF) immunostained neurons in hypothalami of 139H-infected compared to control hamsters.

(8) There was a significant decrease in vasopressin(VP) neurons in the lateral hypothalami(LHy), but not in the dorsalmedial hypothalami(DMH) and supraoptic nuclei(SON), in 139H-infected compared to control hamsters.

(9) I used three-dimensional modeling to demonstrate the changes of CRF- and VP-immunostained neurons in the 139H-infected hamsters.

to

My Mother, Father

and

New York

ACKNOWLEDGEMENTS

I am dedicating this thesis to my parents and New York. My parents have provided me their endless love, support and encouragements since my childhood. This small dedication is not enough to repay them for their love and support over these years.

New York is a city from which I can seek the best education. During the past years, New York has provided me with fellowship and with the best academic environment. I have attended different courses in many colleges and universities in New York. New York has provided me a great deal that I will never forget.

I would like to express my sincere gratitude to my mentor Dr. R.I. Carp and his family. I feel very fortunate to have had the opportunity to work with him. As my mentor for the past years, he has given me everything to mature myself as a scientist. I would like to thank Dr. Carp for his supervision, patience, and guidance during these studies. I feel privileged to have him in my life.

I would like to thank Drs. David Soifer, Richard Kascsak, Yigal H. Erlich, Jose Cara and Salvador Castells for their patience, understanding and thoughtful suggestions. I would especially like to thank Dr. Soifer for his warm caring and for allowing me to have the opportunity to study and to do research in CSI/IBR Center for Developmental Neurosciences. I would also like to thank Drs. Soifer, Kascsak, Erlich, Cara and Castells for their valuable advice in writing this dissertation.

I would like to thank Ms. Sharon Callahan, Mr. Richard Weed, Dr. Judy Shek, Dr. Louis Faso, Dr. Rafia Kozielski, Dr. Peter Kozlowski and Mr. Yangiang Yu for their assistance in my study. Without their assistance, it would have been much more difficult to accomplish this project.

I would also like to thank Dr. R.I. Carp and his wife, Ms. S. Carp, and my English teachers Mr. J.F. Riedel and Ms M. Savova for their critical reading of this dissertation.

I would also like to thank Mr. Y. Yu for his expertise which is of invaluable help in this project.

Finally, I would like to thank all the people in this Institute who directly or indirectly contributed to this study in their various capacities.

TABLE OF CONTENTS

ABBREVIATIONS

Aci:	acini
ACTH:	adrenocorticotropic hormone
AD:	Alzheimer's disease
AM:	adrenal medulla
APP:	b-amyloid precursor protein
bFGF:	basic fibroblast growth factor
BV:	blood vessel
BVC:	blood vessel core
CA:	commissura anterior, pars anterior
Cap:	capillary
CGRP:	calcitonin gene-related peptide
CJD:	Creutzfeldt-Jakob disease
CLIP:	corticotropin-like intermediate peptide
CRF:	corticotropin releasing factor
DMH:	dorsalmedial hypothalamus
DV:	diffuse vacuolization
ES:	extracellular space
EV:	extracellular vacuolization
FSH:	follicle stimulating hormone
GH:	growth hormone
Glu:	glucagon
GSS:	Gerstmman-Straussler-Sherker syndrome
Hy:	hypothalamus
IAPP:	amyloid polypeptide
IL-1:	interleukin-1
In:	insulin
InD:	interlobular duct
InS:	interlobular septum
ir:	immunoreactive
IRI:	immunoreactive insulin
Is:	islet
IV:	intracellular vacuolization
LH:	luteinizing hormone
LHy:	lateral hypothalamus
LV:	localized vacuolization
Max:	maximum
Min:	minimum
N:	number of animals
NGF:	nerve growth factor
NHB:	control hamster
NIDDM:	non-insulin-dependent diabetes mellitus
OD:	optical density
OT:	optic tract
PA:	positively stained area
pan:	pancreatic section area
PAP:	peroxidase-antiperoxidase
PAS:	periodic acid schiff
PD:	pars distalis

PI:	pars intermedia
PIn:	proinsulin
PN:	pars nervosa
PON:	preoptic nucleus
PP:	pancreatic polypeptide
PPS:	PAS positive substance
PRL:	prolactin
PrP:	proteinase K resistant protein
PVH:	paraventricular hypothalamus
SCN:	nucleus of suprachiasmaticus
Si:	sinusoid
SON:	supraoptic nuclei
SS:	somatostatin
T. OD:	total OD
TSH:	thyroid stimulating hormone
III-V:	third ventricle
VP:	vasopressin

LIST OF TABLES

LIST OF FIGURES

I. INTRODUCTION

A. General Background

Scrapie is a neurodegenerative disease of sheep and goats (Dickinson, 1976). It has an insidious onset beginning with the animal scraping its fleece against fence objects. The disease progresses with tremors and ataxia. It culminates in death within 6 weeks to 6 months without any clinical evidence of infection.

The scrapie agent has been passaged in a number of laboratory animal species, including mice and hamsters (Chandler, 1963, Kimberlin and Walker, 1986). Scrapie is a direct model for several human diseases, such as Creutzfeldt-Jakob disease (CJD), Kuru and Gerstmann-Straussler syndrome (GSS) (Gajdusek, 1977).

There are also a number of characteristics of scrapie and the other unconventional slow infectious diseases that are shared with Alzheimer disease (AD) and Down syndrome. They all have some kind of amyloid plaques, the presence of host-coded aberrant fibrillar proteins (scrapie associated fibers in unconventional slow infections and amyloid fibers and paired helical filaments in AD) and a strong genetic influence on the occurrence of the disease process. It also appears that changes in the neuroendocrine system may be an additional shared characteristic of the unconventional slow infections and AD (Carp, personal communication).

Although the nature of the causative infectious agent remains unknown (Carp et al., 1989), extensive work has been done on genetic and pathogenic aspects of scrapie disease. Advances in these areas have been aided by the fact that if the strain of agent, host strain, dose of infectious agent and route of infection are kept constant, there is a remarkable consistency in all aspects of disease pathogenesis (Outram, 1976).

B. Recent Studies

Recent studies in Dr. Carp's laboratory have demonstrated that in some scrapie strain-mouse strain or hamster strain combinations, there is an increase in body weight that starts prior to the onset of typical motor disfunction that signals the start of clinical disease (Carp et al., 1990). For their studies in hamsters, animals were injected intra-cerebrally with scrapie strains 139H or 22CH or with normal hamster brain (NHB). Animals were then assessed periodically for body weight, insulin level and glucose tolerance throughout the incubation periods. Animals injected with the scrapie strains became obese prior to the appearance of the motor changes that are indicative of the start of a clinical disease. During the latter part of the pre-clinical and throughout the clinical phase of disease, animals were hypoglycemic and showed marked hyperinsulinemia with values as much as 49X higher than those

seen in controls. At autopsy, there was marked hyperplasia and hypertrophy of the cells of the islets of Langerhans. The thyroid, adrenal glands, liver and kidneys were also enlarged. In contrast, hamsters injected with the commonly used 263K strain of hamster-adapted scrapie did not show any of the above changes. For example, the total body weight of these animals was the same as that of the ones injected with normal hamster brain throughout the preclinical and clinical periods (Kascsak et al., 1991).

The differences observed between 139H-, 22CH- and 263K-infected hamsters are probably a function of differences in targeting of brain regions and/or of neuronal cell types by the different scrapie strains. It is known that targeting can vary for different scrapie strains (Carp et al., 1990).

While the data for the 139H and 22CH strains suggest that they induce a severe generalized endocrinopathy, the pathological changes in the islets of Langerhans are most prominent (Carp et al., 1990). It seems that the pancreatic changes could play an important role in the obesity of 139H-infected hamsters. Obviously, the next step is to study further the pathological changes in the islets of Langerhans in 139H-infected hamsters.

C. Specific Aims and Significance of the Study

There is a specific and unique architecture in the normal

islet of Langerhans. The islet contains cords and irregular clumps of cells, with highly sophisticated systems of capillaries and nerve terminals. The islet of Langerhans show pathological changes in many diseases such as diabetes (Pohl et al., 1981); nesidioblastoma (Gould et al., 1983; Newman et al., 1986) and in 139H-infected scrapie-positive hamsters (Carp et al., 1990). In my studies:

1) I will determine the quantitative changes in the number and size of the pancreatic islet profiles.

2) I will find out what happens to the four cell types (A, B, D, and F cells) in the islets and the responses that each type of cell produces in 139H-infected hamsters.

3) I will examine the pathological changes that occur in the pancreatic islet architecture and at the cellular, subcellular and molecular levels in the cells of pancreatic islets in 139H-infected hamsters.

4) I will investigate the basis of these pathological changes in the islets of Langerhans and determine whether they are related to pathological changes occurring in the central nervous system.

These studies will provide information concerning the islet of Langerhans damage and dysfunction. This knowledge will in turn yield clues about the fundamental processes in human endocrine diseases such as diabetes, obesity, and hypoglycemia and hyperinsulinemia syndrome in human and nesidioblastoma in infancy.

In the course of the study, I have used

immunocytochemical, histological and cytological methods in combination with the Quantimet 970 image analyzer (Cambridge Instruments).

II. EXPERIMENTAL DESIGN AND METHODS

A. Experimental Design

1. Experiment One: Study of the Quantitative Changes in the Number and Size of the Islets and Immunostaining Areas of A, B, D, and F Cells.

There were two groups of hamsters for injection. Each group was made up of ten or more animals. One group was injected with normal hamster brain homogenate and the other group was injected with scrapie strain 139H. Each homogenate was a 1% weight/volume suspension.

At the time of sacrifice the animals were perfused appropriately, the brain and the splenic portion of the pancreas were removed, fixed, dehydrated, embedded, and paraffin sections were prepared. The pancreatic sections were then immunostained using the peroxidase-antiperoxidase (PAP) or the supersensitive alkaline phosphatase (Biogenex Laboratories, San Ramon, CA) methods. Antisera for insulin, glucagon, somatostatin, and pancreatic polypeptide were used.

The immunostains were done with the Histomatic Slide Stainer-Code On Series (Fisher Scientific), and the stained area and stain intensity were analyzed using the Quantimet 970 image analyzer.

2. Experiment Two: Study of the Pathological Changes in the Pancreatic Islets in 139H-infected Hamsters with Light Microscopy.

Sections of pancreas were stained with hematoxylin and eosin, Periodic acid schiff (PAS) and orange G, Gomori's one step trichrome, Congo red, and thioflavin-S. The sections were observed with standard light microscopy and were examined carefully for a number of pathological changes such as hypertrophy, atrophy, cell shape and orientation, nuclear morphology and other cytological characteristics. For thioflavin-S stain, the sections were viewed under U.V. light, and for Congo red stain, sections were examined by polarized light.

3. Experiment Three: Study of the Pathological Changes in the Pancreatic Islets in 139H-infected Hamsters with Semi-thin Sections.

There were two groups of hamsters for injection. Each

group was made up of five or more animals. One group was injected with normal hamster brain homogenate and the other group was injected with scrapie strain 139H.

Semi-thin sections of pancreatic islets were stained with toluidine blue. The slides were observed with standard light microscopy and were examined carefully for a number of pathological changes such as hypertrophy, atrophy, cell shape and orientation, nuclear morphology and other cytological characteristics.

4. Experiment Four: Study of the Pathological Changes in the Adrenal Gland and the Pituitary in 139H-infected Hamsters with Light Microscopy.

There were three groups of hamsters for injection. Each group was made up of ten or more animals. The first group was injected with normal hamster brain homogenate, the second group was injected with scrapie strain 139H and the third group was injected with scrapie strain 263K. Each homogenate was a 1% weight/volume suspension.

Sections of adrenal glands and pituitaries were stained with hematoxylin and eosin, PAS and orange G, Gomori's one step trichrome, Congo red, and thioflavin-S. The sections were observed with standard light microscopy and were examined carefully for a number of pathological changes as indicated in Experiment Two.

5. Experiment Five: Immunostaining Study of the Pathological Changes in the Pituitary in 139H-infected Hamsters.

Pituitary sections were immunostained using the PAP or the supersensitive alkaline phosphatase (Biogenex Laboratories, San Ramon, CA) methods. Antisera for adrenocorticotropic hormone$_{1-24}$ (ACTH$_{1-24}$), ACTH$_{17-39}$, growth hormone (GH), luteinizing hormone (LH), follicle-stimulating hormone (FSH), prolactin (PRL) and thyroid-stimulating hormone (TSH) were used. The immunostains were done with the Histomatic Slide Stainer-Code On Series, and the stained area and stain intensity were analyzed using the Quantimet 970 image analyzer.

6. Experiment Six: Immunostaining of Hypothalamus with Anti-CRF and Anti-VP.

Immunocytochemical localization of CRF and VP were performed on colchicine-treated hamsters. There were two groups of hamsters for injection. Each group consisted of ten or more animals. One group was injected with normal hamster brain homogenate. The other group was injected with scrapie strain 139H. Two days before sacrifice the animals were infused with colchicine (120μg/15μl) into a lateral ventricle. Colchicine can enhance the CRF immunostaining in neuronal

perikarya (Palkovits et al., 1087). After 48 hours the animals were perfused appropriately, and the brain and pancreas were removed and fixed. Brain coronal sections of 50μm thickness were cut through the forebrain from the diagonal band of Broca to the substantia nigra with a vibratome (Lancer, series 1000). Immunostaining for CRF and VP were processed as free floating sections using PAP methods. The number of CRF immunostained neurons in the hypothalamus and VP immunostained neurons in the supraoptic nucleus were determined with a light microscope. The VP immunostained areas in lateral hypothalamus and dorsomedial hypothalamus were analyzed using the Quantimet 970 image analyzer. I also employed the Quantimet 970 image analyzer to reconstruct and analyze populations or areas of CRF and VP immunostained neurons in three dimensions in both control and 139H-infected hamsters.

B. Materials and Methods

1. Animals.

Female, weanling LVG/LAK hamsters were obtained from Charles River (Wilmington, MA) and maintained in a temperature- and humidity-controlled room of our animal colony. Hamsters were given food and water ad libitum. Animals were injected with 40μl intracerebrally (ic) 1-2 weeks

after arrival.

2. Inocula.

Three inocula were used: normal hamster brain (NHB), scrapie strain 139H and scrapie strain 263K. Scrapie strains were provided by Dr. Richard H. Kimberlin (Neuropathogenesis Unit, Edinburgh, UK), and are being maintained in our laboratory by hamster-to-hamster passage. The characteristics of our passaged materials are exactly the same as those of the strains we obtained from Dr. Kimberlin. Passages were done by routine intracerebral injection of 40μl of brain homogenate prepared in cold (4 ^{o}C) phosphate-buffered saline (PBS). Homogenization was done using 20 strokes of a hand-operated Ten-Broeck homogenizer (see Carp et al., 1990).

3. Tissue Preparation.

In our experiments, we used paraffin sections for histological staining, and paraffin sections and vibratome sections for immunostaining. At the end of incubation period (about 115-125 days post-injection for 139H and 65-70 days for 263K), the animals were anesthetized with nembutal (nembutal : heparin, 2 : 1, 3-4 ml/kg body wt).

For paraffin sections, anesthetized animals were perfused

through the heart with saline (0.9%) at room temperature for a few minutes followed by perfusing with either Bouin solution in Experiment One or 4% paraformaldehyde and 0.05% glutaraldehyde in 0.1M sodium phosphate buffer (Ph 7.4) in Experiment Four for 10-15 min. Animals were then decapitated. Small areas of the skull bone below the area encompassed by the pituitary and hypothalamus were removed with the brain. The splenic portion of the pancreas was also rapidly removed, then fixed in the fixative solution for 24 hours. If the tissues were fixed in Bouin solution, they were then washed in ammoniated 70% alcohol (in which a few drops of NH_4OH were added to the alcohol) for 2-3 days, changed into new ammoniated 70% alcohol for 2-3 days until the solution cleared (not yellow). If the tissues were fixed in 4% paraformaldehyde and 0.05% glutaraldehyde in 0.1M sodium phosphate buffer (Ph 7.4), they were in the buffer solution for 2-3 days. The tissues were then drained thoroughly. Tissues were then cut into small blocks, which were put into labeled carriers.

After immersion-fixation, brain blocks containing hypothalamic paraventricular (PVH) and supraoptic (SON) nuclei, and pituitary were decalcified in decalcifying solution (Calex, Fisher Scientific, Springfield, N.J.) for two days, and drained thoroughly in tap water for one day. Brain blocks were then dehydrated in graded alcohols and embedded in paraffin. Six micrometer thick coronal (or sometimes sagittal) serial sections were mounted on gelatin-coated

slides and allowed to dry overnight at 37°C. Adjacent sections were mounted on sequential slides (or on "probe on" slides).

Immunocytochemical localization of CRF and VP were performed on colchicine-treated hamsters. Colchicine (120μg/15μl saline) was infused into the lateral ventricle. After 48 hours, animals were anesthetized and perfused through the heart with a fixative containing 4% paraformaldehyde and 0.05% glutaraldehyde in 0.1M sodium phosphate buffer (Ph 7.4). Each brain was removed and placed in fixative for an additional 24 hours before being transferred to a phosphate buffer. Coronal sections of 50μm thickness within the hypothalamus region were cut with the vibratome. Prior to the immunostaining, sections were rinsed for at least 6 hr in several changes of phosphate buffer and were processed as free floating sections.

4. Histology and Cytology Staining Methods.

Sections of the adrenal gland, pancreas, pituitary, and brain were stained with routine histological stains including hematoxylin and eosin (H & E), PAS and orange G, Gomori's one step trichrome, Congo red, and thioflavin-S. Gomori's one step trichrome can stain collagen fibers yielding a blue-green color. Congo red and thioflavin-S have been used clinically for diagnosis of amyloidosis. Congo red can stain amyloid

with orange color and has an intense green-red birefringence when viewed with polarized light. Thioflavin-S can stain amyloid with fluorescence when observed with U.V. light. The slides were also observed with standard light microscopy for other changes. All the photos and slides of the histological and immunoreactive stained sections in this study were taken from a Carl Zeiss Axiophot.

5. Semi-thin Section Study.

At the end of the incubation period, animals of both sexes were anesthetized with nembutal (nembutal : heparin, 2 : 1, 3-4 ml/kg body wt). Blood was taken before perfusion (at about 10:00 am to 1:00 pm) from the heart and collected in labeled polyethylene tubes. Plasma were stored at -80°C for later assay. Anesthetized animals were perfused through the heart with saline (0.9%) at room temperature for a few minutes followed by perfusing with 2% paraformaldehyde and 1% glutaraldehyde in 0.1M Cacodylate buffer solution for 10-15 min. Animals were then decapitated. Small areas of the skull bone below the area encompassed by the pituitary and hypothalamus were removed with the brain. The splenic portion and the duodenal portion of the pancreas were also rapidly removed, then fixed in the same fixative solution.

After immersion-fixation overnight at 4°C, the pancreas blocks were rinsed twice in 0.1M Cacodylate buffer with 10% sucrose. The pancreas tissue with islets inside were trimmed

so that the size of the tissue was about 1 mm^3. The tissue blocks were post-fixed in osmic acid for one hour at 4°C, then they were rinsed twice in 0.1M Cacodylate buffer with 10% sucrose and rinsed once in distilled water for 10 minutes. The tissue blocks were stained with 0.5% uranyl acetate overnight. The specimens were dehydrated in increasing concentrations of alcohol, which was then replaced by propylene oxide. The specimens were then infiltrated with unpolymerized Spurr embedding medium. The embedded specimens were kept in an oven at 60°C for several days before they were sectioned. Semi-thin sections (0.5 μm) were cut on the Sorvall JB-4A Porter-Blum microtome, and stained with toluidine blue. The specimens were then observed with a light microscope.

6. Immunostaining Study.

a. Sources of Reagents.

BioGenex Laboratories, San Ramon, CA: anti-FSH, anti-LH, anti-PRL, anti-insulin, HistoGen PAP insulin kit, supersensitive kits.

Peninsula Lab. Inc. CA: anti-$ACTH_{17-39}$.

Incstar Corporation, Stillwater, Minnesota: anti-CRF.

Chemicon International Inc. Temecula, CA: anti-HGH, anti-TSH, anti-somatostatin.

ICN Biomedical Inc, Illinois: anti-VP, anti-pancreatic polypeptide, anti-$ACTH_{1-24}$.

DAKO Corporation, Santa Barbara, CA: anti-glucagon.

Cappel Organon Teknika Co. Durham, NC: sheep serum, sheep anti rabbit antibody, rabbit PAP.

(Note that all antibodies mentioned above are produced in rabbits.)

b. Immunostaining Methods.

Sections were stained using the PAP or the supersensitive alkaline phosphatase methods (BioGenex). Antisera for CRF, Arg-vasopressin, ACTH, FSH, LH, PRL, TSH, GH, insulin, glucagon, somatostatin, and pancreatic polypeptide were used. Three controls were done:

1) negative control: a specimen, processed in the same way as the unknown, which did not contain the antigens to be stained.

2) reagent control: a slide that was treated with a non-immune serum instead of the primary antibody. This slide should show no staining.

3) neutralized control: a slide that was treated with an antisera that had been exposed to an excess of the specific antigen. This slide should show no staining.

For each primary antibody, our initial pilot experiment used the dilution recommended by the supplier plus dilutions

that are two-fold higher and two-fold lower than the recommended dilution.

The immunostains were done with the Histomatic Slide Stainer-Code On Series, which is an autostainer using the capillary action system developed by Brigati et al. (1988) for immunocytochemistry studies. The capillary action system is automated and very accurate. Capillary action technology solves the drying, heating, and control problems of standard manual technology because the reagents, trapped in the gap, do not evaporate as easily as they do in standard tabletop technology. The capillary action design changes the physics of immunocytochemistry and traps the liquid between two glass "probe on" slides which are in close parallel array. One slide performs the function of a coverslip for its partner. This lowers reagent consumption to the point where the volume barrier that existed to automating immunocytochemistry is now broken. The capillary gap evenly disperses the smallest volume of liquid needed to cover a tissue section (Brigati et al., 1988). Our experiments proved that the capillary action system is a most useful and efficient immunostaining technique.

7. Assessment of Immunostaining.

Analysis of the distribution and intensity of immunostaining were computer-assisted. We used the Quantimet

970 image analyzer which has a very high degree of precision and satisfies the need for increased objectivity and accuracy. A stained slide was scanned by a scanner mounted on a microscope. In order to maintain efficiency, the Quantimet 970 utilizes an interactive user-programming interface, "QUIPS/MX, Version V07.00", which allows the user to establish routines for image analysis which will produce the desired sensitivity and quantification. Some of these measurements may include stained cell count, cell area, and optical density.

Data were analyzed using the Lotus 123 program and the CSS statistics software packages. We have obtained information on the stained area of the region of interest, the area that shows positive staining and the optical density of the stained areas. This information was stored, analyzed statistically and compared by Student's t-test or analysis of variance with the data from sections obtained from animals injected with normal hamster brain.

8. Computer Reconstructions of Three-dimensional Models.

The tissues used for three-dimensional reconstructions were sections through the basal forebrain from the diagonal band of Broca to the substantia nigra. All sections of the basal forebrain were prepared with the vibratome for free-floating section immunostaining. All sections were 50

micrometers thick. CRF immunostained neurons in hypothalamus and VP immunostained neurons in SON were difficult to identify by the Quantimet 970 image analyzer because the high background, but they were easily quantitated using light microscopy. VP immunostained neurons in LHy and DMH regions were easily quantitated by the Quantimet 970 image analyzer.

The position of each immunostained cell was mapped on a photocopy of an atlas figure outlined from the section taken from one brain. In this study, eight outlines of sections were taken to reconstruct the brain model. The outlines of the brain were obtained from selected sections of one animal with the DL-2 microfiche projector. The atlas number of the eight standard outlines were most closely matched to the atlas figures from Sidman et al. (1971).

The mapping procedure was done for all immunostained sections, which represented one third of the total number of sections through the basal forebrain from the diagonal band of Broca to the substantia nigra. The immunostained neurons reconstructed for each group of animals utilized sections from ten animals. The number of neurons on each outline represented the average number of immunostained neurons in the test sections closest to the corresponding standard section. In case of VP immunostained neurons in LHy and DMH, single neurons represented a 400 μm^2 immunostained area.

The position of each immunostained neuron detected was entered into the Quantimet 970 image analyzer with its built-in digitizer. Three-dimensional reconstruction was performed

using a QUIPS program, which was written by Mr. Y. YU, who is a Ph.D. student in the Department of Computer Science, the City University of New York. The cell bodies were plotted as small colored dots. The CRF or VP immunostained neurons for each group of animals were viewed singly or simultaneously with the other group. The VP immunostained neurons in LHy, DMH and SON regions were also viewed simultaneously in the control or 139H-infected groups. Photographs of displays were taken with the Nikon HP F3 model camera.

III. RESULTS

A. Experiment One: Study of the Quantitative Changes in the Number and Size of the Islets and in Immunostaining Areas of A, B, D, and F Cells

1. Results of Quantitative Changes in the Number and Size of the Islets.

Using the Quantimet 970 image analyzer system, I have quantitated the changes in the number and size of the pancreatic islet profiles in 139H-infected hamsters.

Figure 1 shows the H & E staining of pancreatic islets in a normal and in a 139H-infected hamster, a and c are pancreatic islets of a control hamster, b and d are pancreatic islets of a 139H-infected hamster. The size of the islets in the 139H-infected hamster is larger than in the control hamster. As observed by Carp et al. (1990), clear spaces in islets of 139H-infected hamster are probably areas of hemorrhage in which blood cells were washed away during fixation and staining process. The pancreatic islets were classified into three sizes with the image analyzer. As shown in Figure 2, the number of "small" (areas less than 0.01 mm^2) islets was reduced from 28.0 ± 2.8 /50 mm^2 pancreatic area (pan) in control animals to 15.0 ± 1.9 /50 mm^2 pan in 139H-infected hamsters. In contrast, the number of "medium" (areas larger

than or equal to 0.01 mm^2 and less than 0.1 mm^2) islet profiles was increased significantly from 19.4±2.6 /50 mm^2 pan in the control animals to 46.1±3.7 /50 mm^2 pan in the 139H-infected hamsters. The "large" (areas larger than or equal to 0.1 mm^2) islet profiles were not found in the control animals, but there were 15.0±3.6 /50 mm^2 pan in the 139H-infected hamsters. The total number of pancreatic islet profiles was much greater in the scrapie (76.1±6.6 /50 mm^2 pan) than in the normal animals (47.4±5.5 /50 mm^2 pan). As shown in Figure 3, the total area covered by "small" islets was reduced from 0.13±0.02 mm^2/50 mm^2 pan in the control animals to 0.08±0.01 mm^2/50 mm^2 pan in the 139H-infected hamsters. In contrast, the area of "medium" islet profiles was increased significantly from 0.42±0.07 mm^2/50 mm^2 pan in the control animals to 1.82±0.18 mm^2/50 mm^2 pan in the 139H-infected hamsters. The "large" islet profiles were not found in the control hamsters, but there was 2.97±0.77 mm^2/50 mm^2 pan large islet profiles in the 139H-infected hamsters. The proportion of area of pancreas covered by islet tissue was much greater in the scrapie (4.21±0.73 mm^2/50 mm^2 pan, that was 8.42% of the pancreatic area) than in the normal animals(0.55±0.08 mm^2/50 mm^2 pan, that was 1.1% of the pancreatic area).

2. Analysis of A, B, D, and F Cell Ratios.

In my studies, I have determined the immunostaining area,

the ratio and the percentage changes of A, B, D, and F cells in the pancreatic islet profiles in 139H-infected hamsters.

By using antibodies against insulin, glucagon, somatostatin and pancreatic polypeptide, the immunostaining areas of B, A, D, and F cells, respectively, were measured by the Quantimet 970 image analyzer system. Figure 4 shows the pictures of pancreatic sections immunostained with insulin (ir-In) in islets of normal and 139H-infected hamsters; we can see that the stained density was less in the pancreatic islets of the 139H-infected hamsters than in the control hamsters.

Figure 5 shows the positively stained areas of ir-In per 50 mm^2 pan in control hamsters and 139H-infected hamsters. The area of ir-In was increased significantly from 0.46 ± 0.07 $mm^2/50$ mm^2 pan in the normal animals to 3.53 ± 0.61 $mm^2/50$ mm^2 pan in the 139H-infected animals. The percentage of positively stained areas of ir-In did not differ significantly in the 139H-infected hamsters ($85.75\pm1.61\%$) from the stained area in the control animals ($82.71\pm2.40\%$).

Figure 6 shows the immunostained glucagon (ir-Glu) in islets of control and 139H-infected hamsters. We can see that the ir-Glu is located in the outer rim of the islets in both the control and the 139H-infected hamsters. Figure 7 shows the immunostained somatostatin (ir-SS) in the islets of control and 139H-infected hamsters. The ir-SS is also located in the peripheral mantle of the islets in both control and 139H-infected hamsters.

Table I shows the analysis of ir-Glu and ir-SS in the

pancreatic islets of control and 139H-infected hamsters. Although the positively stained areas of ir-Glu were increased significantly from 0.09±0.02 mm^2/50 mm^2 pan in control animals to 0.20±0.04 mm^2/50 mm^2 pan in 139H-infected hamsters, the percentage of positively stained areas of ir-Glu compared to the total islet area was decreased significantly from 17.5±2.4% in control animals to 5.6±0.8% in 139H-infected hamsters. There was no a significant difference between the positively stained areas of ir-SS in control and 139H-infected animals, however, the percentage of positively stained areas compared to the total islet area was decreased significantly from 3.2±0.6% in control animals to 0.99±0.2% in 139H-infected hamsters.

Figure 8 shows the immunostained pancreatic polypeptide (ir-PP) in islets of a control and a 139H-infected hamster. The positively stained areas of ir-PP were not significantly different in control animals (0.0006±0.0003 mm^2/50 mm^2 pan) and 139H-infected hamsters (0.0011±0.0005 mm^2/50 mm^2 pan). The percentage of positively stained areas of ir-PP compared to the total islet area was not significantly different in the control than from that of the 139H-infected hamsters in this study.

Figure 9 shows the positively stained areas of B, A, D, and F cells. The immunostained areas of insulin and glucagon were increased significantly in 139H-infected animals compared to that of control animals. The immunostained areas of somatostatin and pancreatic polypeptide did not change

significantly. The proportion of B, A, D, and F cells was determined. With somatostatin positive cells arbitrarily given a value of 1, the ratio of B:A:D:F cells in the islets of normal hamsters was 27:5:1:0.04, whereas, in the islets of 139H-infected hamsters it was 122:7:1:0.04. Our results indicate that the increase in B cells could serve as a major component in the enlargement of pancreatic islets and play an important role in the hypoglycemia-hyperinsulinemia seen in hamsters infected with the 139H scrapie strain.

As shown in Figure 10, the average optical density per pancreatic area (OD/pan) of ir-In was decreased in 139H-infected hamsters compared to that of control animals. The OD/pan of ir-In "small" islets was decreased significantly from 0.4307 ± 0.0288 in the control animals to 0.3303 ± 0.0201 in the 139H-infected hamsters. The OD/pan of ir-In "medium" islets was decreased significantly from 0.4030 ± 0.0280 in the control animals to 0.3093 ± 0.0175 in the 139H-infected hamsters. There were no "large" islets in the control animals, the OD/pan of ir-In "large" islets in the 139H-infected hamsters was very low (0.2288 ± 0.0250). The OD/pan of ir-In total islets was decreased significantly from 0.3662 ± 0.0121 in the control animals to 0.2837 ± 0.0131 in the 139H-infected hamsters. The results suggested that in islets of 139H-infected hamsters, the concentration of insulin in B granules was decreased or the number of B granules was decreased, or both.

The OD/pan of ir-Glu did not differ significantly between

control animals (0.248±0.011) and 139H-infected hamsters (0.238±0.015). Though the OD/pan of ir-SS differed between control animals (0.169±0.017) and 139H-infected hamsters (0.214±0.029), the difference was not significant. The OD/pan of ir-PP did not differ significantly in control animals (0.264±0.031) and 139H-infected hamsters (0.282±0.020).

Figure 1. Hematoxylin and Eosin Stain of Pancreatic Islets.

a. Pancreatic islets of a control hamster at low power (82x).

b. Pancreatic islets of a 139H-infected hamster at low power (82x).

c. Pancreatic islet of the control hamster at high power (328x).

d. Pancreatic islets of the 139H-infected hamster at high power (328x).

Note: the size of the islets in the 139H-infected hamster is larger than that in the control hamster. Aci: acini, Is: islet.

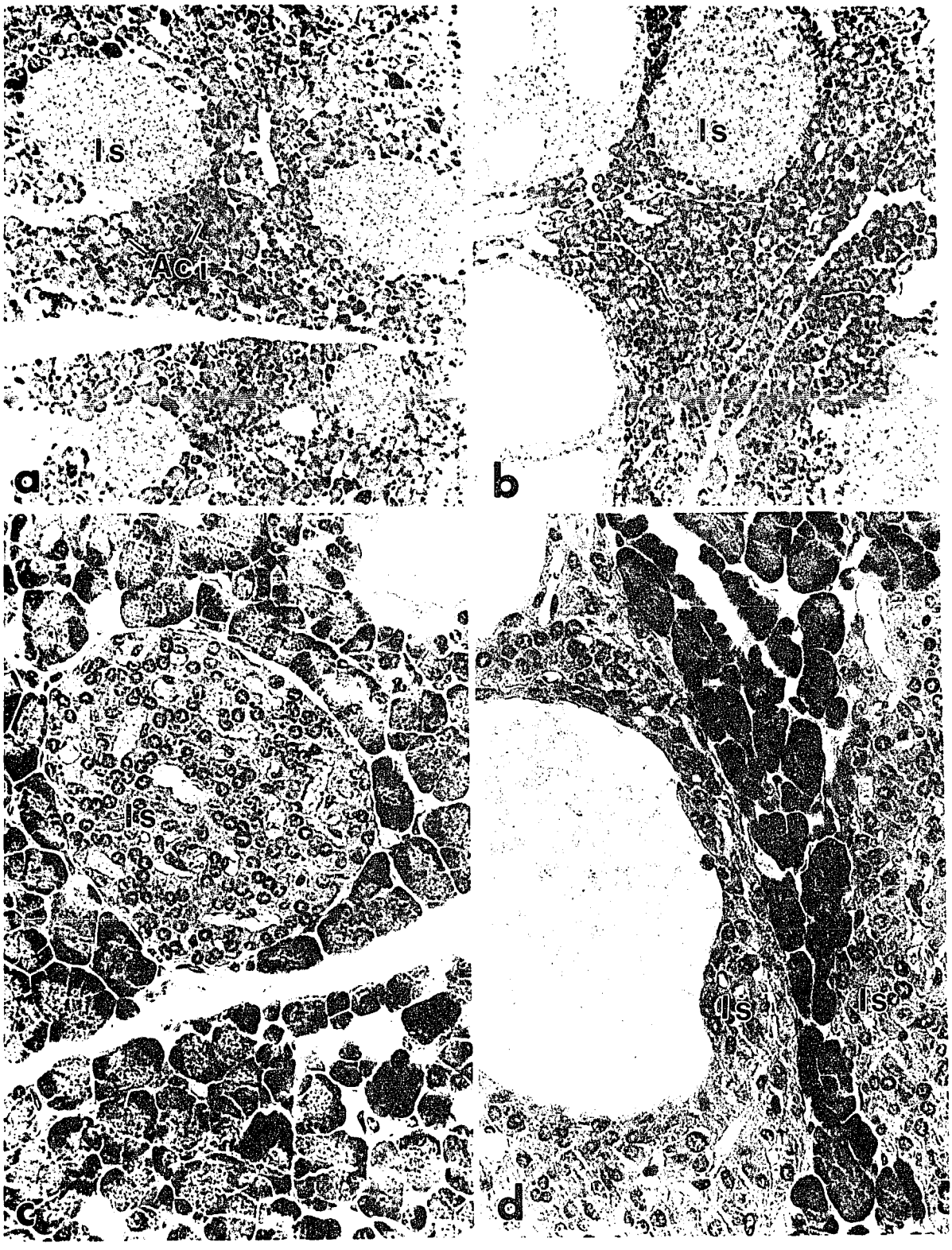
ls
Aci
a
ls
b
ls
c
ls
ls
d

Figure 2. Comparison of the Number of Pancreatic Islets of Different Sizes per 50 mm^2 Pancreatic Section in Control Hamsters (NHB, N=14) and 139H-infected Hamsters (N=20).

Note: *: p value < 0.05; **: p value < 0.01; ***: p value < 0.001; small islets < 0.01 mm^2; medium islets ≥ 0.01 mm^2 and < 0.1 mm^2; large islets ≥ 0.1 mm^2.

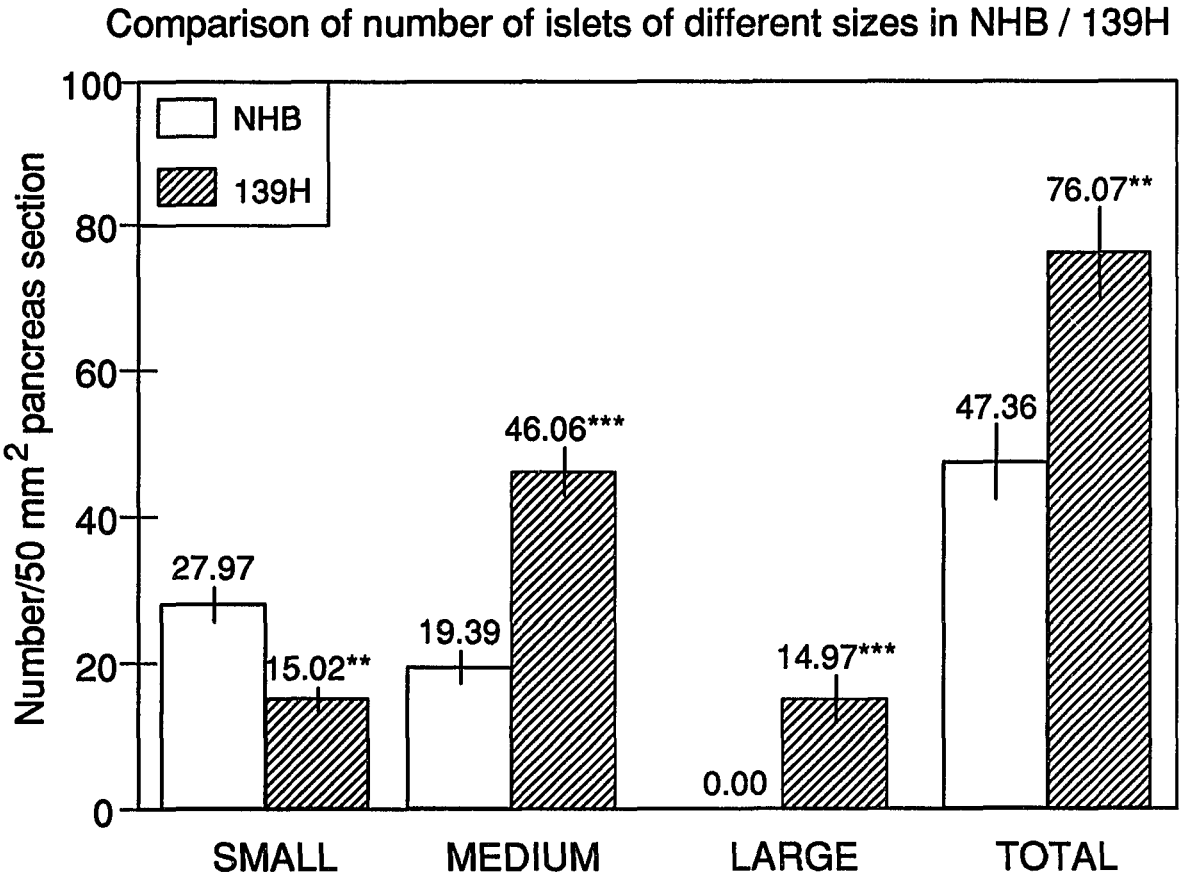
Comparison of number of islets of different sizes in NHB / 139H
Number/50 mm2 pancreas section
100
80
60
40
20
0
NHB
139H
27.97
15.02**
19.39
46.06***
0.00
14.97***
47.36
76.07**
SMALL
MEDIUM
LARGE
TOTAL

Figure 3. Comparison of the Area of Pancreatic Islets of Different Sizes per 50 mm^2 Pancreatic Section in Control Hamsters (NHB, N=14) and 139H-infected Hamsters (N=20).

Note: *: p value < 0.05; **: p value < 0.01; ***: p value < 0.001; small islets < 0.01 mm^2; medium islets ≥ 0.01 mm^2 and < 0.1 mm^2; large islets ≥ 0.1 mm^2.

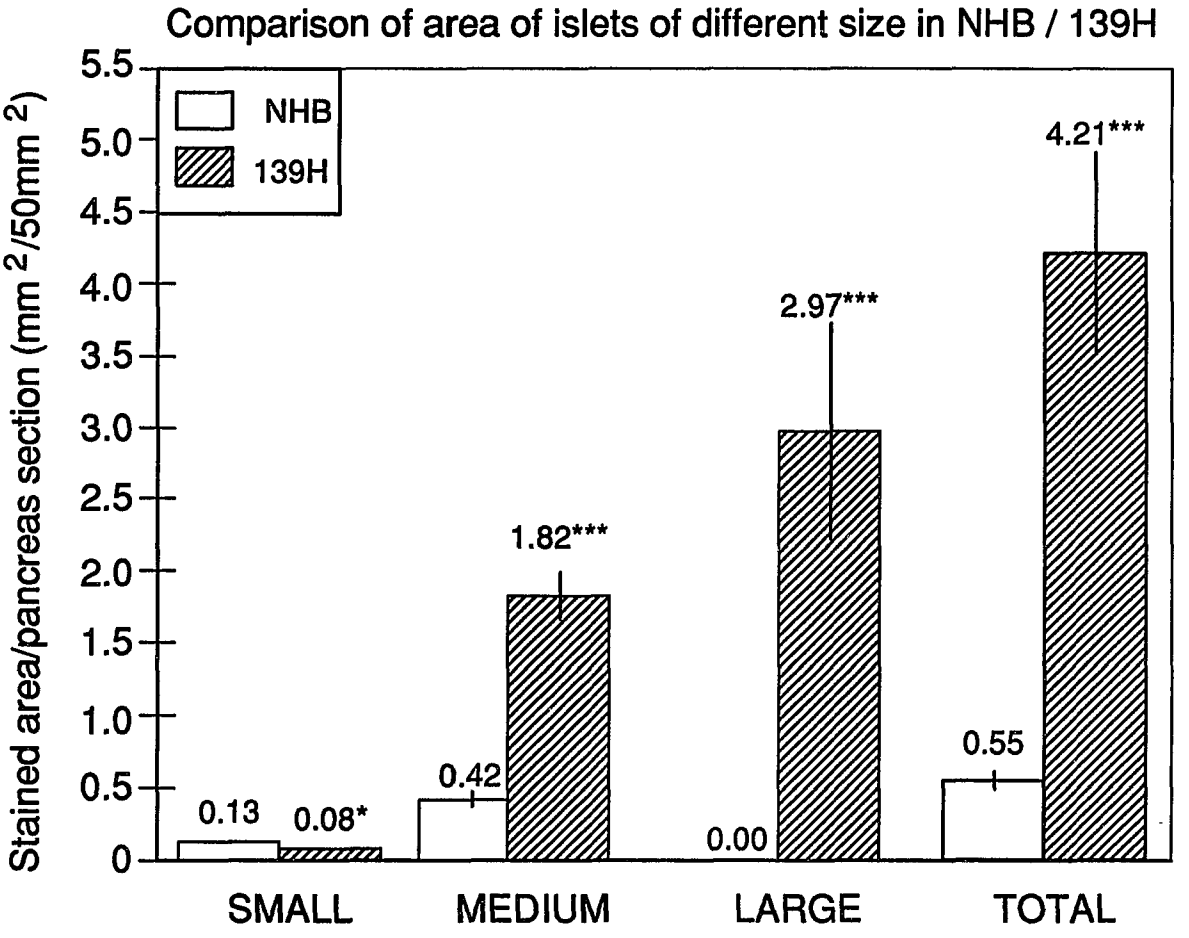
Comparison of area of islets of different size in NHB / 139H
Stained area/pancreas section (mm 2/50mm 2)
5.5
5.0
4.5
4.0
3.5
3.0
2.5
2.0
1.5
1.0
0.5
0
NHB
139H
0.13
0.08*
0.42
1.82***
0.00
2.97***
0.55
4.21***
SMALL
MEDIUM
LARGE
TOTAL

Figure 4. Immunostained Insulin in Islets.

a. Pancreatic islets of a control hamster at low power (82x).

b. Pancreatic islets of a 139H-infected hamster at low power (82x).

c. Pancreatic islet of a control hamster at high power (245x, H & E counterstain).

d. Pancreatic islet of a 139H-infected hamster at high power (245x, H & E counterstain).

Note: the immunostained insulin (ir-In; arrowhead) is less intense in the islets of the 139H-infected hamsters than in the control hamsters.

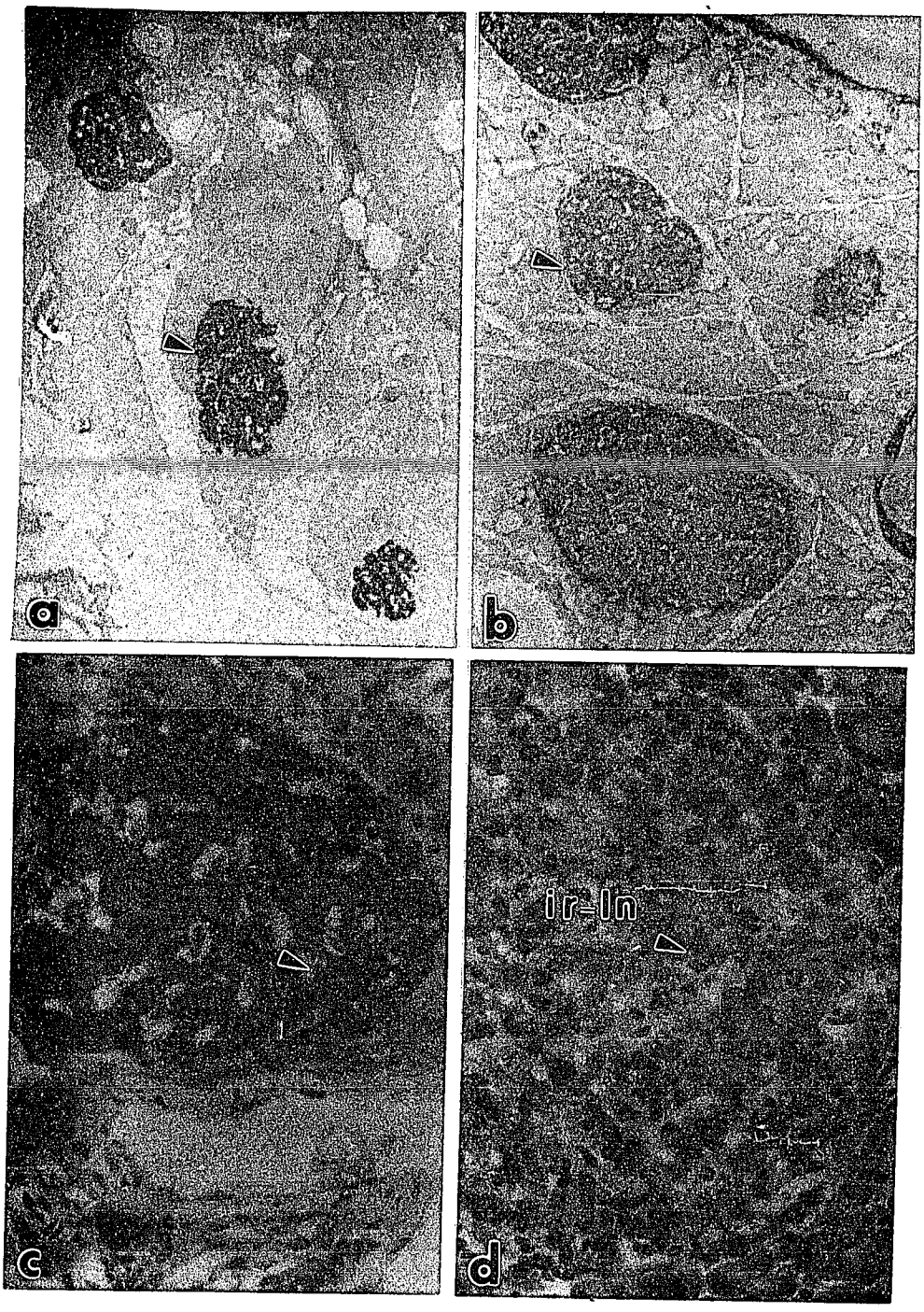
a
b
c
d
ir-ln

Figure 5. Positively Stained Area of Immunoreactive Insulin per 50 mm^2 Pancreatic Section in Control Hamsters (NHB, N=14) and 139H-infected Hamsters (N=20).

***: p value < 0.001.

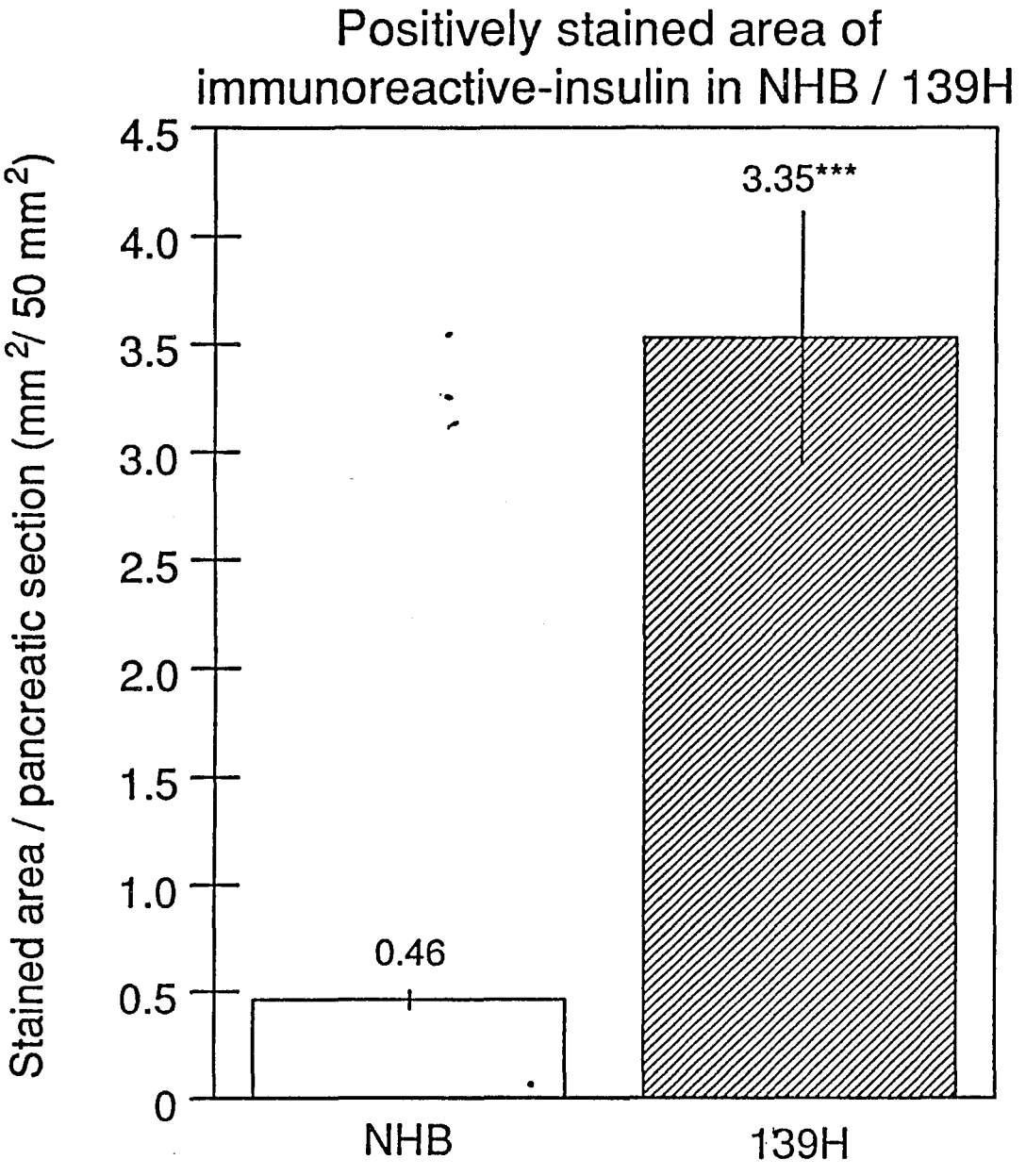
Positively stained area of
immunoreactive-insulin in NHB / 139H
Stained area / pancreatic section (mm 2/ 50 mm 2)
4.5
4.0
3.5
3.0
2.5
2.0
1.5
1.0
0.5
0
3.35***
0.46
NHB
139H

Figure 6. Immunostained Glucagon in Islets.

a. Pancreatic islet of a control hamster at 245x.

b. Pancreatic islet of a 139H-infected hamster at 245x.

c. Pancreatic islet of a control hamster at 245x.

d. Pancreatic islet of a 139H-infected hamster at 245x.

Note: the immunostained glucagon (ir-Glu, arrowhead) is located in the outer rim of both the control and the 139H-infected hamsters; the ir-Glu cells might form a spherical shell around the islet. The ir-Glu cells show a circle in this section and many of them are parallel to the mantle in the control hamsters in Figures 6a and 6c, but the ir-Glu cells are scattered in the peripheral mantle in the 139H-infected hamsters, and these cells are not parallel to the mantle as seen in the control hamsters (Figures 6b and 6d).

Small arrow shows that the orientation of the islet cells is changed in the 139H-infected hamsters. We can also see that there is marked hyperplasia and hypertrophy of the islet cells and marked swelling of the cell nuclei in the 139H-infected hamsters.

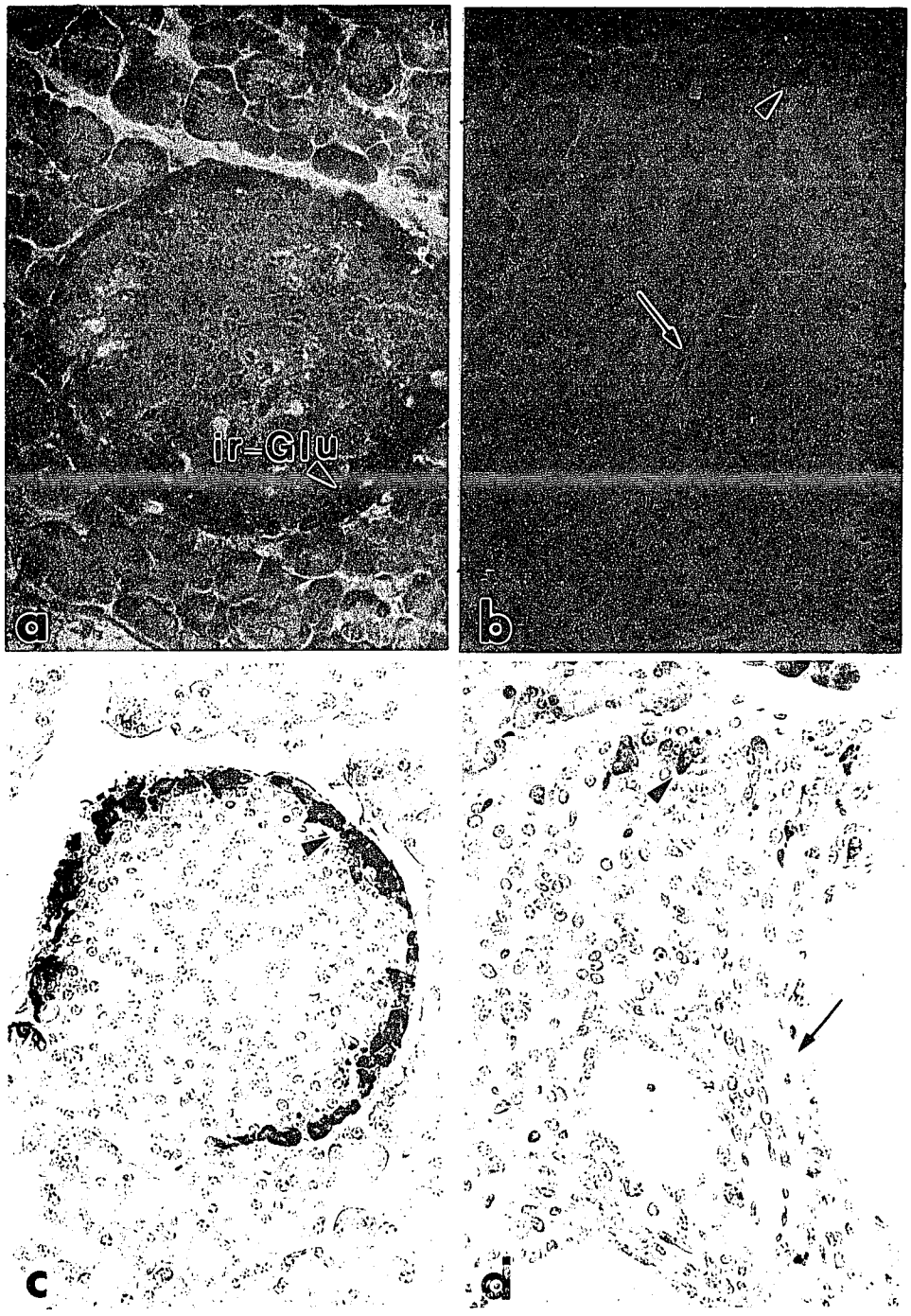
ir-Glu
a
b
c
d

Figure 7. Immunostained Somatostatin in Islets.

a. Pancreatic islet of a control hamster at low power (82x).

b. Pancreatic islets of a 139H-infected hamster at low power (82x).

c. Pancreatic islet of the control hamster at high power (328x).

d. Pancreatic islet of the 139H-infected hamster at high power (328x).

Note: the immunostained somatostatin (ir-SS, arrowhead) is located in the outer rim of the islets of both the control and the 139H-infected hamsters. Many of the ir-SS cells are parallel to the mantle in Figures 7a and 7c in the control hamster, but the ir-SS cells are scattered in the peripheral mantle in the 139H-infected hamsters, and these cells are not parallel to the mantle as seen in the control hamster (Figures 7b and 7d).

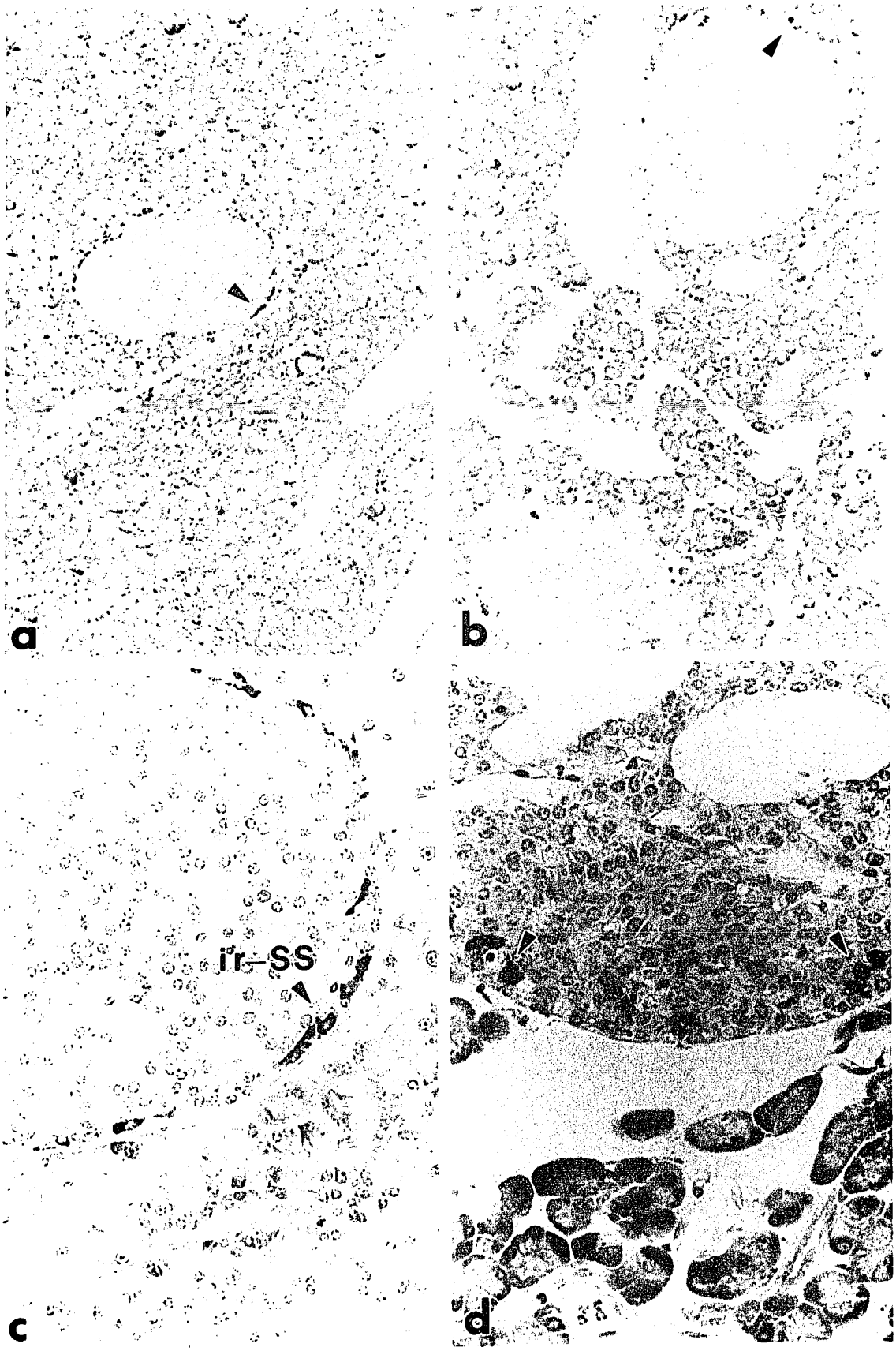
a
b
ir-SS
c
d

Table I. Analysis of Immunoreactive Glucagon and Somatostatin in the Pancreatic Islets of NHB and 139H Hamsters

Inoculum	N	ir-Glu		N	ir-SS	
		PA	PA%		PA	PA%
NHB	15	0.09 ±0.02	17.5 ±2.4	16	0.017 ±0.004	3.2 ±0.6
139H	20	0.20 ±0.04*	5.6 ±0.8***	18	0.029 ±0.006	0.99 ±0.2**

Note: N: number of animals; PA: positively stained area ($mm^2/50\ mm^2$); PA%: percentage of positively stained area in total islets. *: $p < 0.05$; **: $p < 0.01$; ***: $p < 0.001$.

Figure 8. Immunostained Pancreatic Polypeptide in Islets.

a. Pancreatic islet of a control hamster at low power (328x).

b. Pancreatic islets of a 139H-infected hamster at low power (328x).

Note: the immunostained pancreatic polypeptide (ir-PP, arrowhead) is located in the outer rim of the islets of both the control and the 139H-infected hamsters. Is: islet.

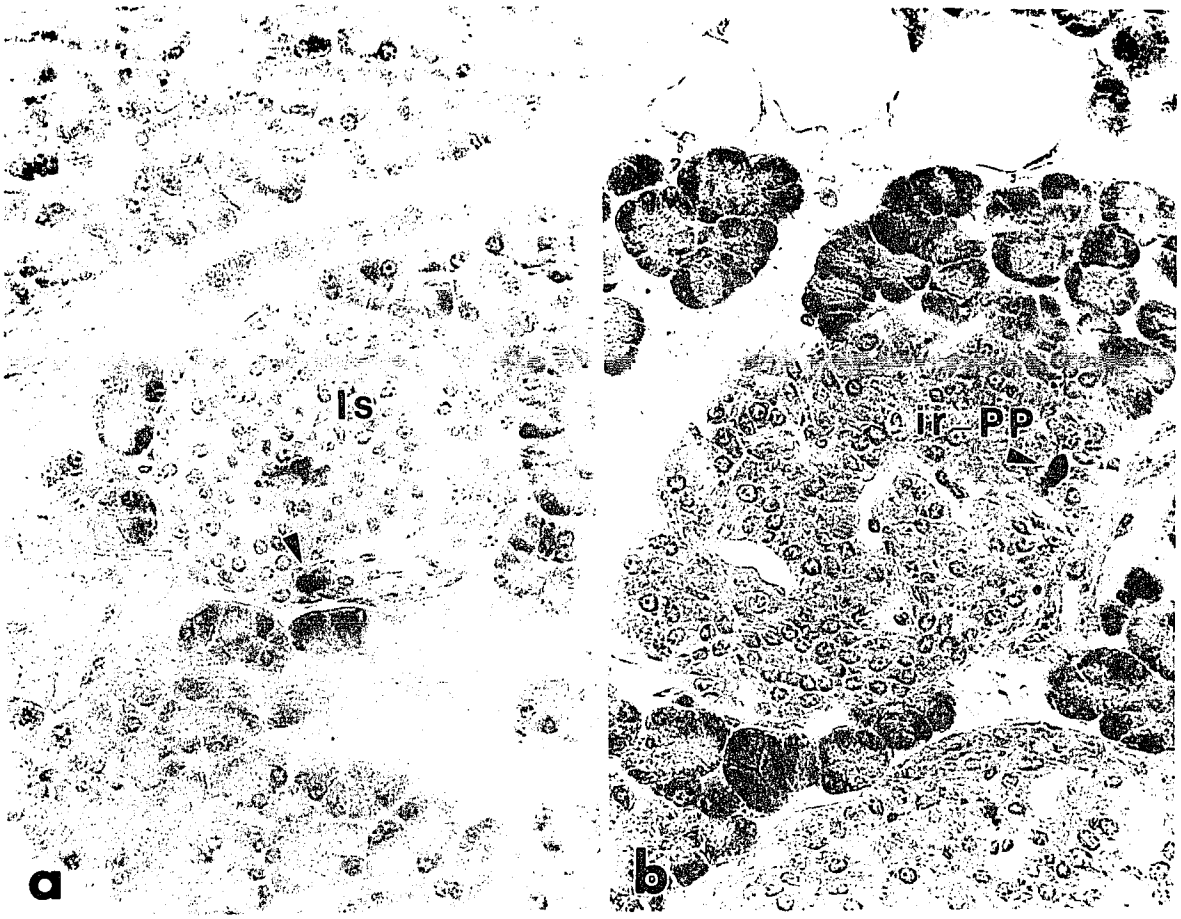
a
ls
b
ir
PP

Figure 9. Comparison of Positively Stained Areas of B, A, D, and F Cells in Control Hamsters (NHB, N=14) and 139H-infected Hamsters (N=20).

*: p value < 0.05; **: p value < 0.01; ***: p value < 0.001.

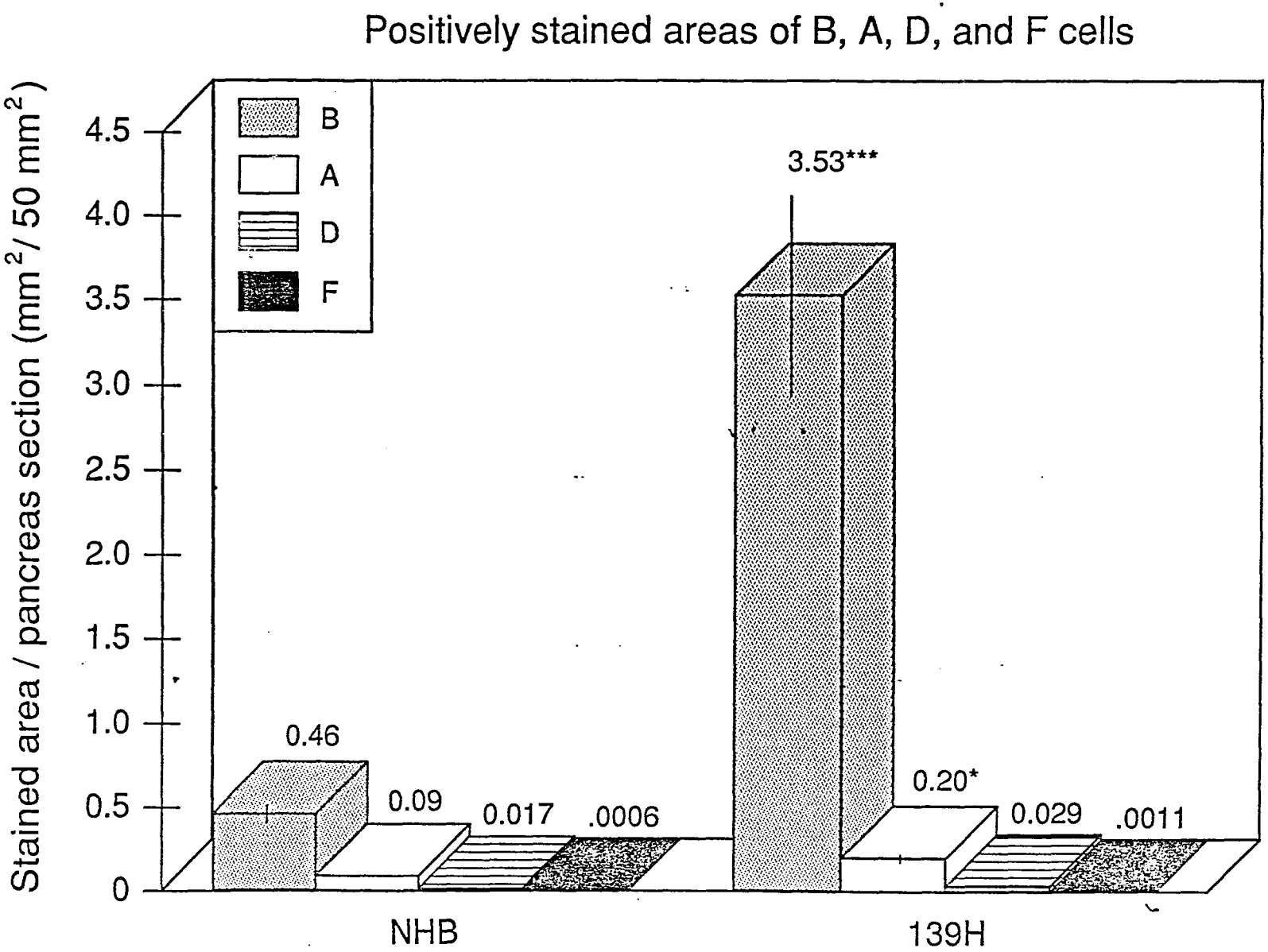
Positively stained areas of B, A, D, and F cells
Stained area / pancreas section (mm²/ 50 mm²)
4.5
4.0
3.5
3.0
2.5
2.0
1.5
1.0
0.5
0
B
A
D
F
0.46
0.09
0.017
.0006
3.53***
0.20*
0.029
.0011
NHB
139H

Figure 10. The Average Optical Density per Pancreatic Area (OD/pan) of ir-In 139H-infected Hamsters (N=20) and Control Animals (NHB, N=14).

Note: *: p value < 0.05; **: p value <0.01; ***: p value < 0.001; S: small islets < 0.01 mm^2; M: medium islets ≥ 0.01 mm^2 and < 0.1 mm^2; L: large islets ≥ 0.1 mm^2; T.OD: average of stained cells optical density per pancreatic area.

Stained cells' OD of ir-In in NHB/139H

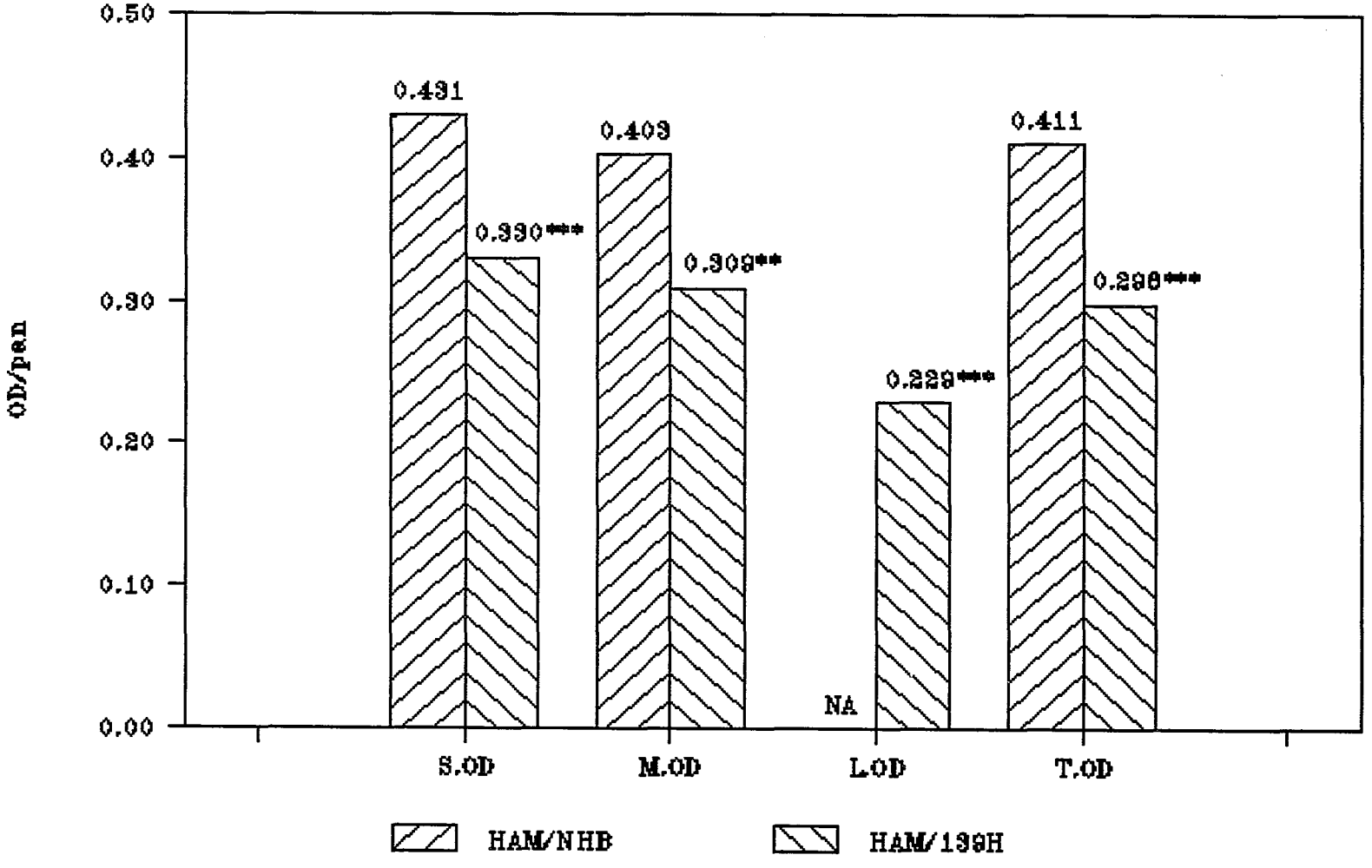

B. Experiment Two: Study of the Pathological Changes in the Pancreatic Islets in 139H-infected Hamsters with Light Microscopy

As shown in Figures 11 and 12, there were histopathological changes in the islets of Langerhans in hamsters infected with the 139H scrapie strain. We can see fibrosis (arrowhead, in Figures 11b and 11d), vacuolization (Figures 11b; 11d; 12f; 12h; 12i and 12j), cellular atrophy (Figures 11b; 11d; 12f; 12h; 12i and 12j), cellular elongation (Figures 12d; and 12f), changes in cell shape and orientation (Figures 11b; 11d; 12f and 12j). There were also nuclear pathological changes such as swelling (Fig 12i, double arrowheads), changes in shape, pyknosis, karyorrhexis and karyolysis (Figures 11b; 11d and 12h). There were no such changes in 263K-infected hamsters (Figure 12b).

There are two kinds of vacuolization that we can see in this study. I refer to call the first one as "intracellular vacuolization" (IV). IV is located inside the islet cells and is near the nuclei of islet cells (as seen in Fig 12h and 12i, star). The other vacuolization I would call "extracellular vacuolization" (EV). EV is found outside the islet cells (as seen in Fig 11d, 12f and 12j, asterisk). IV might be the beginning of cell death and EV might be the result of cell death.

As shown in Figure 11 and 12, the vascular pattern was disturbed significantly in the islets of the 139H-infected

hamsters. There was a large mass of blood cells which did not appear to be surrounded by traditional arterial, venous or capillary wall cells. I refer to this structure as "blood vessel core" (BVC). These structures were almost always centrally located within the islets and surrounded by B cells, some of which were elongated abnormally.

As shown in Figure 13, using PAS and orange G stain, I noted an abnormal PAS positive substance in plaque-like form located in the islets of Langerhans and in BVC (Figures 13b and 13c) in the 139H-infected hamsters, but not in the control hamsters. This substance was located both inside and outside the cells in the endocrine organs. I refer to this PAS positive substance as "PPS".

In normal animals, islets are separated from acinar tissue by a thin layer of reticular tissue (see Figure 11c). However, in Figure 12g, we can see that the structure of the islet is destroyed and we do not see the thin layer of reticular tissue.

Using Congo red and thioflavin-S stain, I did not find any amyloid formation in the pancreatic islets of the 139H-infected hamsters.

Figure 11. Gomori's One-step Trichrome Stain of Pancreatic Islets.

a. Pancreatic islet of a control hamster at low power (61x).

b. Pancreatic islets of a 139H-infected hamster at low power (61x).

c. Pancreatic islet of a control hamster at high power (244x).

d. Pancreatic islet of a 139H-infected hamster at high power (244x).

Note: abbreviations and symbols used in denoting the histopathological changes in the islets of Langerhans in the hamsters infected with the 139H scrapie strain.

BV: blood vessel; BVC: blood vessel core; Cap: capillary; InD: interlobular duct; Is: islet; fibrosis (arrowhead); vacuolization (*); margination of inflammatory cells (small arrow); cellular atrophy; cellular elongation; changes in cell shape and orientation.

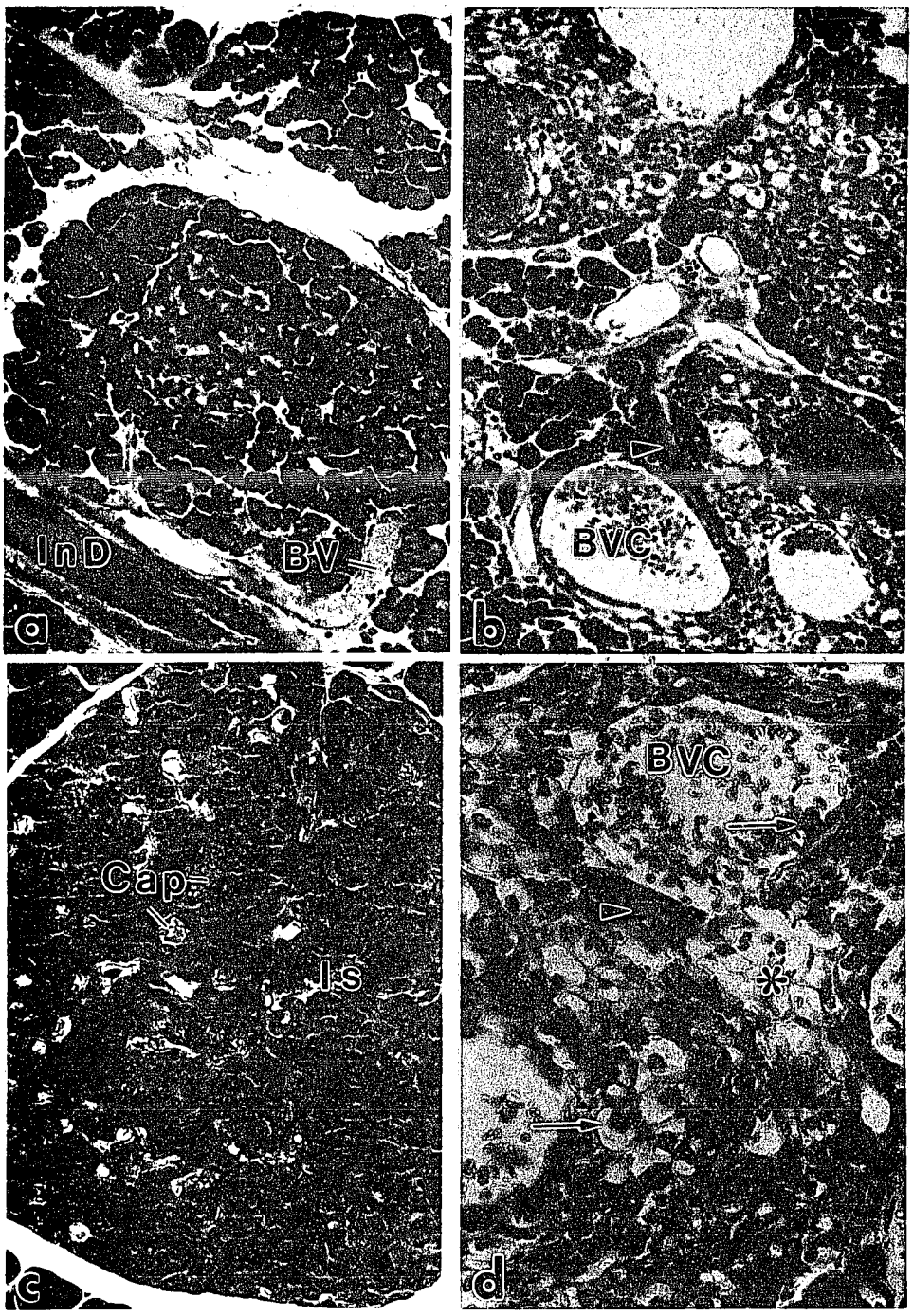
InD
BV
a
BVC
b
Cap
IS
c
BVC
d

Figure 12. Histopathological Changes in Pancreatic Islets.

a. Pancreatic islets of a control hamster at 55x.

b. Pancreatic islets of a 263K-infected hamster at 55x.

c. Pancreatic islets of a 139H-infected hamster at 55x.

d. Pancreatic islet of a 139H-infected hamster at 820x.

e. Pancreatic islet of a control hamster at 164x.

f. Pancreatic islet of a 139H-infected hamster at 328x.

g. Pancreatic islet of a 139H-infected hamster at 82x.

h. Pancreatic islet of a 139H-infected hamster at 164x.

i. Pancreatic islet of a 139H-infected hamster at 164x.

j. Pancreatic islet of a 139H-infected hamster at 382x.

Note: H and E stains show the histopathological changes in the islets of Langerhans in the hamsters infected with the 139H scrapie strain.

Aci: acini; BVC: blood vessel core; InS: interlobular septum; Is: islet; intracellular vacuolization (star); extracellular vacuolization (*); cellular atrophy (Figure 12f); cellular elongation (arrowhead); changes in cell shape and orientation (arrowhead).

There are also nuclear pathological changes such as swelling (double arrowheads). The structure of the islet is destroyed and the thin layer of reticular tissue is not found (Fig 12g; small arrow). There were no such changes in 263K-infected hamsters (Figure 12b).

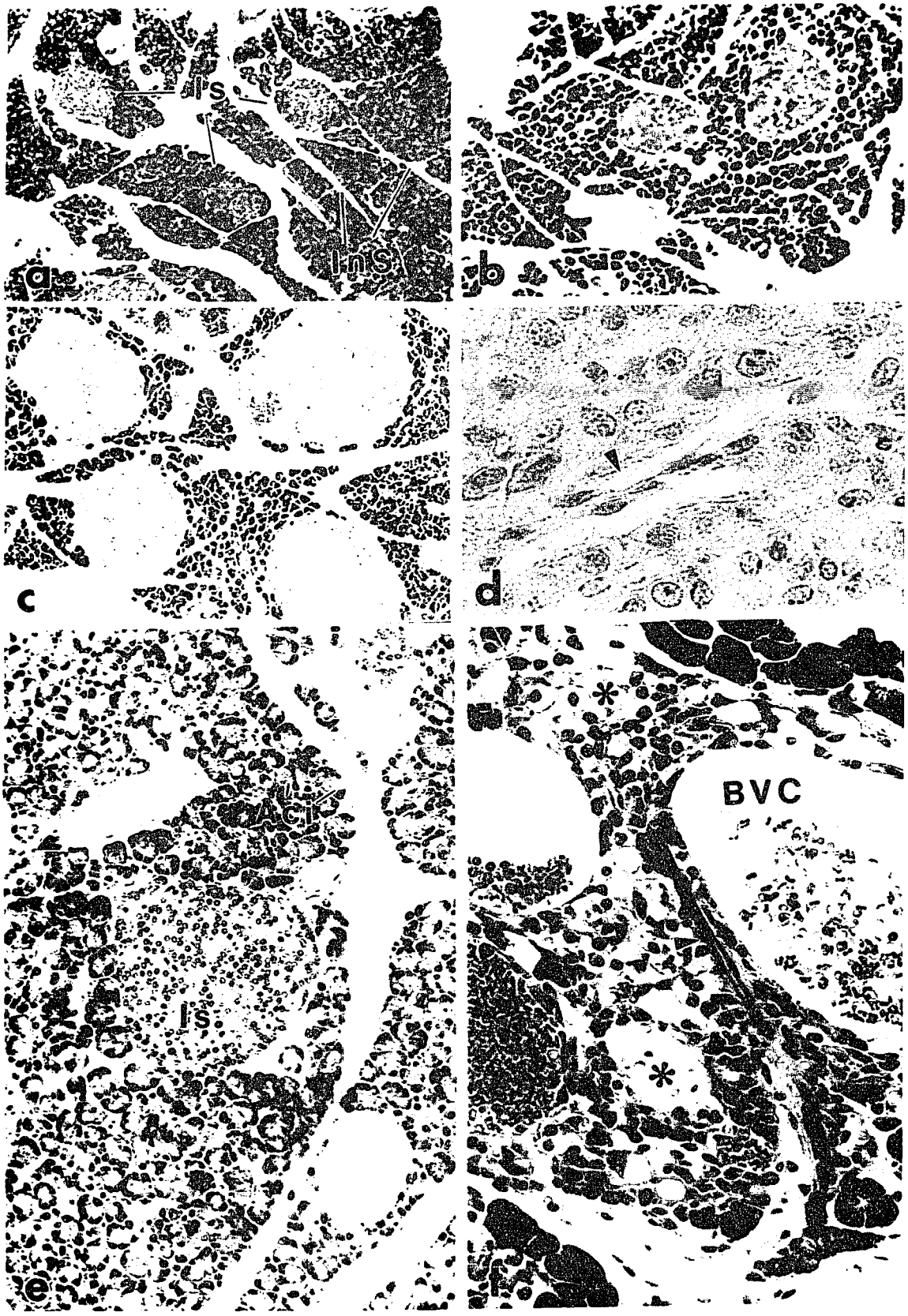
IS
InS
a
b
c
d
ACi
IS
e
BVC

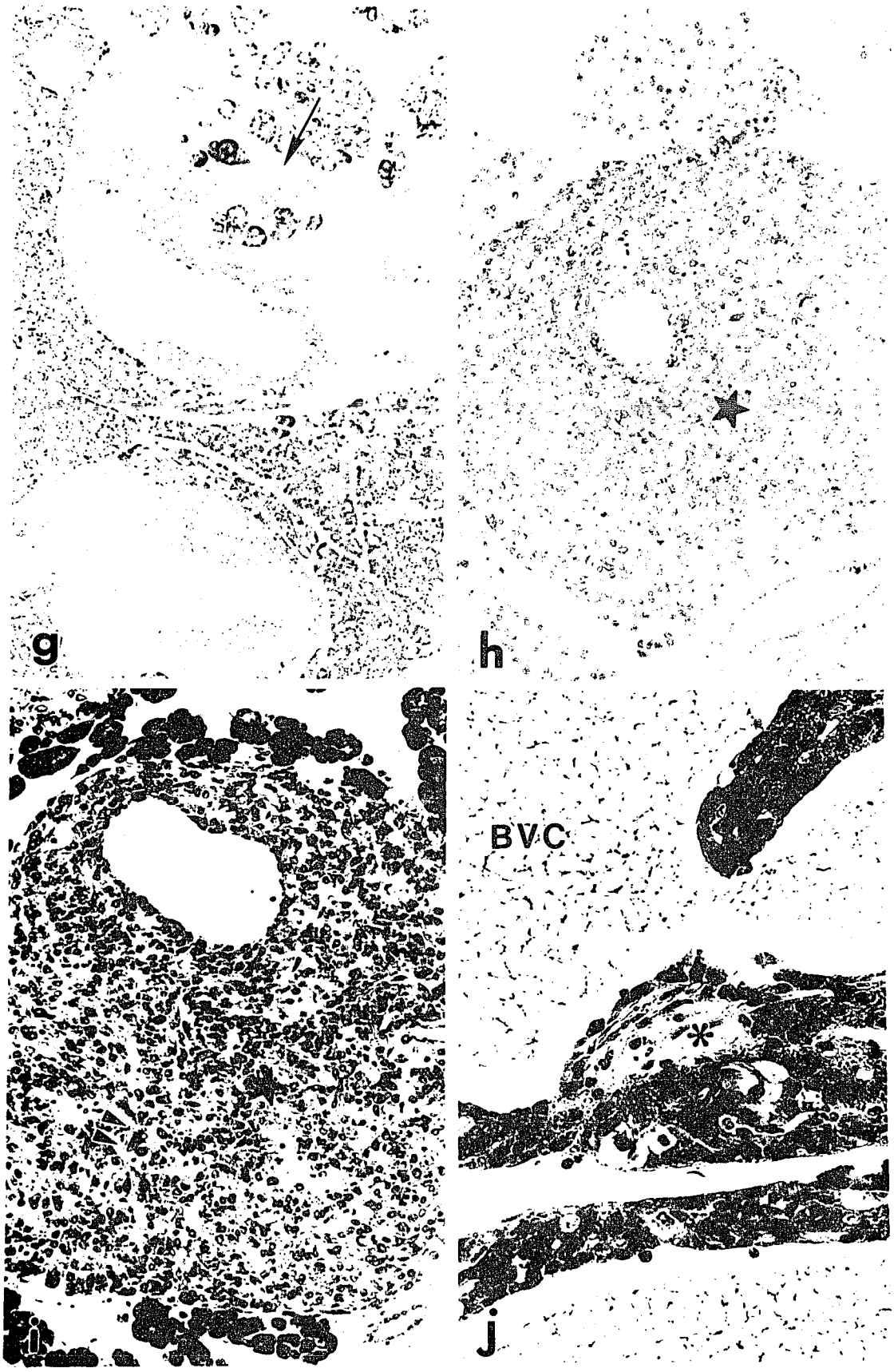
g
h
BVC
j

Figure 13. PAS and Orange G Stain of Pancreatic Islets.

a. Pancreatic islet of a control hamster at 610x, shows the normal structure and no PPS. Is: islet.

b. Pancreatic islet of a 139H-infected hamster at 610x, shows abnormal PPS in plaque-like form located in the pancreatic islets. This PPS (arrowhead) is located both inside and outside the islet cells. Note: the nuclei of the islet cells in 139H-infected hamsters are enlarged (arrow).

c. Pancreatic islet of a 139H-infected hamster at 820x, shows abnormal PPS in plaque-like form located in the pancreatic islets. Note: this PPS is located both inside and outside the islet cells, in the lumen of BVC and attached to the wall of BVC (arrowhead).

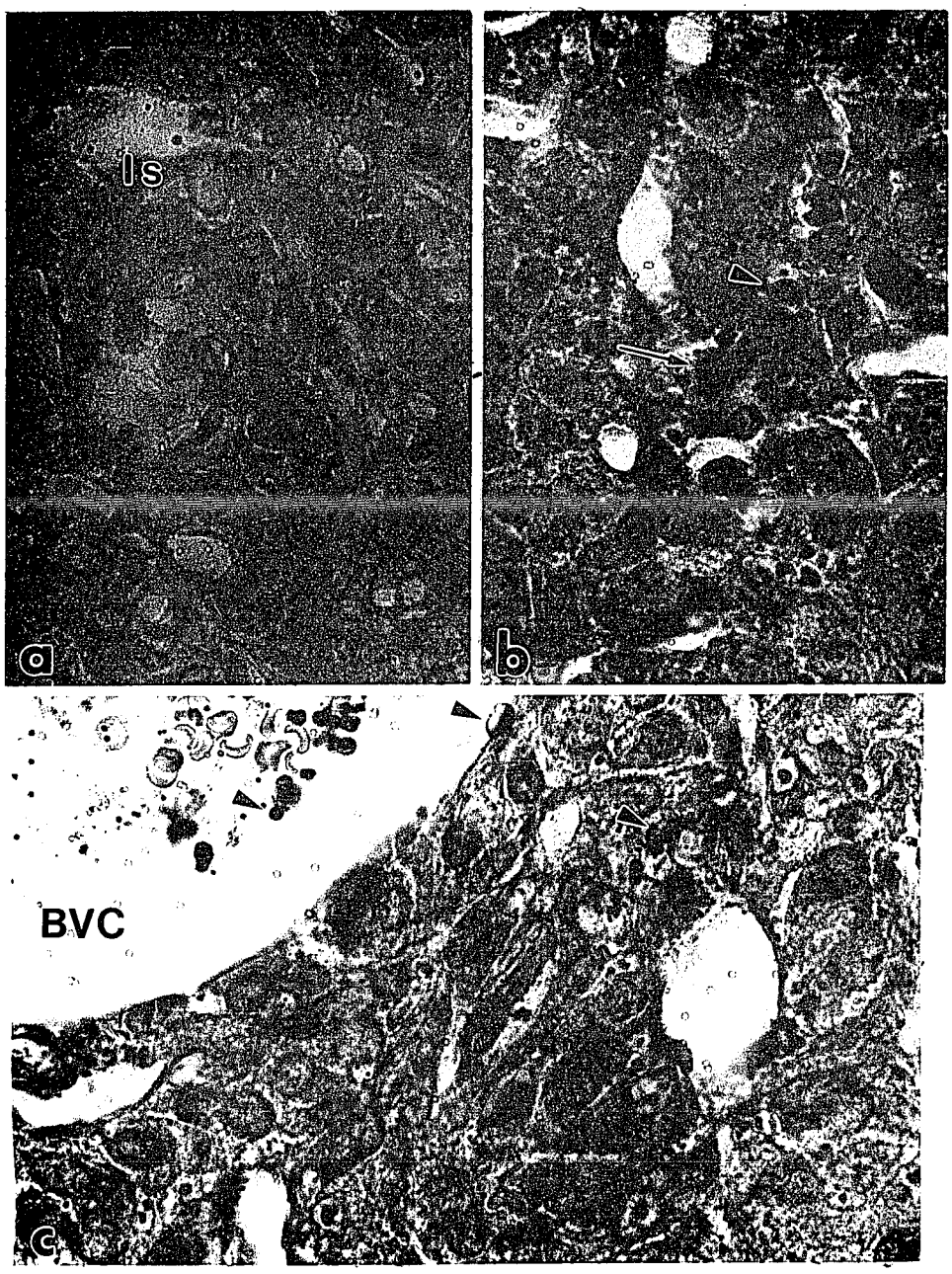
ls
a
b
BVC
c

C. Experiment Three: Study of the Pathological Changes in the Pancreatic Islets in 139H-infected Hamsters with Semi-thin Sections

As shown in Figures 14 and 15, using semi-thin sections stained with toluidine blue, we can see the pathological changes in the islets of 139H-infected hamsters in much more detail. There were cytoplasmic vesicles, nuclear swelling, vacuolization in the islet cells of 139H-infected hamsters. There were also two types of vacuolization that we can see in the semi-thin sections. One type of vacuolization I would call "localized vacuolization" (LV). LV has a clear edge and is restricted or confined within the cell (Figures 14c and 15b). The other type of vacuolization I would call "diffuse vacuolization" (DV). DV has no clear edge, and is scattered within tissues either inside or outside of cells (Figures 14d and 15b). These Dvs may span intracellular and extracellular regions of the tissues.

There were also many nuclei, which resembled the nuclei of macrophages between the islet cells in the 139H-infected hamsters. The extracellular spaces were enlarged in the islets of the 139H-infected hamsters compared to the spaces in the control hamsters. In my studies, I observed the following phenomenon: pathological changes are similar in a specific region. That is to say, if you see a LV in one cell, you might also find other Lvs in the nearby cells (Figures 14c and 15b). That is also true for many pathological changes such as

DV (Figures 14d and 15b), IV (Figures 12h and 12i), EV (Figures 12f and 12j), changes in cell orientation and shape (Figures 12d, and 12f), cellular hypertrophy (Figures 14c and 14d), atrophy (Figures 11d and 12f), nuclear swelling (Figures 14b and 14d), pyknosis (Figures 11d and 12f), and karyolysis (Figure 12j). I would call this phenomenon "pathological pattern synchronism". I will discuss the pathological significance of pathological pattern synchronism later.

In addition, I also observed different phenomena of margination and diapedesis of inflammatory cells (macrophages, neutrophils and lymphocytes) through the membranes of B-cells (the wall of the BVC) in 139H-infected hamsters: (1) only a single macrophage-like inflammatory cell (Figure 15a); (2) only a single lymphocyte (Figure 16); (3) a group of two or more lymphocytes (Figure 17); (4) a group of mixed lymphocytes and macrophages or neutrophils (Figure 18); (5) a group of two or more macrophages (Figures 15b; 19a; 19b and 19c).

My studies showed that lymphocytes could come into close contact with one another and also with macrophages, neutrophils or with B-cells at the wall of BVC. Furthermore, I have also observed another phenomenon: the interaction between a group of macrophages and/or other inflammatory cells with B-cells at the wall of BVC. I refer to this phenomenon as "linkage reaction"; this group of macrophages or inflammatory cells as "linkage-macrophages" or "linkage-inflammatory cells". I will discuss the functional significance of "linkage reaction" later.

Figure 14. Semi-thin Sections of Pancreatic Islets Stained with Toluidine Blue.

a. Pancreatic islet of a control hamster at 820x.

b. c. and **d.** Pancreatic islets of 139H-infected hamsters at 820x.

Note: the histopathological changes in the islets of Langerhans in the 139H-infected hamsters.

BVC: blood vessel core; Cap: capillary; DV: diffuse vacuolization; LV: localized vacuolization; cellular hypertrophy (small arrow); cytoplasmic vesicles, and the extracellular spaces (ES) enlarged.

There are also nuclear pathological changes such as swelling (small arrow), changes in shape. There are also many nuclei (arrow head), which look like the nuclei of macrophages between the islet cells in the 139H-infected hamsters.

In spite of many dilations of the extracellular spaces in forms of necklace-like chains between cells, islet cells maintain intimate contacts with each other at several points in both the control and the 139H-infected hamsters. The contact points consist of a close relationship of the respective islet cell plasma membranes with no intervening extracellular spaces. Such a zone might correspond to a tight junction. Those contact points are changed significantly in the 139H-infected hamsters compared with the control hamsters.

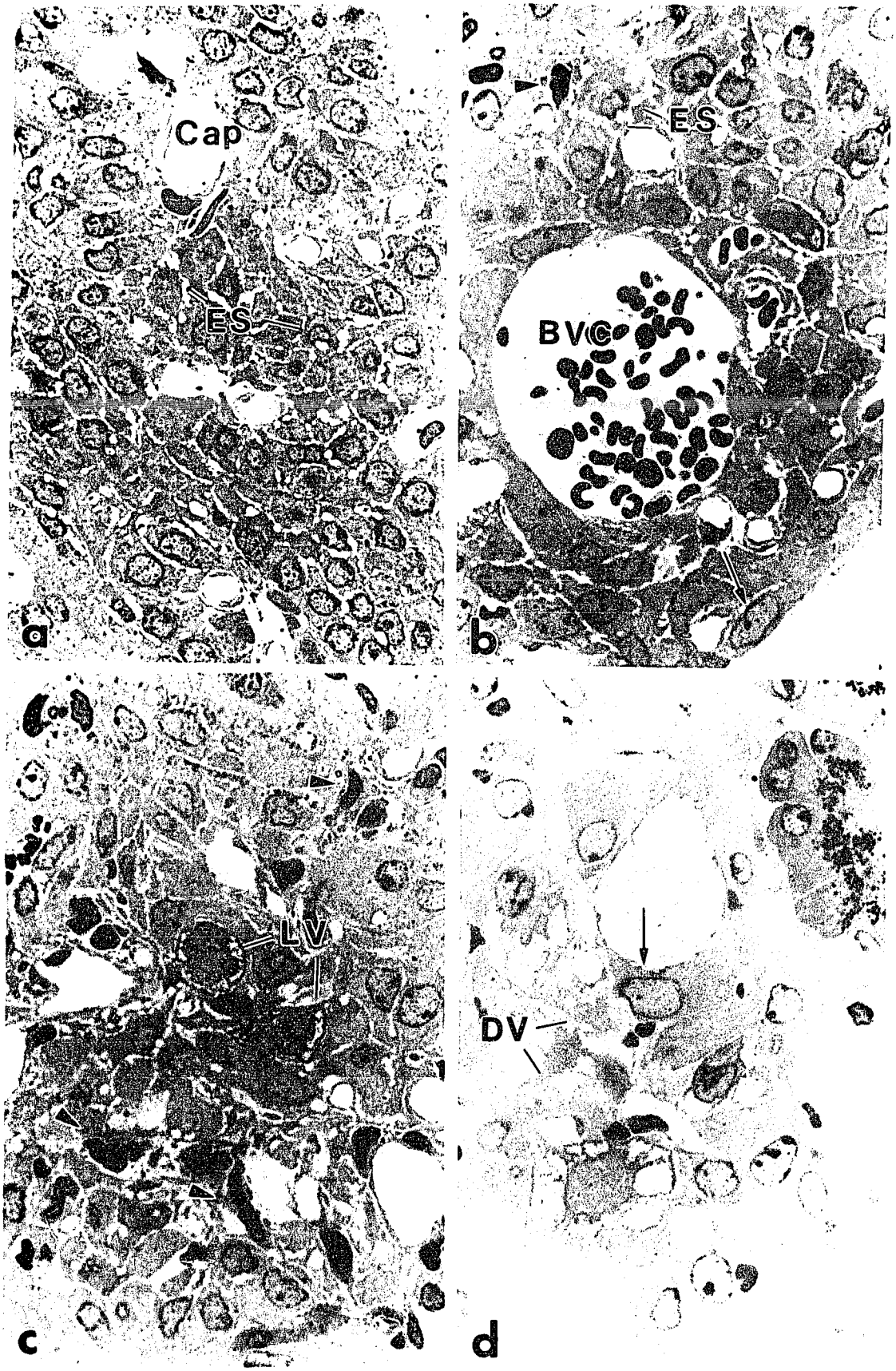
Cap
ES
a
ES
BVC
b
LV
c
DV
d

Figure 15. Margination and Diapedesis of Macrophages through the B-cells (the Wall of the BVCs) in 139H-infected Hamsters.

a. b. and **c.** Pancreatic islets of 139H-infected hamsters at high power (semi-thin section, 820x).

d. Pancreatic islet of a control hamster at high power (semi-thin section, 820x).

Note: the histopathological changes in the islets of Langerhans in the 139H-infected hamsters.

BVC: blood vessel core; DV: diffuse vacuolation; ES: extracellular space; LV: localized vacuolization; cellular hypertrophy and elongation (small arrow); a single macrophage (arrow head).

There are also nuclear pathological changes such as swelling, and changes in shape (small arrow). There are also some nuclei which resemble those of macrophages between the islet cells in the 139H-infected hamsters. The extracellular spaces (ES) are enlarged in the islets of the 139H-infected hamsters compared to the control hamsters. A single macrophage (arrowhead) and several macrophages (double arrowheads) attached to B-cells at the wall of BVC.

We can also see a channel connection between the BVC and the central islet (three medium arrows).

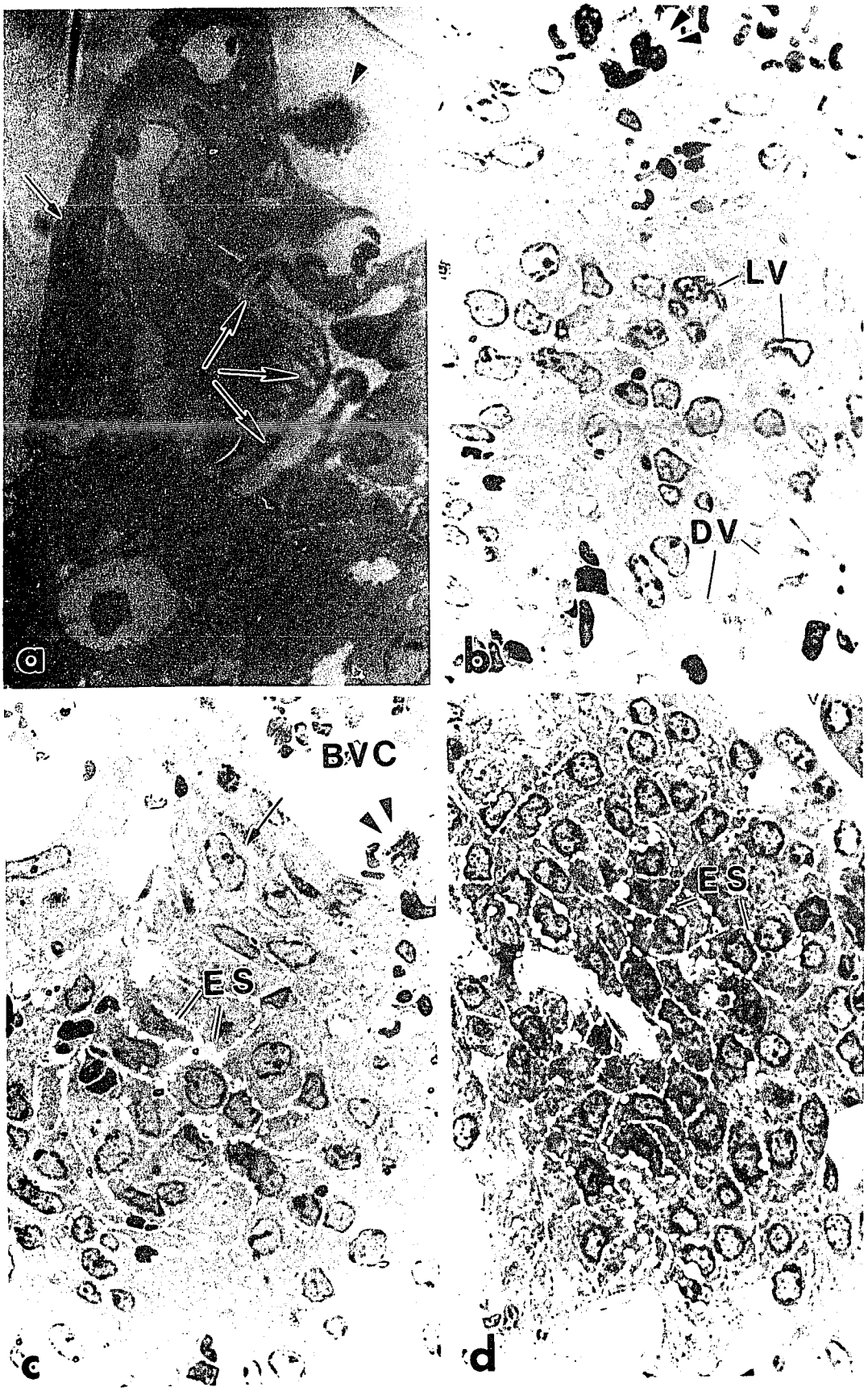
a
LV
DV
b
BVC
ES
c
ES
d

Figure 16. Margination and Diapedesis of Lymphocytes through B-cells (the Wall of the BVCs) in 139H-infected Hamsters.

a. and b. Pancreatic islets of 139H-infected hamsters (H and E stain, 164x).

c. and **d.** Pancreatic islets of 139H-infected hamsters (Gomori's one-step trichrome stain, 382x).

Note: a single lymphocyte (arrowhead); a group of inflammatory cells (small arrow); BVC: blood vessel core; extracellular vacuolization (*); intracellular vacuolization (star).

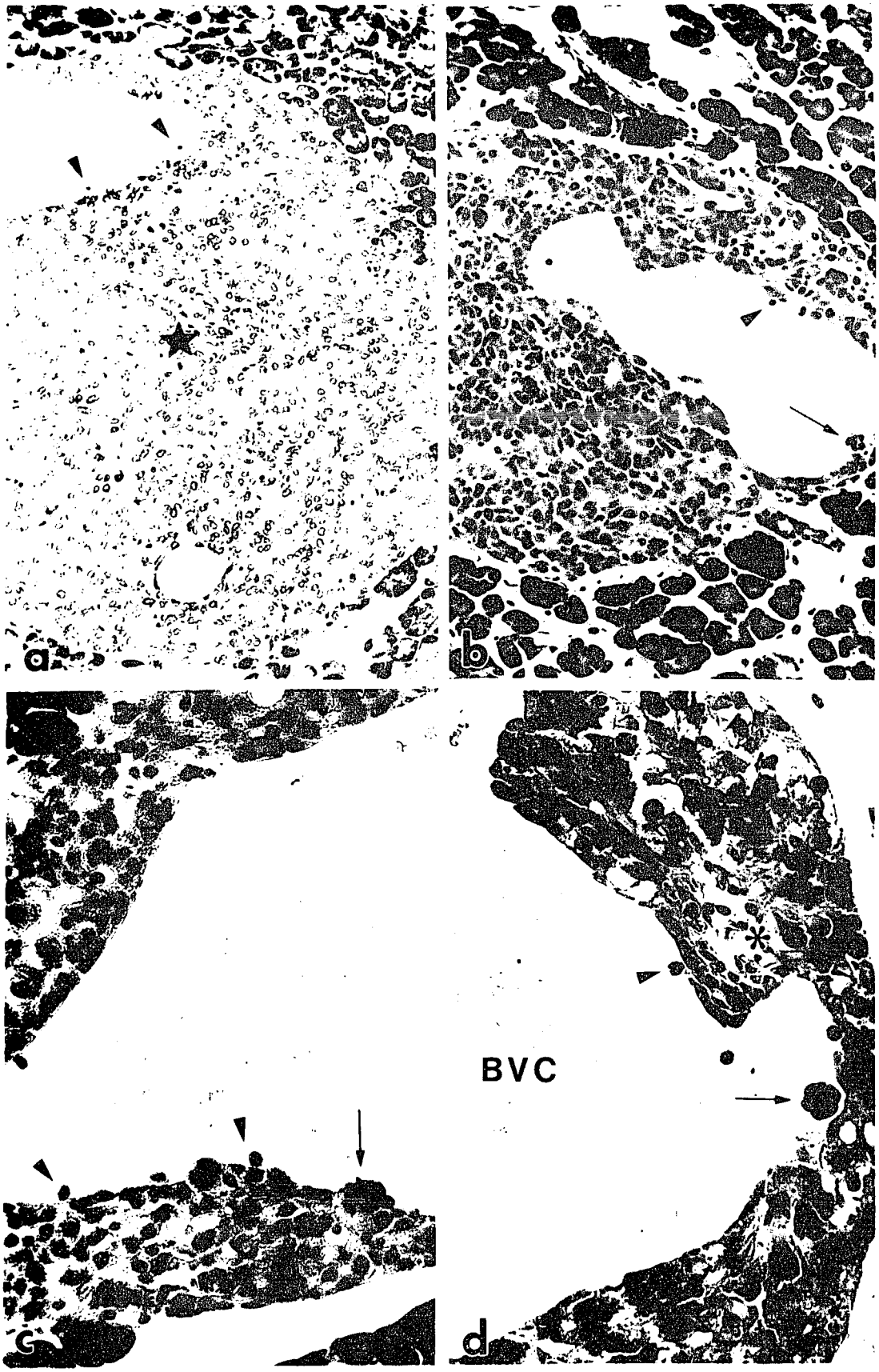
a
b
c
d
BVC

Figure 17. Margination and Diapedesis of a Group of Lymphocytes through B-cells (the Wall of the BVCs) in 139H-infected Hamsters.

Pancreatic islets of 139H-infected hamsters with H and E stain. **a.** 382x; **b.** 164x; **c.** 382x; **d.** 820x.

Note: a group of lymphocytes (medium arrow); extracellular vacuolization (*); BVC: blood vessel core.

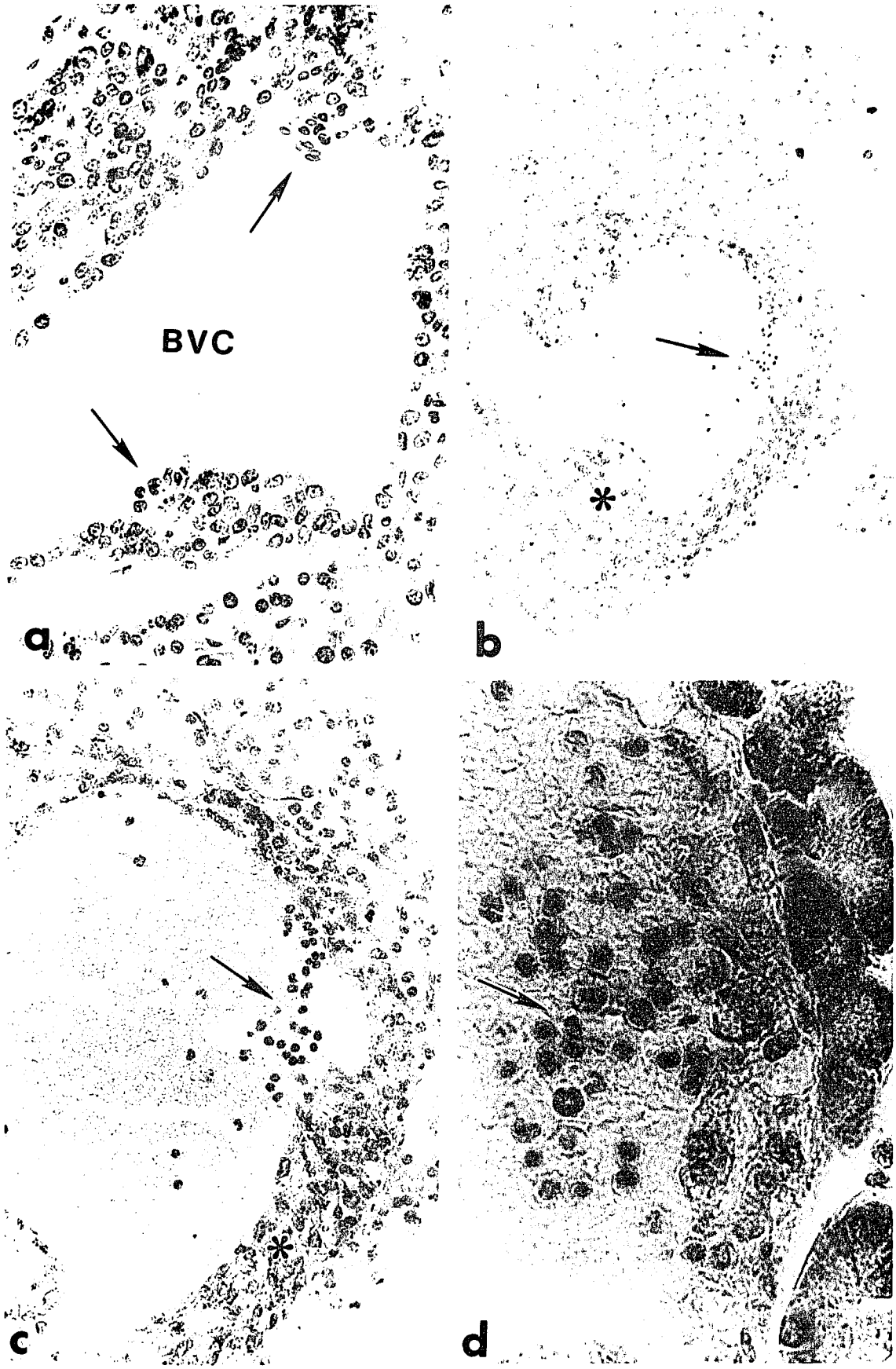
BVC
a
b
c
d

Figure 18. Margination and Diapedesis of Groups of Mixed Lymphocytes and Macrophages or Neutrophils through B-cells (the wall of the BVCs) in 139H-infected Hamsters.

a. and b. Pancreatic islets of 139H-infected hamsters (Gomori' one step trichrome stain, 820x).

c. Pancreatic islet of a 139H-infected hamster (H and E stain, 820x).

d. Pancreatic islet of a 139H-infected hamster (insulin immunostain, 820x).

Note: a group of mixed lymphocytes and macrophages or neutrophils (small arrow); extracellular vacuolization (*); ir-In: immunoreactive insulin; BVC: blood vessel core.

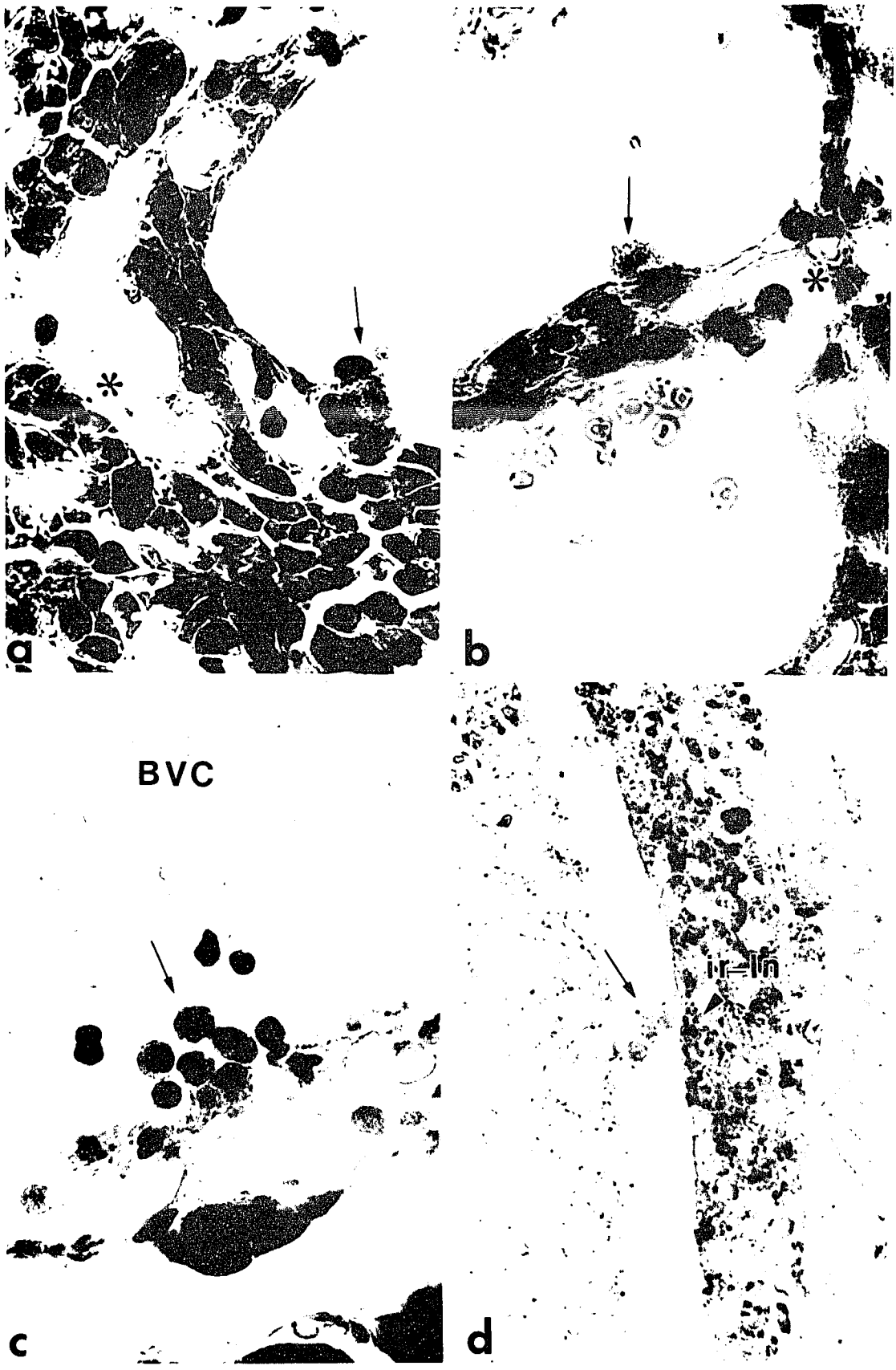
a
b
BVC
c
d
ir-lm

Figure 19. Margination and Diapedesis of a Group of Two or More Inflammatory Cells through B-cells (the Wall of the BVCs) in 139H-infected Hamsters.

a. b. and **c.** Pancreatic islets of 139H-infected hamsters at high power (semi-thin section, 820x). Note: margination of a group of macrophages.

d. Pancreatic islet of a 139H-infected hamster at high power (H and E stain, 820x).

e. Pancreatic islet of a 139H-infected hamster at high power (H and E stain, 382x).

f. g. h. i. and **j.** Pancreatic islets of 139H-infected hamsters at high power (H and E stain, 820x). Note: groups of inflammatory cells, some of them form a ball shape like structure inside the islets (medium arrow); BVC: blood vessel core.

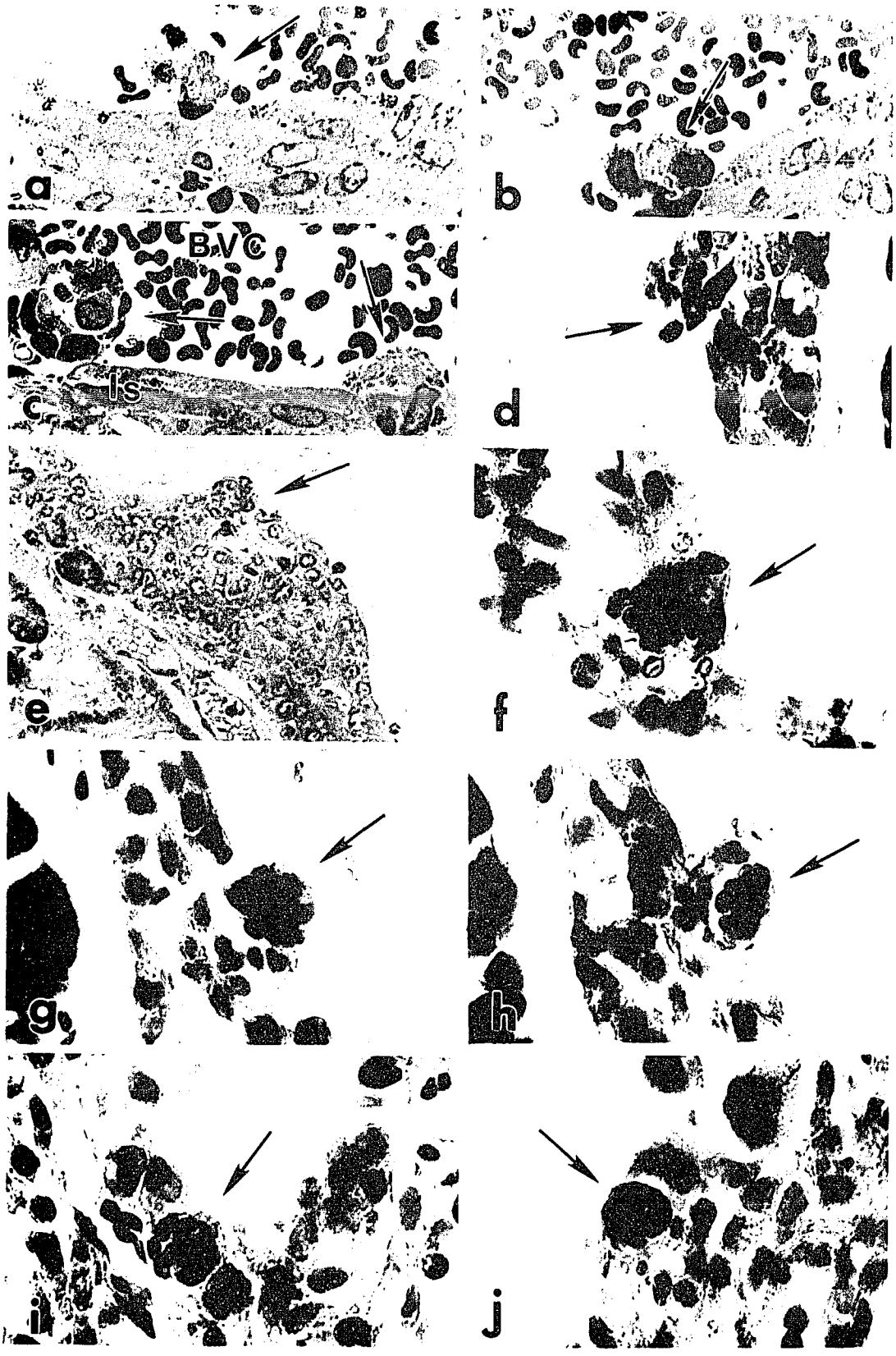
a
b
B.V.
c
ls
d
e
f
g
h
i
j

D. Experiment Four: Light Microscopy Study of the Pathological Changes in the Pituitaries and Adrenal Glands in 139H-infected Hamsters

As shown in Figures 20, 21 and 22, the 139H-infected hamsters showed extensive extracellular vacuolization (EV) in the pituitary. Most vacuoles were located on the ventral and/or ventrolateral parts of the pars distalis. There was comparatively little vacuolization in 263K-infected hamsters (Figures 22b and 22d).

As shown in Figures 20, 21 and 22, the pituitaries of 139H-infected hamsters also showed cellular hypertrophy, cellular atrophy, and cytoplasmic vesicles. There were nuclear pathological changes such as swelling, vesicular changes, pyknosis, karyorrhexis and karyolysis. The cellular and nuclear pathological changes were most pronounced in the regions with vacuolation.

As shown in Figure 23, using PAS and orange G stain, I noted an abnormal PAS positive substance in grape-like or plaque-like forms located in the pituitary in the 139H-infected hamsters but not in the control hamsters.

As shown in Figure 24, I observed similar PAS positive substance in grape-like or plaque-like form in the adrenal medulla and blood stream in the 139H-infected hamsters but not in the control hamsters. This substance was located both inside and outside the cells in the endocrine organs. I have referred to this PAS positive substance as "PPS".

Figure 20. Hematoxylin and Eosin Stain of Pituitaries.

a. Pars distalis of the pituitary of a control hamster (244x) shows the normal structure.

b. c. and **d.** Pars distalis of the pituitaries of 139H-infected hamsters (244x) show extensive EV (*).

Note: most vacuoles (*) are located on the ventral and/or ventrolateral parts of the pars distalis (PD) in the 139H-infected hamsters. Pituitaries of 139H-infected hamsters show cellular hypertrophy (small arrow).

There are nuclear pathological changes such as swelling, ring-form changes (arrowhead); vesicular changes, pyknosis, karyorrhexis and karyolysis (arrowhead) in the 139H-infected hamsters. The cellular and nuclear pathological changes are most pronounced in the regions with vacuolation. Si: sinusoid.

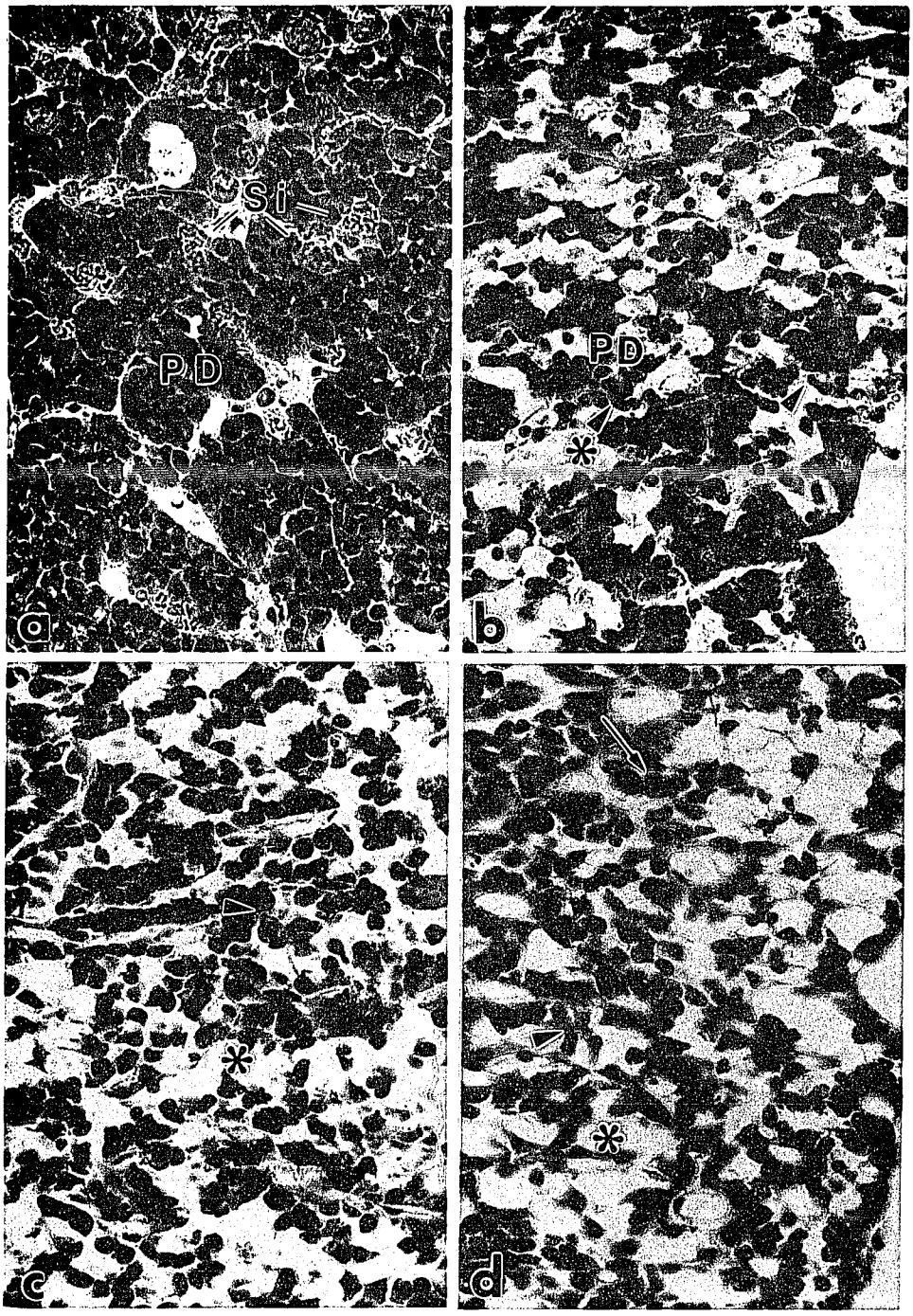
Si
PD
a
PD
b
c
d

Figure 21. Histopathological Changes in the Pituitaries of 139H-infected Hamsters.

a. Pars distalis of the pituitary of a control hamster (164x) shows the normal structure.

b. Pars distalis of the pituitary of a control hamster (328x) shows normal structure.

c. Pars distalis of the pituitary of a 139H-infected hamster (328x).

d. Pars distalis of the pituitary of a 263K-infected hamster (328x).

Note: most vacuoles (EV) (*) are located on the ventral and/or ventrolateral parts of the pars distalis (PD) in the 139H-infected hamsters but not in the 263K-infected or in the control hamsters. PN: pars nervosa, PI: pars intermedia.

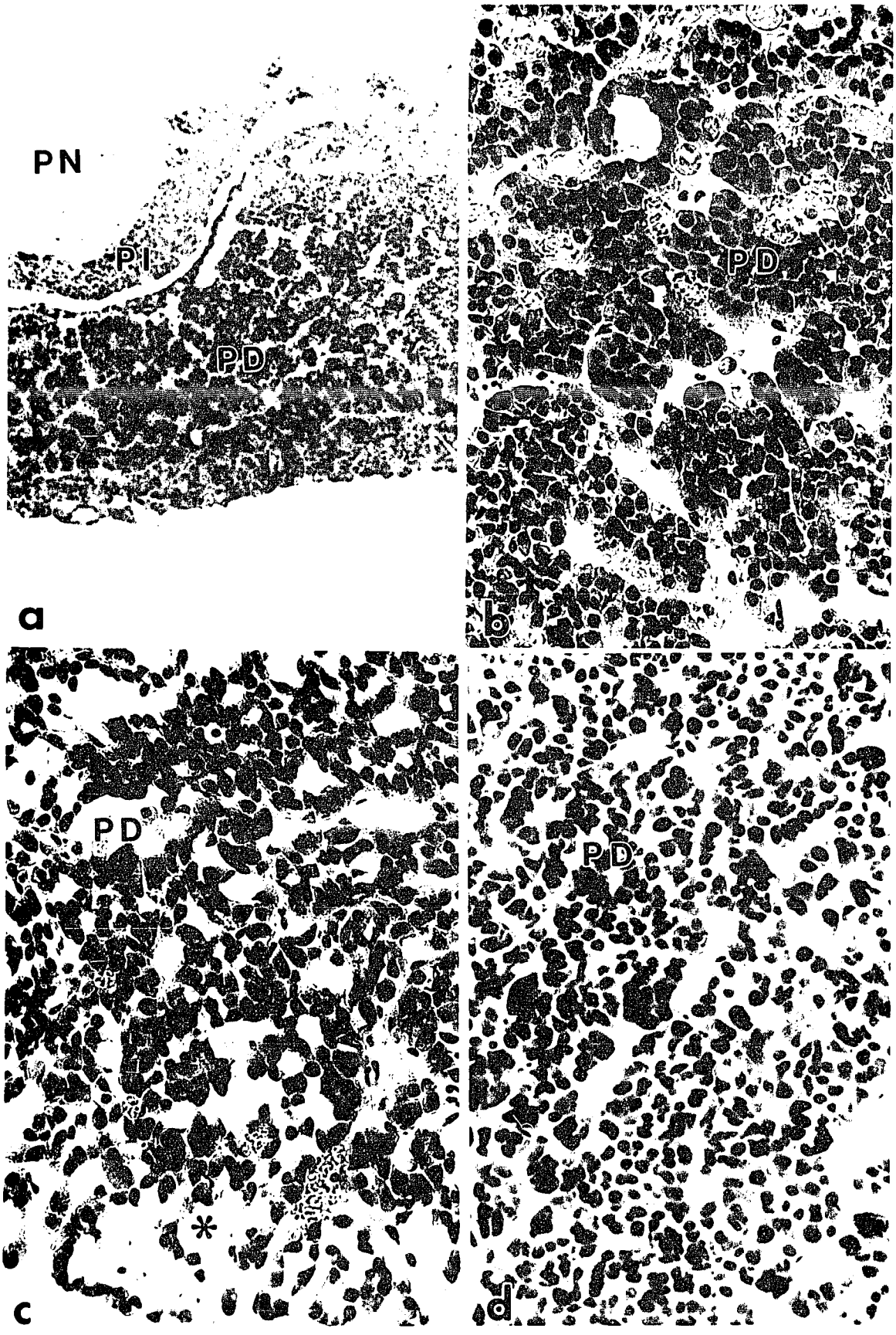
PN
PI
PD
a
PD
b
PD
c
*
PD
d

Figure 22. Comparison of Pituitaries in 139H-infected and 263K-infected Hamsters with Gomori's One-step Trichrome Stain.

Pars distalis of the pituitary of a 139H-infected hamster shows extensive EV in the ventral and/or ventrolateral parts of the pars distalis (*). **a.** (41x), **c.** (82x), **e.** (328x) and **g.** (820x).

Pars distalis of the pituitary of a 263K-infected hamster shows comparatively little vacuolization. **b.** (41x), **d.** (82x), **f.** (328x), **h.** (820x).

Note: PI: pars intermedia, PN: pars nervosa, PD: pars distalis.

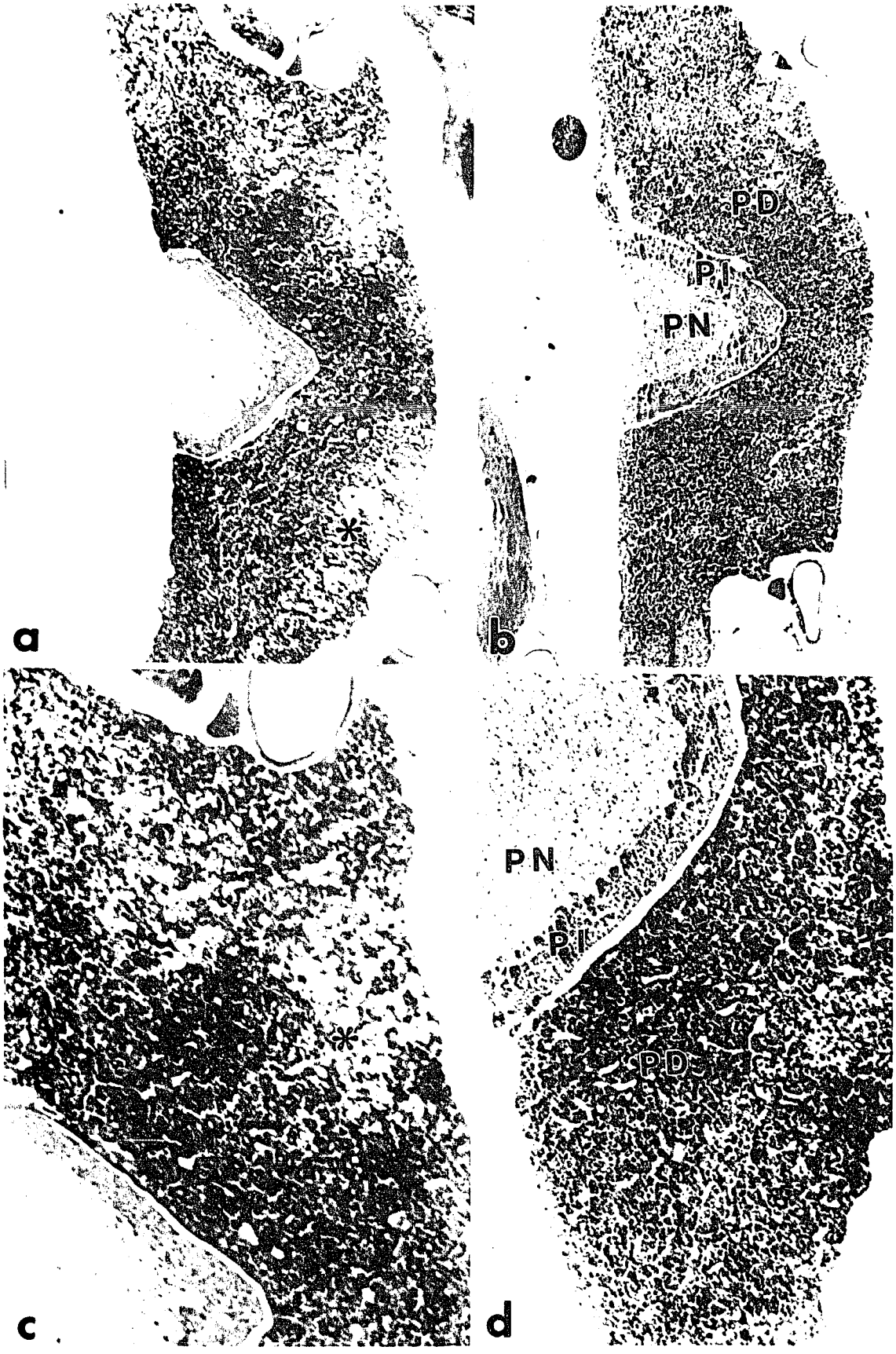
a
b
PD
PI
PN
c
d
PN
PI
PD

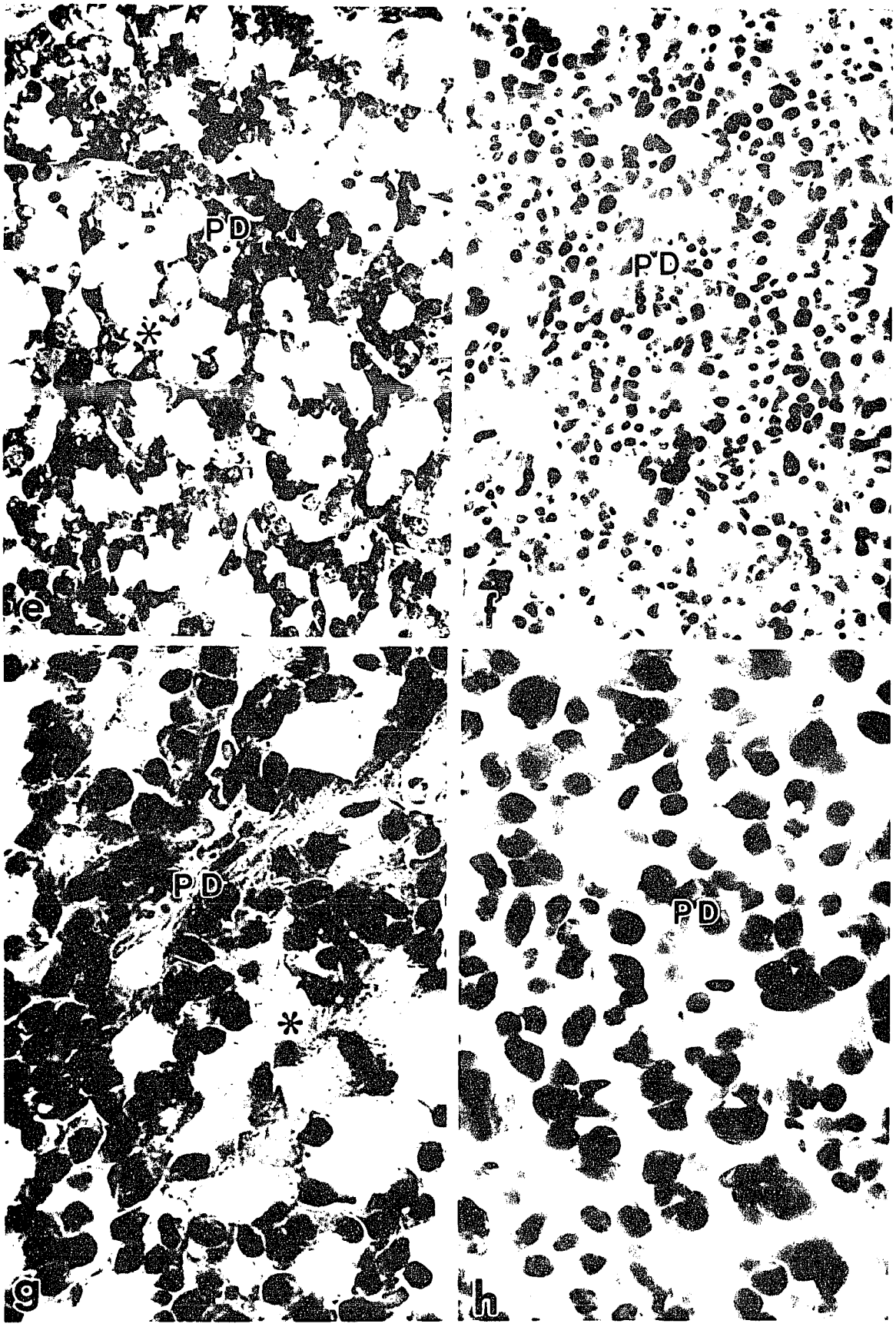
PD
*
e
PD
f
PD
*
g
PD
h

Figure 23. PAS and Orange G Stain of the Pituitaries.

a. Pars distalis of the pituitary of a control hamster (244x) shows the normal structure.

b. Pars distalis of the pituitary of a 139H-infected hamster (244x) shows extensive vacuolization in the ventral and/or ventrolateral parts of the pars distalis (*).

c. Pars distalis of the pituitary of the control hamster (610x) shows the normal structure and no PPS.

d. Pars distalis of the pituitary of the 139H-infected hamster (610x) shows abnormal PAS positive substance, termed PPS (arrowhead). The abnormal PPS in grape-like form is located both inside and outside the cells. Cap: capillary, PD: pars distalis.

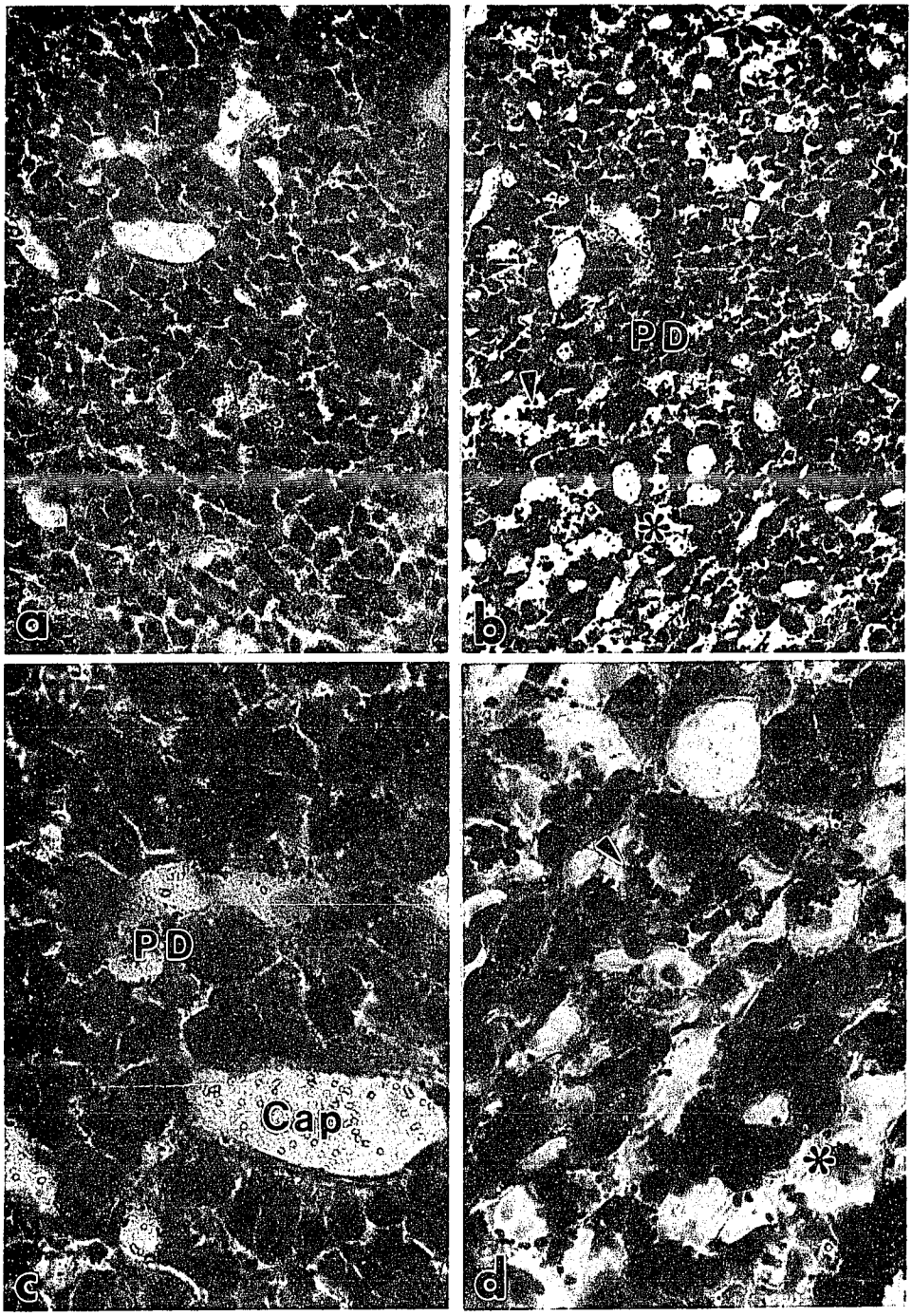
a
b
PD
c
PD
Cap
d

Figure 24. PAS and Orange G Stain of Blood Vessels in Pancreatic Islets and of Adrenal Glands.

a. A blood vessel in the pancreas in a control hamster (244x) shows no PPS in the lumen of the blood vessel.

b. A blood vessel of the pancreas in a 139H-infected hamster (244x) shows abnormal PPS (arrowhead) in the lumen.

c. An adrenal medulla (AM) of a control hamster (610x) shows the normal structure and no PPS.

d. An adrenal medulla of a 139H-infected hamster (610x) shows abnormal PPS in plaque-like form (arrowhead).

Note: PPS is located both inside and outside the cells. BV: blood vessel.

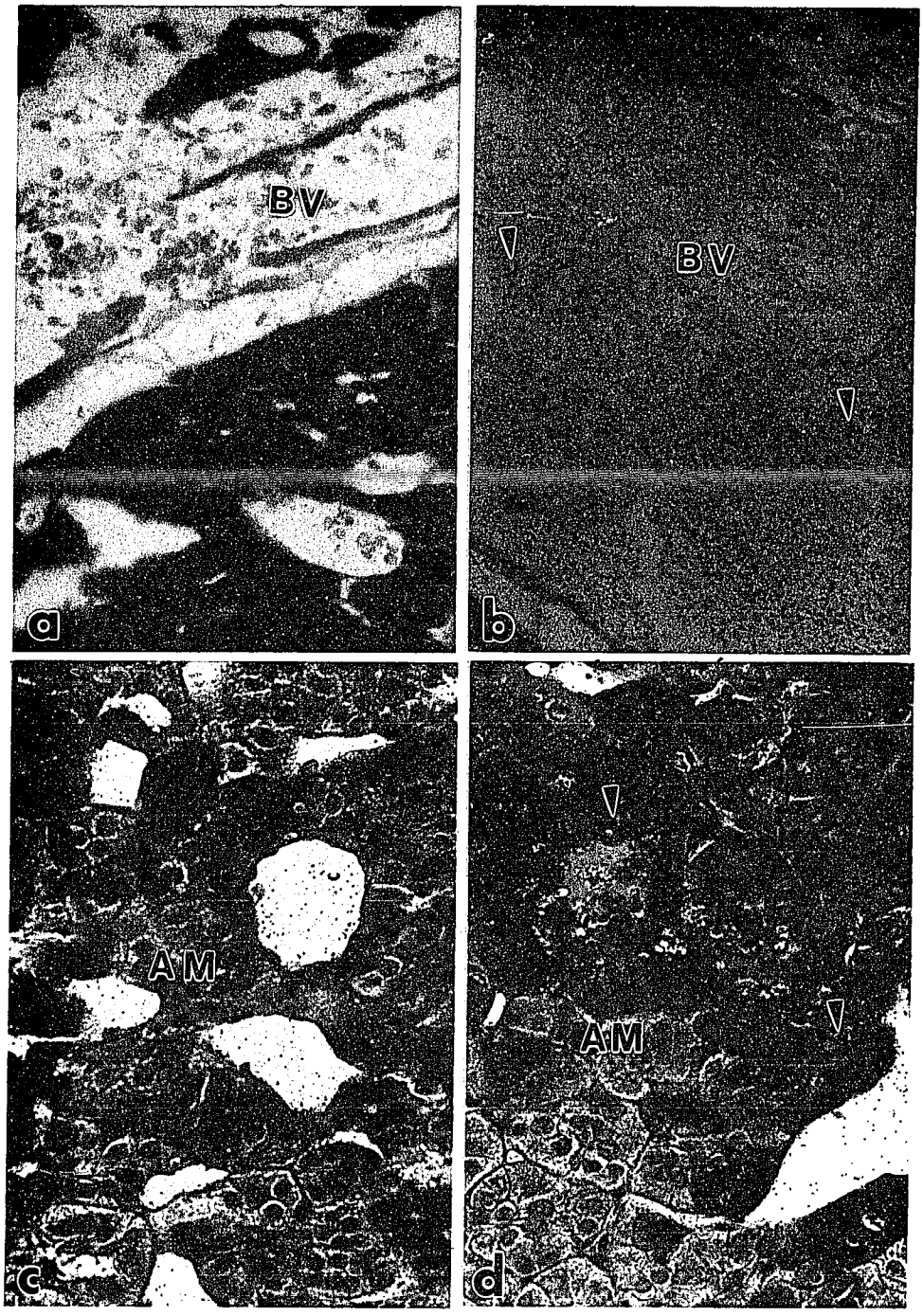
BV
a
BV
b
AM
c
AM
d

E. Experiment Five: Immunostaining Study of the Pathological Changes in the Pituitaries in 139H-infected Hamsters

The results of immunostaining studies of the pathological changes in the pituitaries of 139H-infected hamsters are summarized in Table II. As shown in Figures 25 and 26, the immunostaining patterns of $ACTH_{1-24}$ and $ACTH_{17-39}$ changed dramatically in the pituitaries of 139H-infected hamsters from those in the pituitaries of control animals. The $ACTH_{1-24}$ and $ACTH_{17-39}$ immunostained cells were found in the pars intermedia and pars distalis, but not in the pars nervosa in both control and 139H-infected hamsters. However, I seldom saw $ACTH_{1-24}$ and $ACTH_{17-39}$ immunostained cells in the EV areas of the pars distalis of the 139H-infected hamsters.

As shown in Figure 27, the immunostaining pattern of GH was slightly changed in the pituitaries of 139H-infected hamsters compared to the pituitaries in control animals. GH immunostained cells were mainly found in the pars distalis, a few of them were seen in the pars intermedia and immunostained fibers were seen in the pars nervosa in both the control and the 139H-infected hamsters. GH immunostained cells were low in the ventrolateral area of both control hamsters and 139H-infected hamsters compared to other parts of the pars distalis. Since most of the EV in pituitaries of 139H-infected hamsters was located in the ventrolateral area of the pars distalis, GH immunostained cells might not be affected by the EV. In fact, the GH immunostained area was

slightly larger in 139H-infected hamsters compared to the area in control animals (see Table II).

As shown in Figures 28 and 29, the immunostaining patterns of TSH and PRL were changed but not dramatically in the pituitaries of 139H-infected hamsters compared to the pituitaries in control animals. TSH and PRL immunostained cells were found only in the pars distalis, but not in the pars intermedia nor the pars nervosa of control or 139H-infected hamsters. The number of TSH and PRL immunostained cells was reduced in the vacuolation areas of the pars distalis of 139H-infected hamsters compared to the number in control animals.

Table II. The Results of Immunostaining Studies of the Pituitaries in 139H-infected Hamsters

Immuno-stain	Ino-cula	N	PA (mm^2)	OD	PA%	Max PA%	Min PA%
$ACTH_{17-39}$	NHB	10	0.28 ±0.03	0.30 ±0.02	11.9 ±1.0	17.1	6.2
	139H	11	0.20 ±0.04	0.30 ±0.01	9.6 ±1.6	17.3	2.2
$ACTH_{1-24}$	NHB	11	0.27 ±0.03	0.33 ±0.02	13.1 ±1.3	20.4	6.0
	139H	14	0.23 ±0.03	0.34 ±0.02	11.6 ±1.3	23.3	3.1
GH	NHB	15	0.26 ±0.04	0.27 ±0.02	11.1 ±1.6	24.0	1.8
	139H	13	0.36 ±0.04	0.30 ±0.02	13.0 ±1.7	25.1	6.3
TSH	NHB	15	0.20 ±0.02	0.25 ±0.03	9.0 ±1.1	16.2	0.0
	139H	18	0.22 ±0.02	0.27 ±0.02	9.4 ±0.8	18.6	3.6
PRL	NHB	11	0.23 ±0.06	0.20 ±0.02	10.9 ±3.6	42.8	0.7
	139H	15	0.32 ±0.06	0.19 ±0.02	14.2 ±2.6	30.1	0.6
FSH	NHB	12	0.02 ±.010	0.13 ±0.04	0.9 ±0.4	4.4	0.0
	139H	15	0.02 ±0.01	0.17 ±0.02	1.2 ±0.5	6.3	0.0
LH	NHB	13	0.003 ±0.002	0.03 ±0.02	0.13 ±0.09	1.0	0.0
	139H	14	0.001 ±0.001	0.04 ±0.02	0.04 ±0.03	0.4	0.0

Note abbreviations used: N: number of animals; PA: positively stained area; OD: optical density; PA%: percentage of positively stained area in the section of pars distalis; Max PA%: the maximum PA% in the group; Min PA%: the minimum PA% in the group.

Figure 25. The Immunostaining Patterns of $ACTH_{1-24}$.

a. Pars distalis of the pituitary of a control hamster (82x) shows the normal structure and the immunostaining pattern of $ACTH_{1-24}$.

b. Pars distalis of the pituitary of a 139H-infected hamster (82x) shows the immunostaining pattern and extensive EV (*) in the ventral and/or ventrolateral parts of the pars distalis.

c. Pars distalis of the pituitary of a 139H-infected hamster (164x) shows EV (*).

d. Pars distalis of the pituitary of a 139H-infected hamster (328x) shows EV and ir-$ACTH_{1-24}$ pattern in EV area (*). PI: pars intermedia; PD: pars distalis, Arrowhead shows ir-$ACTH_{1-24}$.

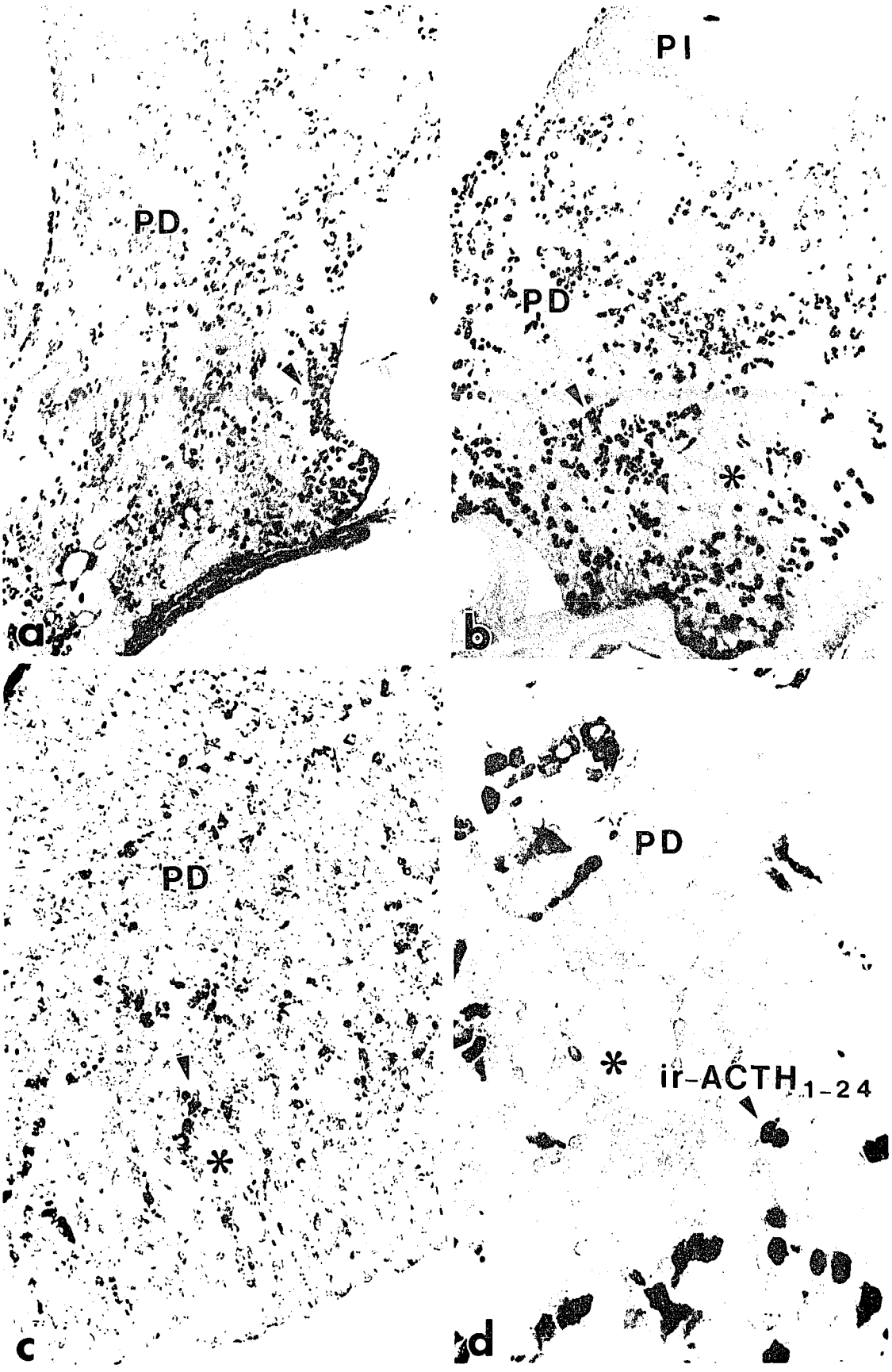
PD
a
PI
PD
b
PD
c
PD
ir-ACTH1-24
d

Figure 26. The Immunostaining Patterns of $ACTH_{17-39}$.

a. Pars distalis of the pituitary of a control hamster (82x) shows the normal structure and the immunostaining pattern of $ACTH_{17-39}$.

b. Pars distalis of the pituitary of a 139H-infected hamster (82x) shows the immunostaining pattern and extensive EV (*) in the ventral and/or ventrolateral parts of the pars distalis.

c. Pars distalis of the pituitary of a 139H-infected hamster (164x) shows EV (*).

d. Pars distalis of the pituitary of a 139H-infected hamster (328x) shows EV and ir-$ACTH_{17-39}$ pattern in EV area (*). PI: pars intermedia; PD: pars distalis, PN: pars nervosa, Arrowhead shows ir-$ACTH_{17-39}$.

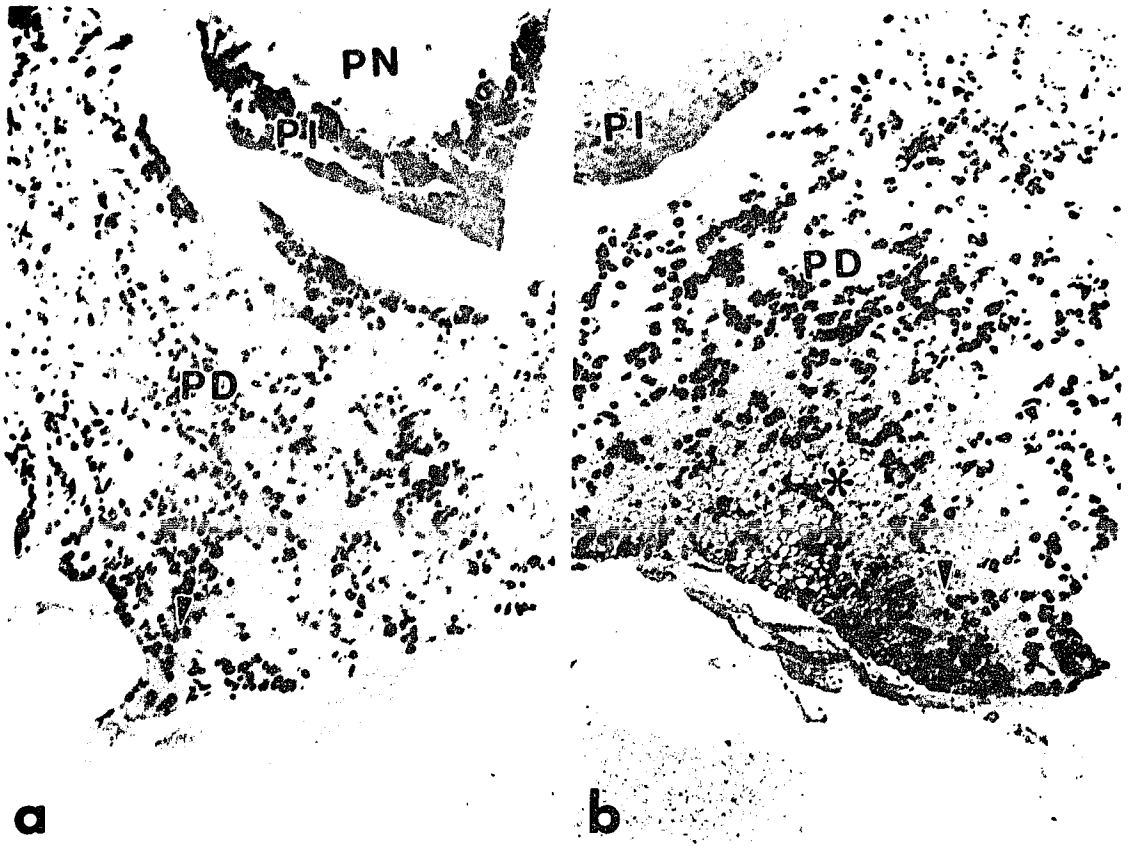
PN
PI
PD
a
PI
PD
b

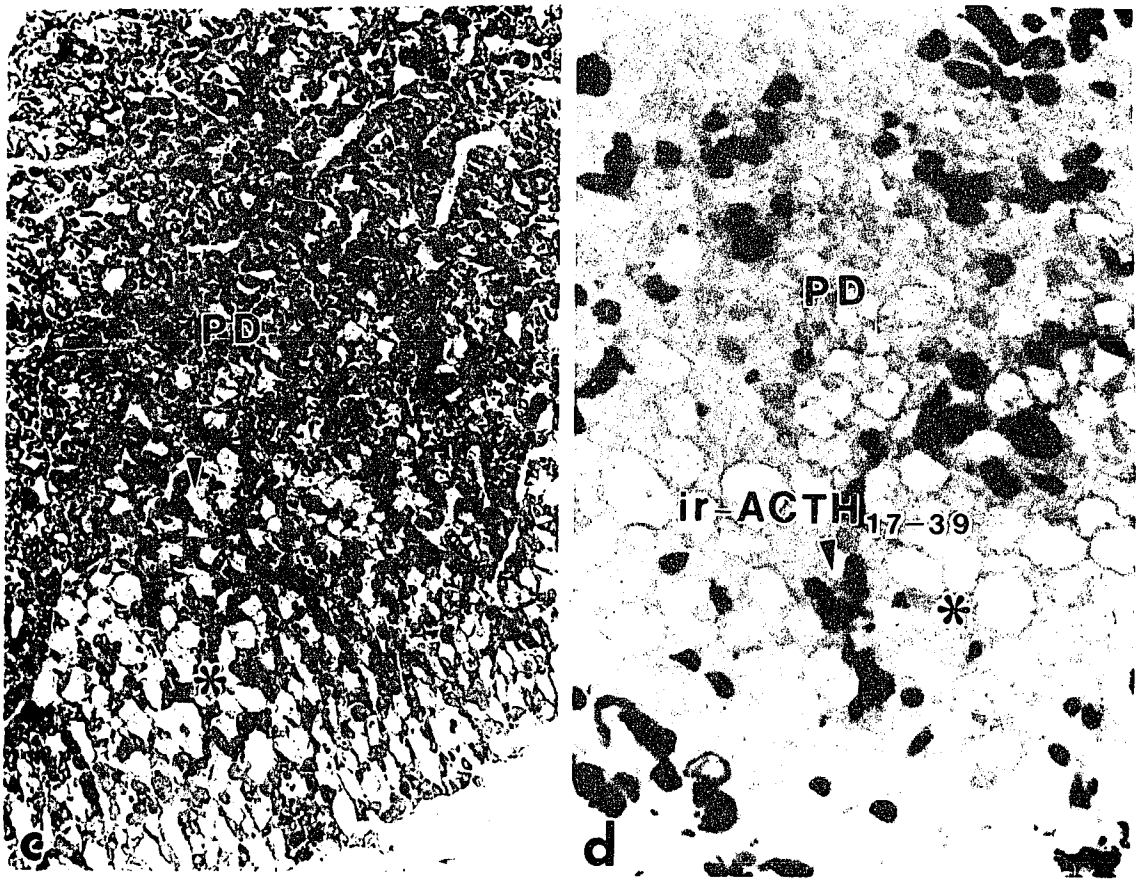
PD
c
PD
ir-ACTH1-39
d

Figure 27. The Immunostaining Patterns of GH.

a. Pars distalis of the pituitary of a control hamster (82x) shows the normal structure and the immunostaining pattern of GH.

b. Pars distalis of the pituitary of a 139H-infected hamster (164x) shows the immunostaining pattern and extensive EV (*) in the ventral and/or ventrolateral parts of the pars distalis.

c. Pars distalis of the pituitary of a control hamster (164x) shows the normal structure and the immunostaining pattern.

d. Pars distalis of the pituitary of a 139H-infected hamster (164x) shows EV and ir-GH pattern in EV area (*). PN: pars nervosa; PI: pars intermedia; PD: pars distalis, Arrowhead shows ir-GH.

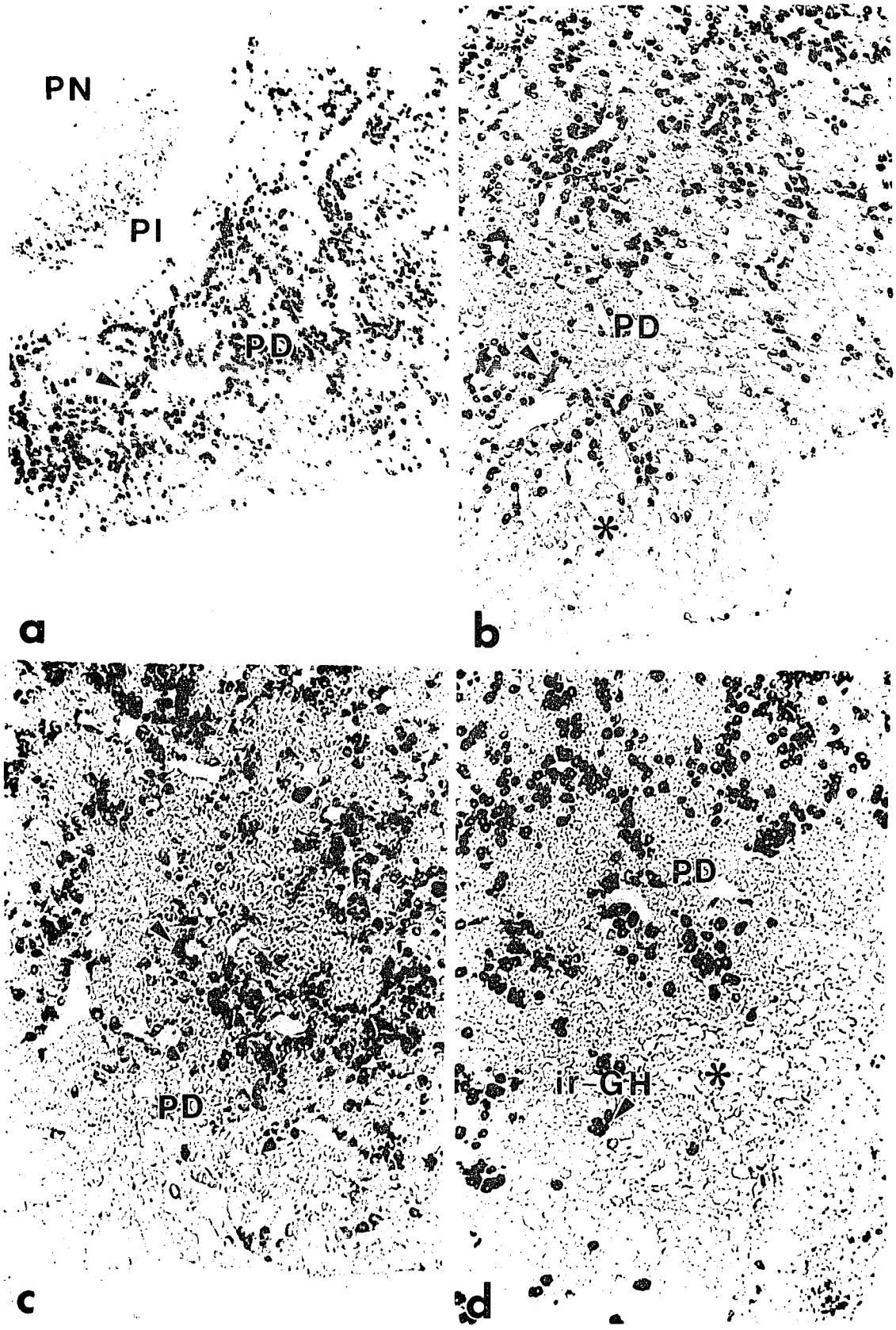
PN
PI
PD
a
PD
b
PD
c
PD
ir-GH
d

Figure 28. The Immunostaining Patterns of TSH.

a. Pars distalis of the pituitary of a control hamster (82x) shows the normal structure and the immunostaining pattern of TSH.

b. Pars distalis of the pituitary of a 139H-infected hamster (82x) shows the immunostaining pattern and extensive EV (*) in the ventral and/or ventrolateral parts of the pars distalis.

c. Pars distalis of the pituitary of a 139H-infected hamster (164x) shows EV.

d. Pars distalis of the pituitary of a 139H-infected hamster (164x) shows EV and ir-TSH pattern in EV area (*). PI: pars intermedia; PD: pars distalis, Arrowhead shows ir-TSH.

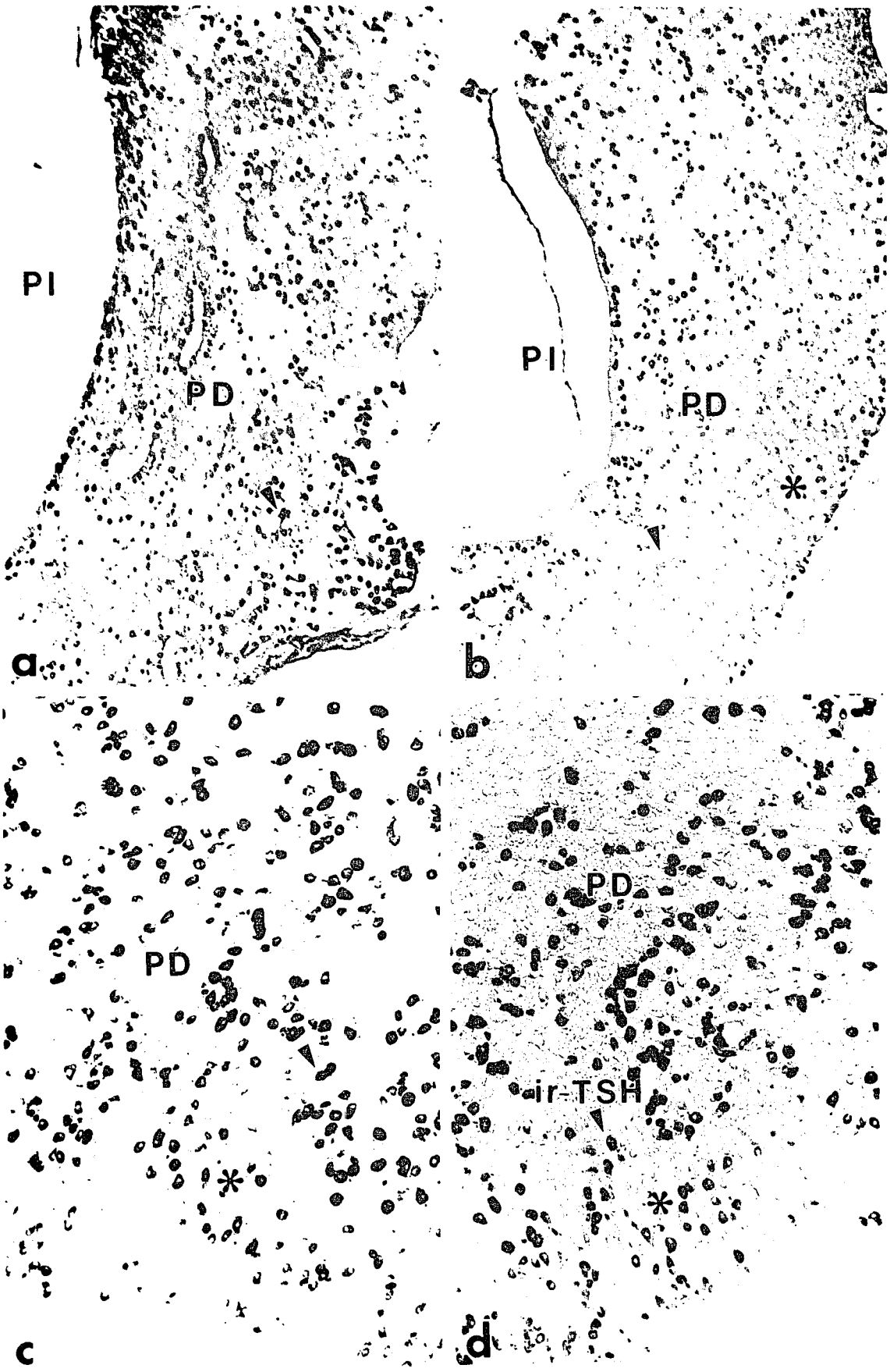
PI
PD
a
PI
PD
b
PD
c
PD
ir-TSH
d

Figure 29. The Immunostaining Patterns of PRL.

a. Pars distalis of the pituitary of a control hamster (82x) shows the normal structure and the immunostaining pattern of PRL.

b. Pars distalis of the pituitary of a 139H-infected hamster (82x) shows the immunostaining pattern and extensive EV (*) in the ventral and/or ventrolateral parts of the pars distalis.

c. Pars distalis of the pituitary of a 139H-infected hamster (328x) shows EV.

d. Pars distalis of the pituitary of a 139H-infected hamster (328x) shows EV and ir-PRL pattern in EV area (*). PI: pars intermedia; PD: pars distalis, Arrowhead shows ir-PRL.

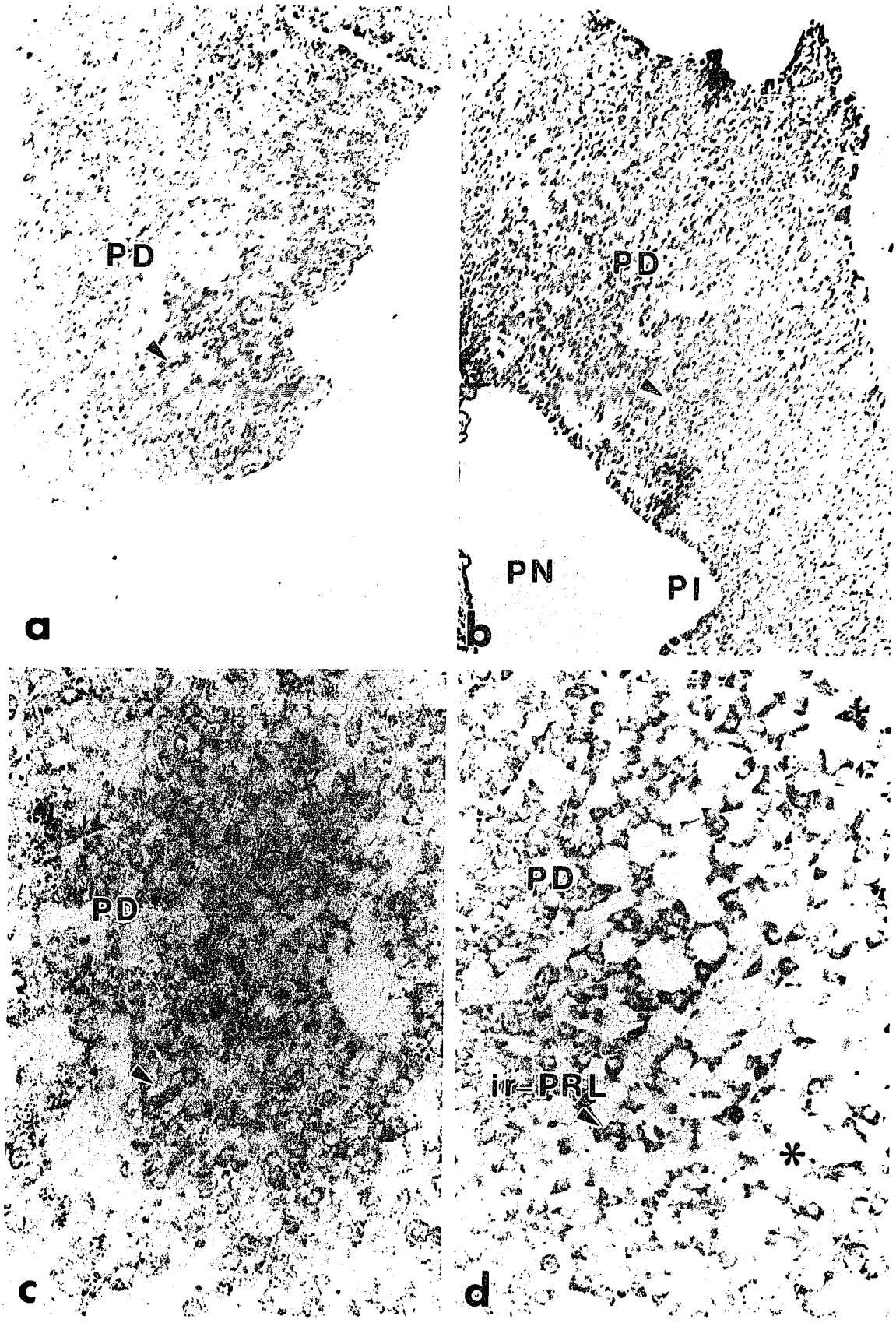
PD
a
PD
PN
PI
b
PD
c
PD
ir-PRL
*
d

F. Experiment Six: Immunostaining of Hypothalamus with Anti-CRF and Anti-VP

The immunostaining study of the hypothalamus with anti-CRF is shown in Figures 30 - 32. As shown in Figure 30, there was a significant increase in the number of CRF immunostained neurons in 139H-infected hamsters (19.4±3.3 neurons/per section) in comparison to that of the control animals (7.5±1.9 neurons/per section). Figure 31 showes the CRF stained cells vs. the atlas number. At present there is no atlas of a hamster brain, so in my studies, I used the atlas of a mouse brain as reference (Sidman et al., 1971) since the major structures of mouse brains are similar to those of hamster brains. We can see that the curve of CRF stained cells in the 139H-infected hamsters is higher than that in the control animals. There is a peak in atlas number 30 which indicates that the number of CRF immunostained neurons in the preoptic area of the 139H-infected hamsters has increased as compared to those in the control animals (see Figure 32). This difference is evident in comparisons of computer-reconstructions of the CRF neuron populations (Figure 33).

The immunostaining study of hypothalamus with anti-VP is shown in Figures 34-42. As shown in Figure 34, there was a significant decrease in the area of ir-VP in the lateral hypothalamus (LHy) of the 139H-infected hamsters (2542.7±481.1 μm^2/per section) compared with that in the control animals

(5273.3±1211.7 μm^2/per section). Figure 35 shows the VP immunostained area in the LHy vs. the atlas number. We can see that the curve of the VP immunostained area in the LHy of 139H-infected hamsters is lower than that of the control animals; there is a peak in atlas numbers 34-36 of the control animals, but not in the 139H-infected hamsters. This indicates that the VP immunostained area in LHy of the 139H-infected hamsters has decreased in comparison to the level found in the control animals (see Figure 39).

As shown in Figure 36, there was no significant difference in the area of ir-VP in dorsomedial hypothalamus (DMH) of the 139H-infected hamsters (7669.4±1800.1 μm^2/per section) compared to those in the control animals (7997±1949.1 μm^2/per section). Figure 37 shows the VP immunostained area in the DMH vs. the atlas number. We can see the curve of the ir-VP area in DMH of the 139H-infected hamsters is almost the same as that of the control animals. There is a shift of the peaks to the left in the 139H-infected hamsters compared to that of the control animals, but the curve pattern is almost the same in both the control and the scrapie hamsters.

Figure 38 shows the outlines of the position of the VP immunoreactive neuronal cell bodies in SON region. There was no significant difference in the number of ir-VP in supraoptic hypothalamus (SON) of the 139H-infected hamsters (14.4±0.317/per section) compared to those in the control animals (14.7±0.2242/per section).

Figure 39 shows the immunostained VP cells in the LHy, DMH and SON regions.

Figures 40, 41 and 42 are the three dimensional reconstruction of VP immunostained neurons in the LHy, DMH and SON, respectively. As shown in Figure 40, the population of VP immunostained neurons was less in the 139H-infected hamsters than that in the control hamsters. As shown in Figure 41, the total number of the VP immunostained neurons in DMH region was not changed significantly, but the population of VP immunostained neurons shifted from caudal to rostral in the 139H-infected hamsters. As shown in Figure 42, there was no significantly changes in VP immunostained neurons in the SON region in the 139H-infected hamsters compared to that in the control hamsters.

Figures 43 shows the CRF or the VP immunostained neurons in both the control and the 139H-infected groups simultaneously.

Figure 44 shows the VP immunostained neurons in the three regions (LHy, DMH and SON) simultaneously in control or 139H-infected hamsters.

Figure 30. CRF Positively Stained Cell Count Comparison in Hy Region.

Note: there was a significant increase in the number of CRF immunostained neurons in the 139H-infected hamsters (19.4±3.3 neurons/per section, N=10) compared with the control animals (7.5±1.9 neurons/per section, N=10).

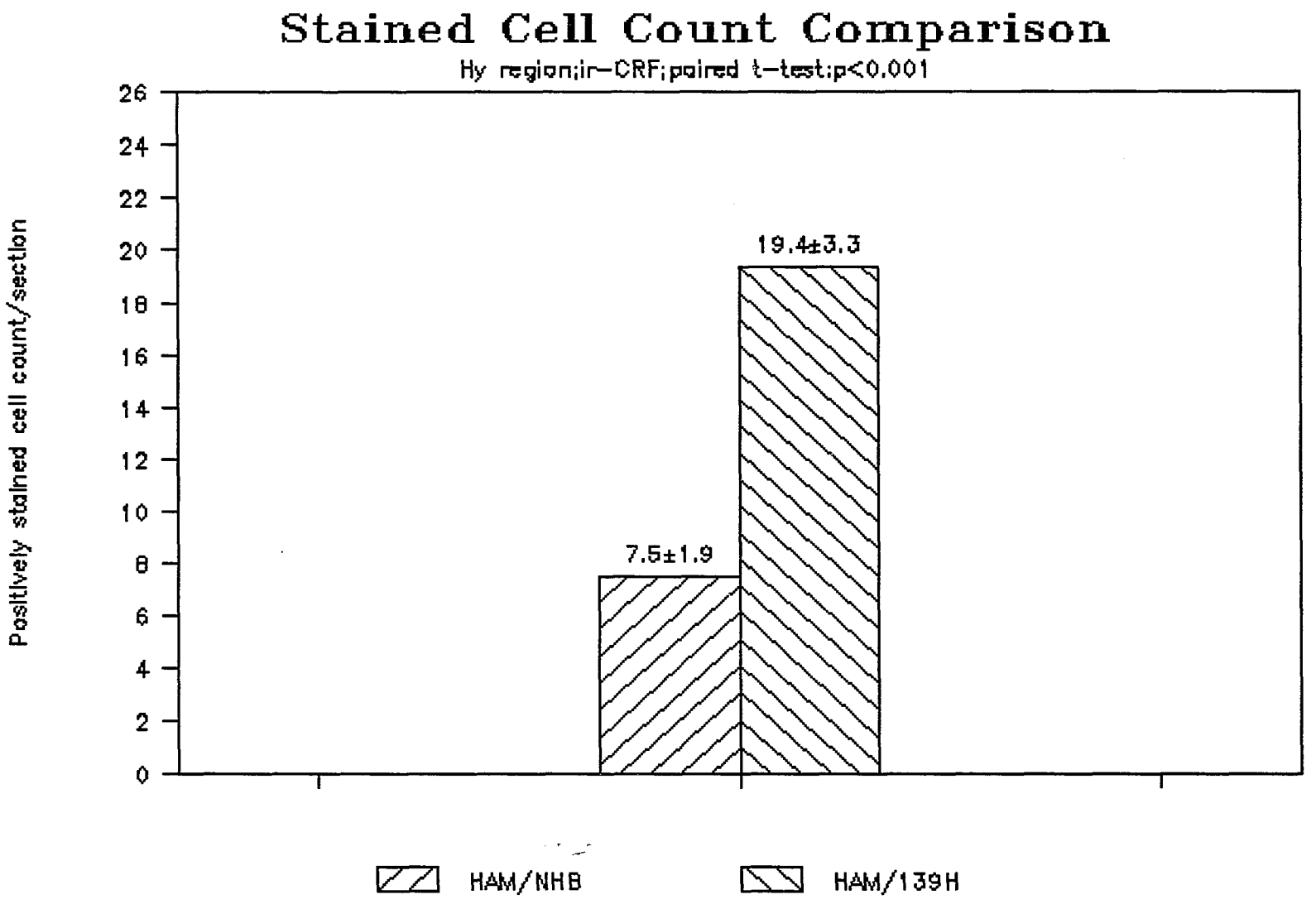
Stained Cell Count Comparison
Hy region;ir-CRF;paired t-test;p<0.001
Positively stained cell count/section
26
24
22
20
18
16
14
12
10
8
6
4
2
0
19.4±3.3
7.5±1.9
HAM/NHB
HAM/139H

Figure 31. CRF Stained Cells vs. Atlas Number.

The number of CRF immunopositive neuronal cell bodies are plotted for each coronal level, from rostral to caudal.

Note: the curve of the CRF stained cells in the 139H-infected hamsters is higher than that of the control animals. There are three peaks from atlas number 24 to 37 which indicate that the number of CRF immunostained neurons in the preoptic area of the 139H-infected hamsters (N=10) has increased in comparison to those in the control animals (N=10).

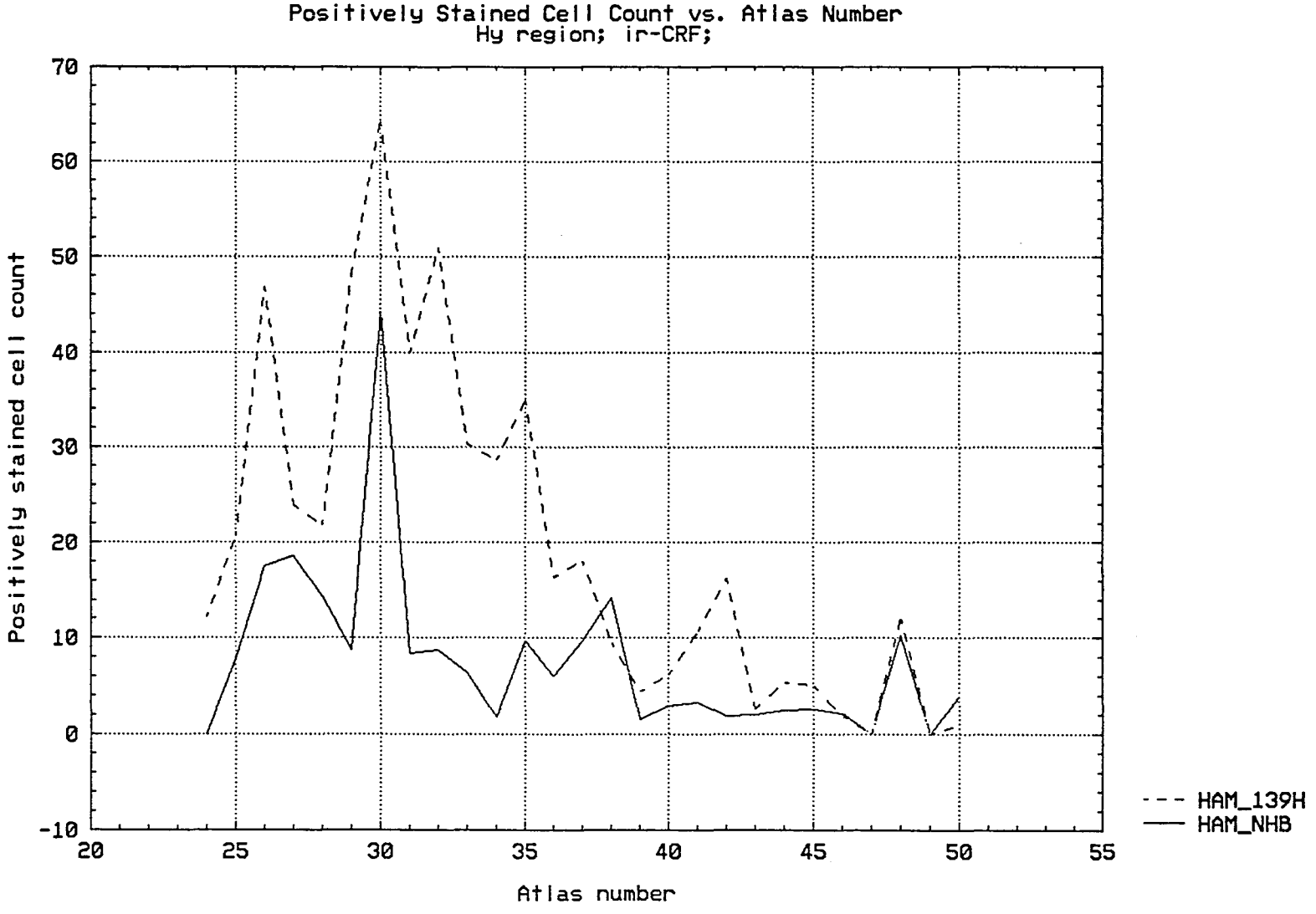
Positively Stained Cell Count vs. Atlas Number
Hy region; ir-CRF;
Positively stained cell count
70
60
50
40
30
20
10
0
-10
20
25
30
35
40
45
50
55
Atlas number
HAM_139H
HAM_NHB

Figure 32. Immunostained CRF Cells in PON Region.

a. Immunostained CRF cells in the PON region in a control hamster at low power (82x).

b. Immunostained CRF cells in the PON region in a 139H-infected hamster at low power (82x).

c. Immunostained CRF cells in the PON region in the control hamster at high power (164x). PON: preoptic nucleus; CA: commissura anterior, pars anterior; Arrowhead shows ir-CRF cells.

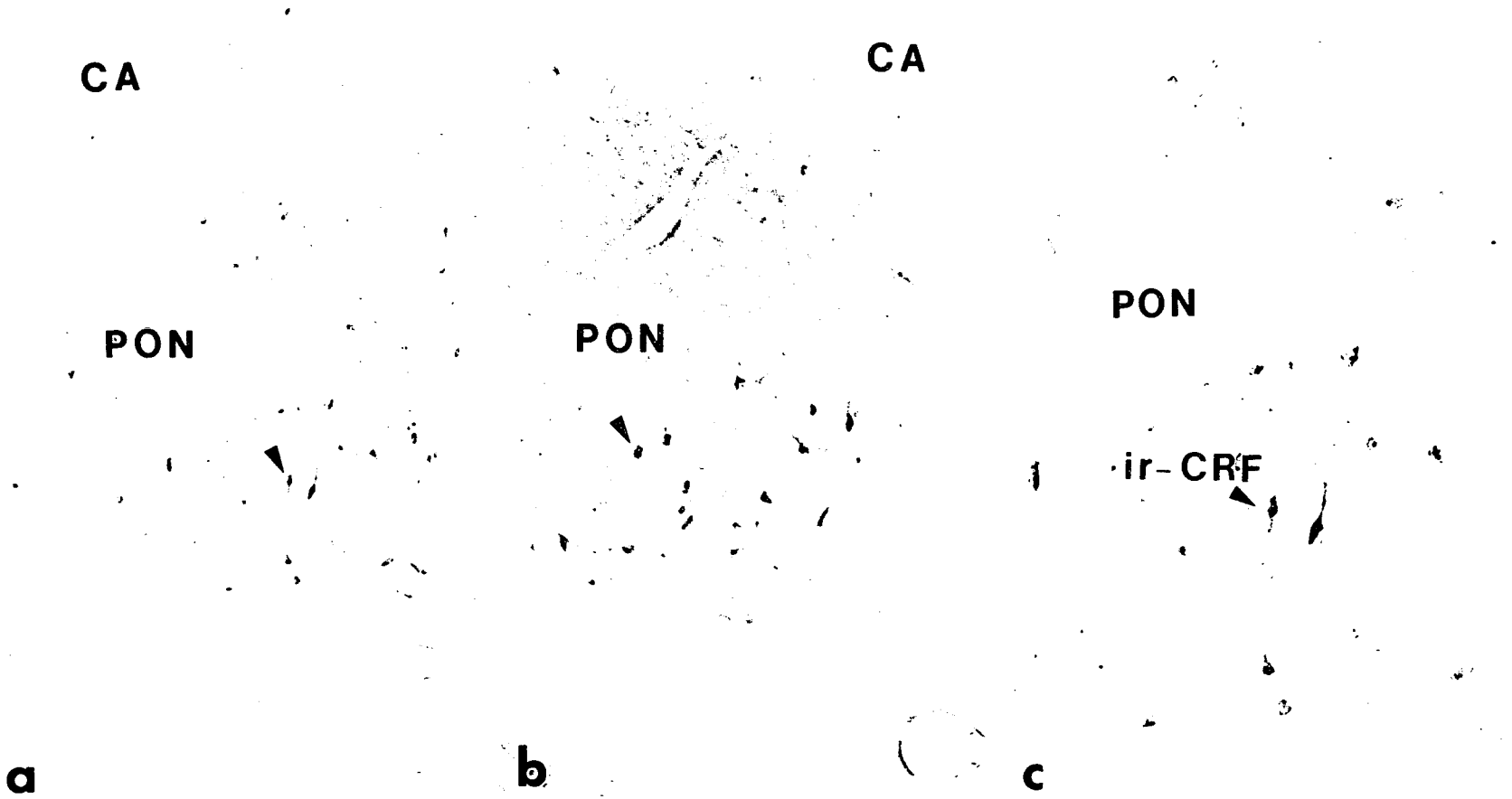
CA
PON
a
CA
PON
b
PON
ir-CRF
c

Figure 33. Three-dimensional Reconstruction of Hypothalamic CRF Immunostained Neurons.

Three-dimensional models of CRF immunostained neurons in the brains of control and 139H-infected hamsters were reconstructed from eight outlines of coronal sections. The models are viewed from a 60 degree rotation about the y axis; rostral, (left); caudal, (right). The cortexes are transparent so that interior structures and the CRF immunostained neurons can be viewed. The right edge of the cortex is colored white. The left edge of the cortex is colored blue. One part of the ventricles (from atlas number 24) and the part of the commissura anterior, pars anterior (from atlas number 24) are colored white. The other parts of ventricles (from atlas numbers 36 and 45) are colored blue. The average population of hypothalamic CRF immunostained neurons in the group of animals (N=10) is colored yellow. **a.** control. **b.** 139H-infected. Note: the population of hypothalamic CRF immunostained neurons was increased in 139H-infected hamsters.

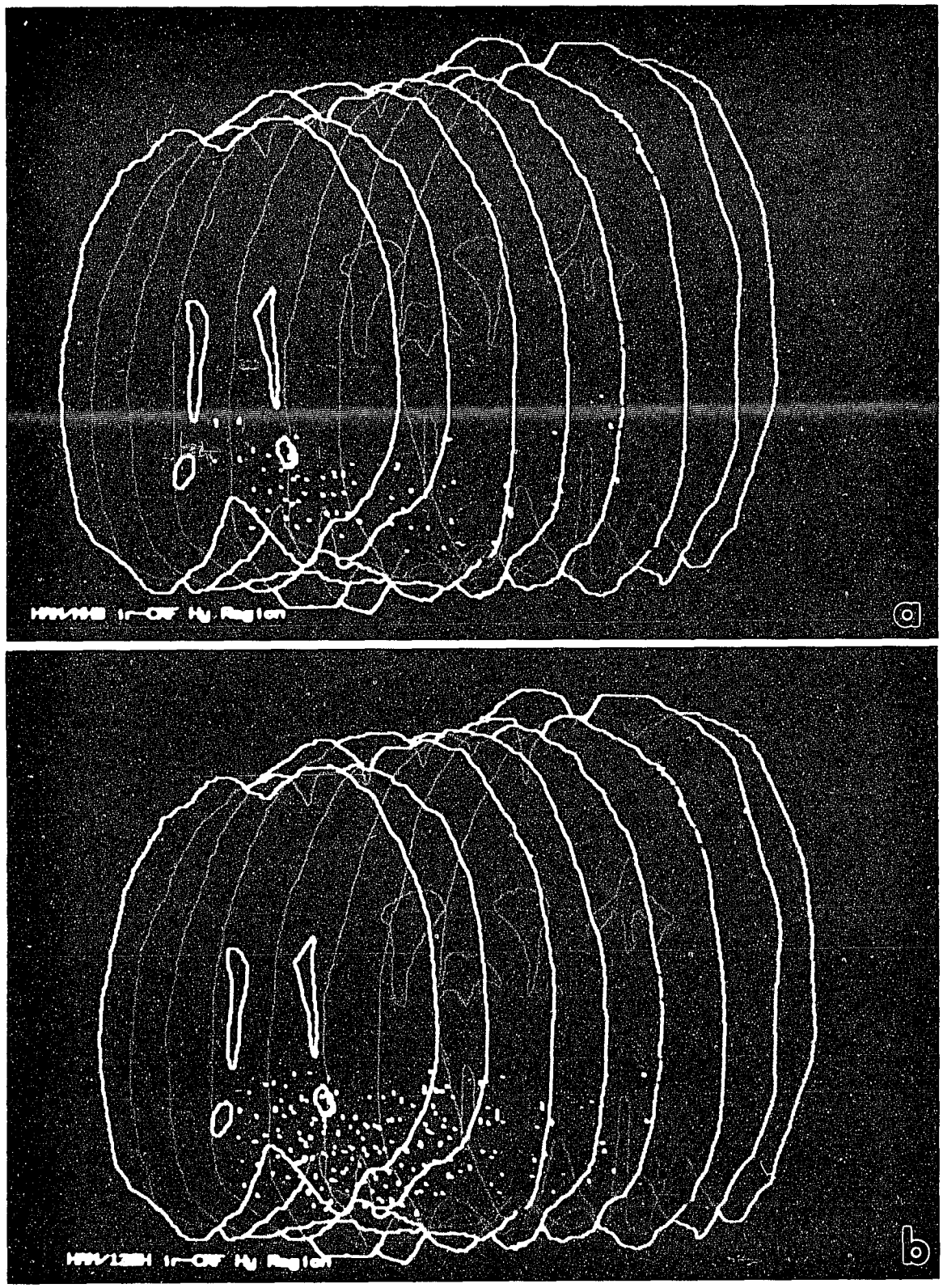
a
b

Figure 34. Comparison of VP Positively Stained Cell Area in LHy Region.

Note: there is a significant decrease in the area of VP immunostained neurons in LHy of the 139H-infected hamsters (2542.7 ± 481.1 μm^2/per section, N=10) in comparison to the control animals (5273.3 ± 1211.7 μm^2/per section, N=10).

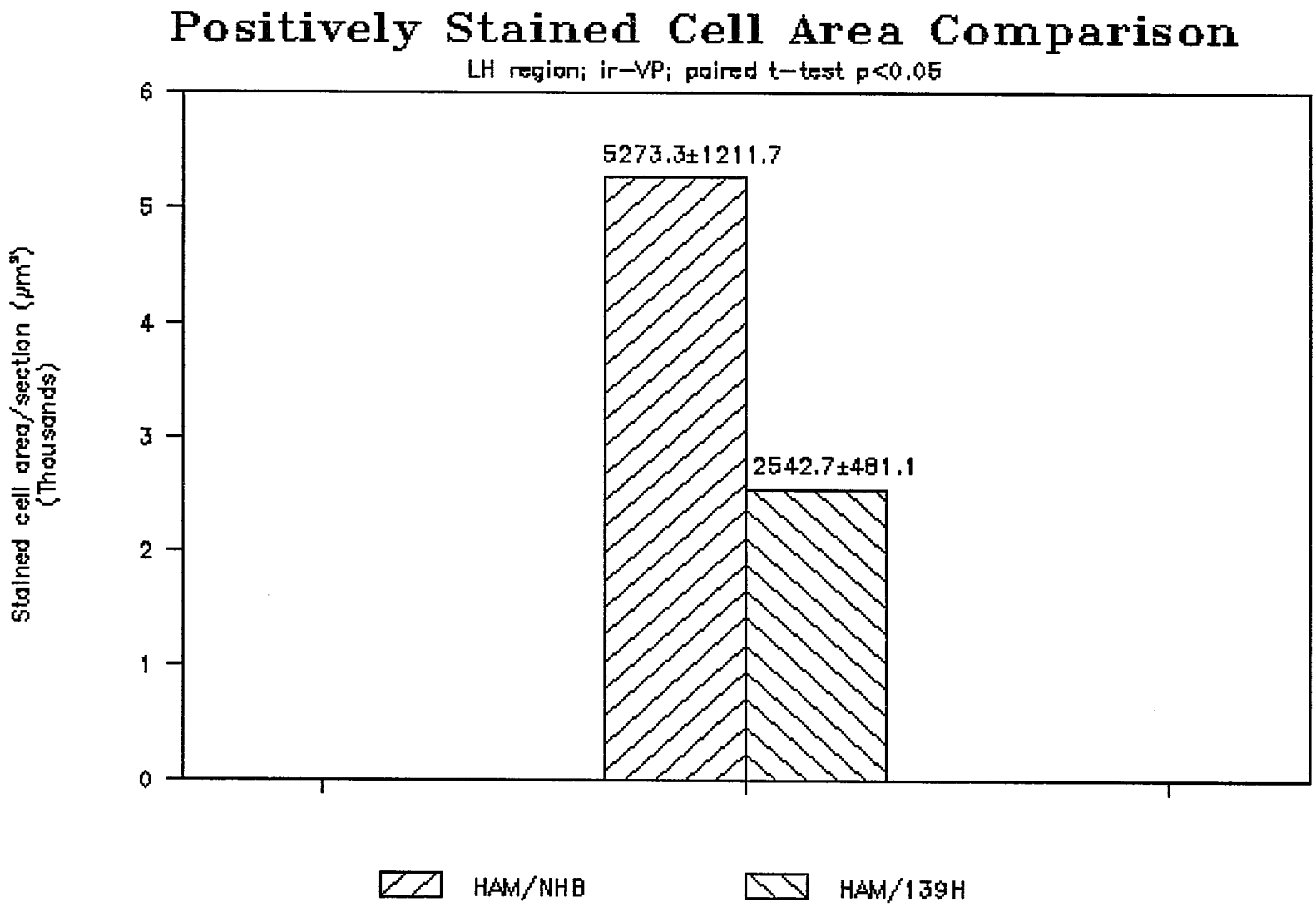
Positively Stained Cell Area Comparison
LH region; ir-VP; paired t-test p<0.05
Stained cell area/section (μm²)
(Thousands)
6
5
4
3
2
1
0
5273.3±1211.7
2542.7±481.1
HAM/NHB
HAM/139H

Figure 35. VP Stained Area in LHy Range vs. Atlas Number.

The area of VP immunopositive neuronal cell bodies in LHy is plotted for each coronal level, from rostral to caudal.

Note: the curve of the VP stained area in the LHy of 139H-infected hamsters is lower than that in the control animals; there is a peak in atlas numbers 34-36 in the control animals, but not in the 139H-infected hamsters which indicates that the ir-VP area in LHy of the 139H-infected hamsters (N=10) is decreased in comparison to that in the control animals (N=10).

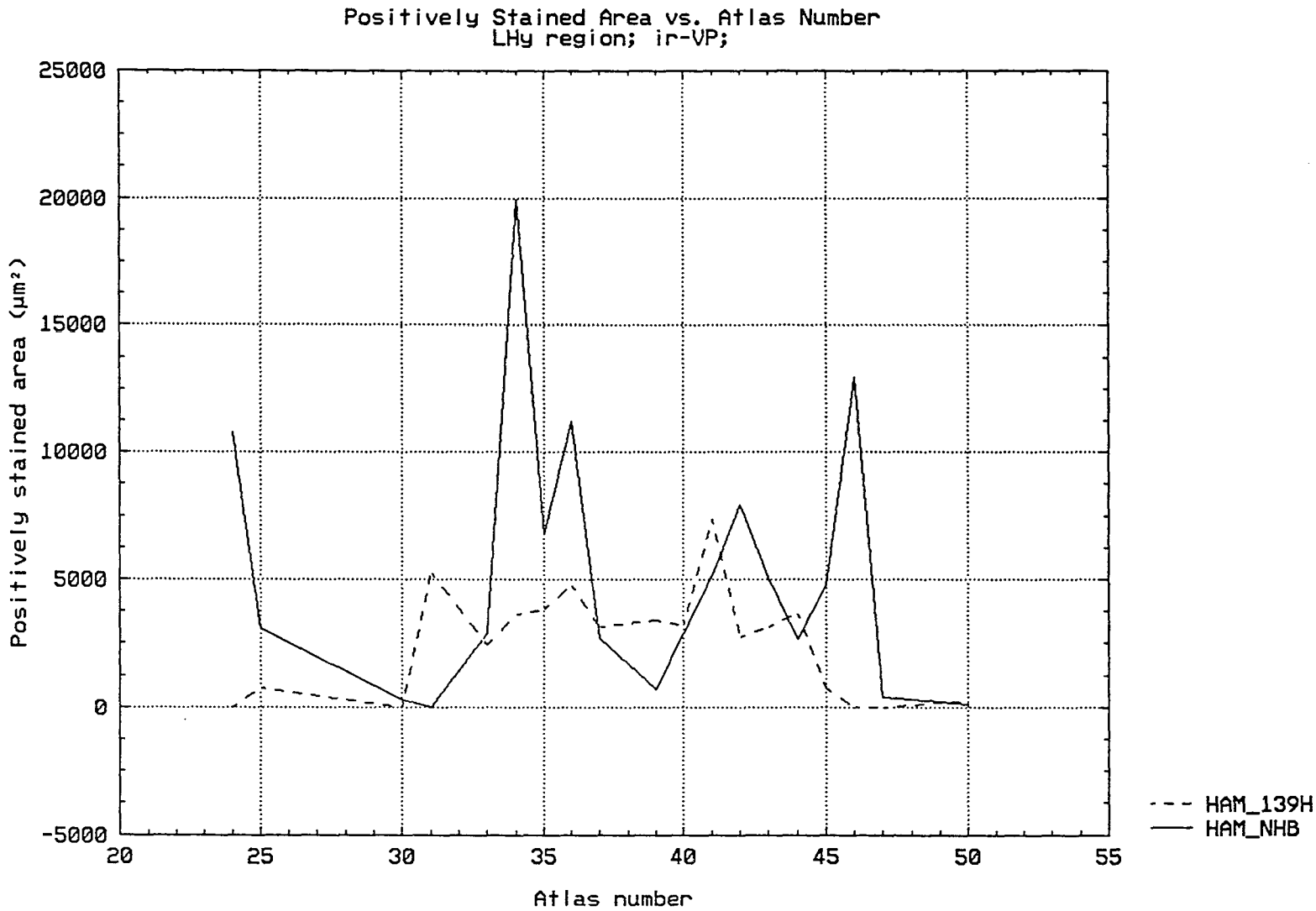
Positively Stained Area vs. Atlas Number
LHy region; ir-VP;
Positively stained area (µm²)
25000
20000
15000
10000
5000
0
-5000
20
25
30
35
40
45
50
55
Atlas number
HAM_139H
HAM_NHB

Figure 36. Comparison of VP Positively Stained Cell Area in DMH Region.

Note: there was no significant difference in the area of VP immunostained neurons in the DMH of the 139H-infected hamsters (7669.4±1800.1 μm^2/per section, N=10) compared with that in the control animals (7997±1949.1 μm^2/per section, N=10).

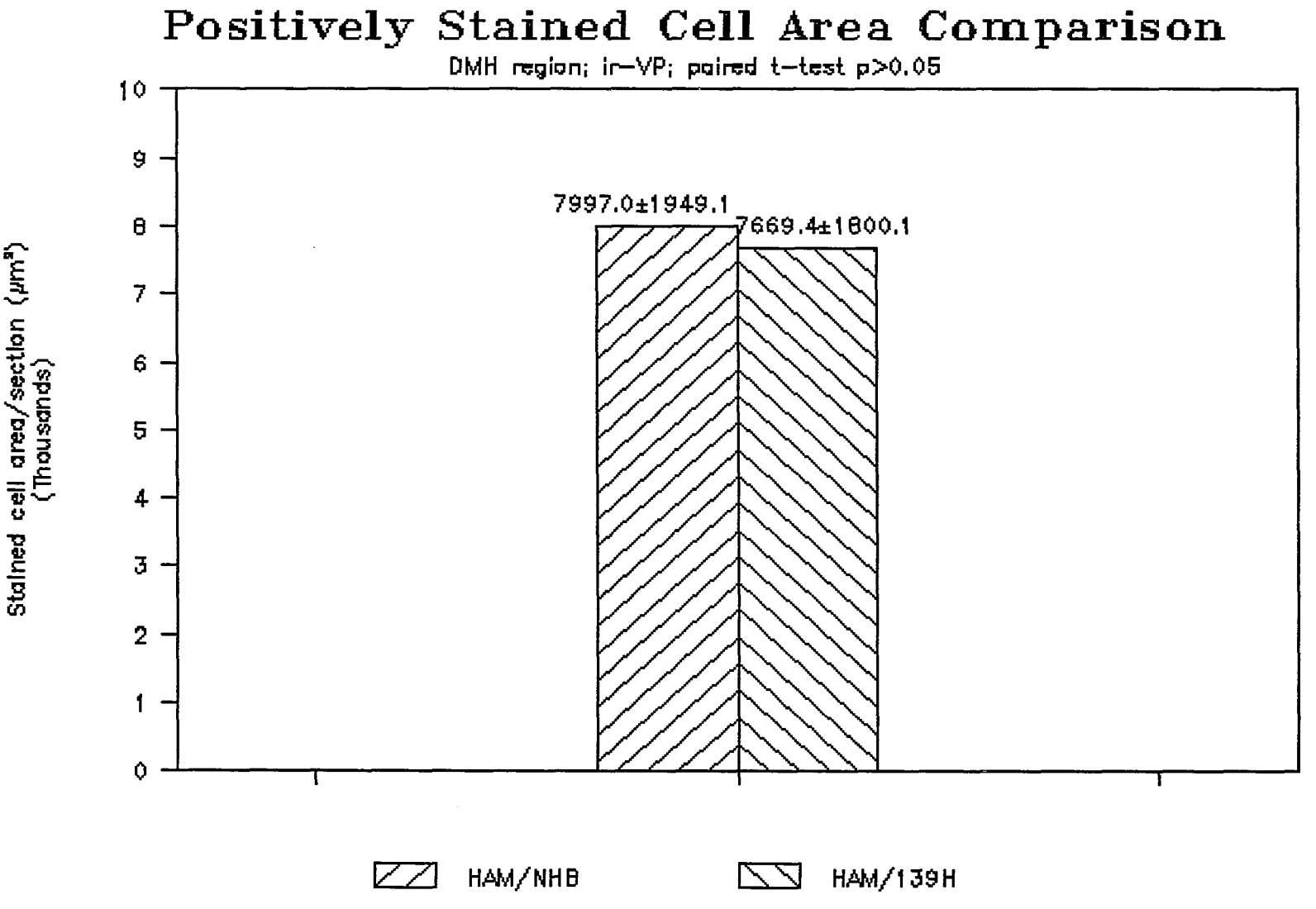
Positively Stained Cell Area Comparison
DMH region; ir-VP; paired t-test p>0.05
Stained cell area/section (μm²)
(Thousands)
10
9
8
7
6
5
4
3
2
1
0
7997.0±1949.1
7669.4±1800.1
HAM/NHB
HAM/139H

Figure 37. VP Stained Area in DMH Range vs. Atlas Number.

The area of VP immunopositive neuronal cell bodies in DMH is plotted for each coronal level, from rostral to caudal.

Note: the curve of the VP stained area in the DMH area of 139H-infected hamsters is almost the same as the curve in the control animals. There is a shift of the peaks to the left in the 139H-infected hamsters compared to those of the control animals, but the curve patterns are almost the same. Control, (N=10); scrapie hamsters, (N=10).

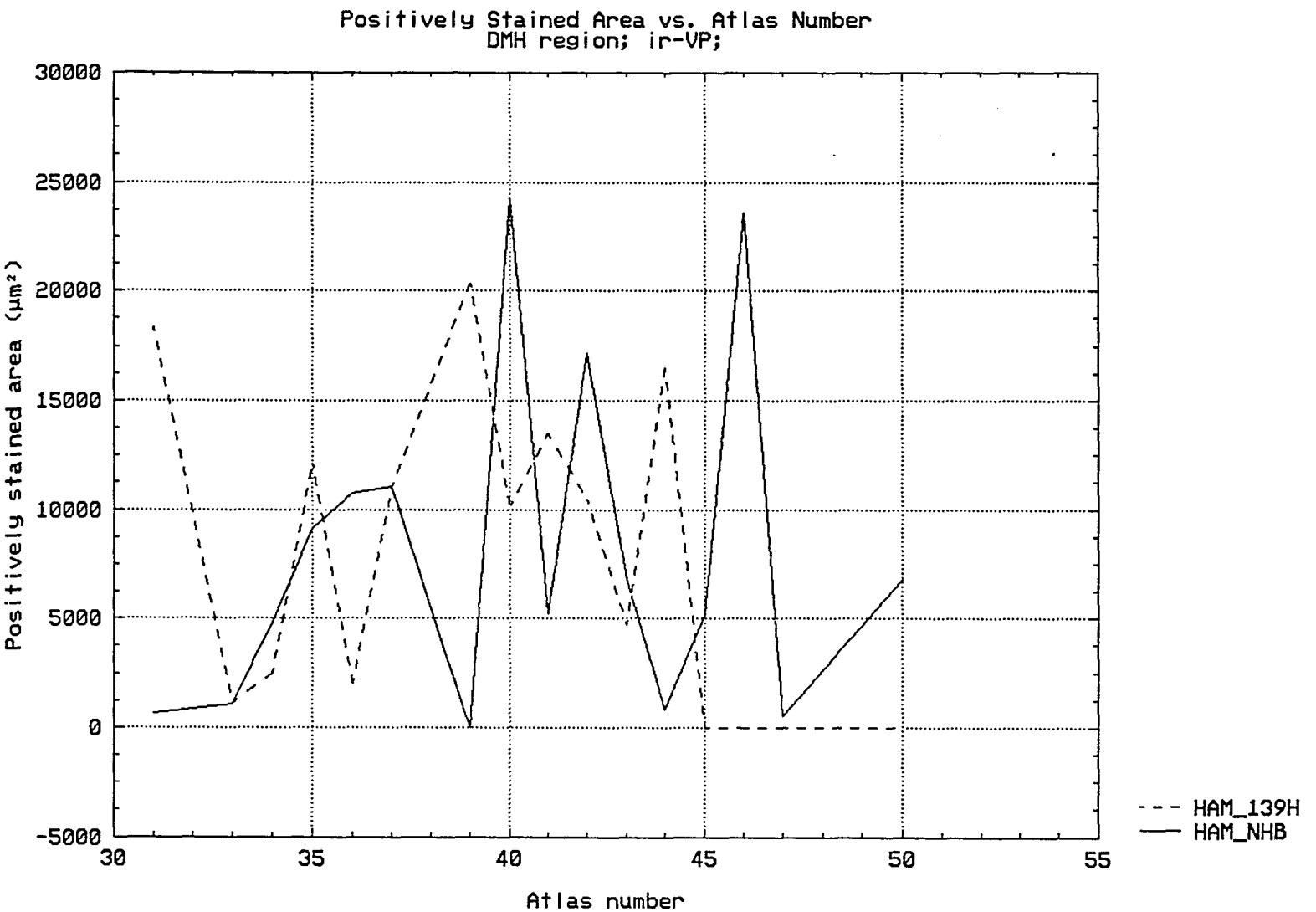
Positively Stained Area vs. Atlas Number
DMH region; ir-VP;
30000
25000
20000
15000
10000
5000
0
-5000
Positively stained area (µm²)
30
35
40
45
50
55
Atlas number
HAM_139H
HAM_NHB

Figure 38. The Outlines of the Position of VP Immunostained Neurons in SON Region.

The position of VP immunostained neurons. They were mapped onto outlines of the atlas figures according to Sidman et al. (1971). The dots represent VP immunostained neurons in the SON region. The outlines of the atlas figures were scanned into a NEC Powermate/SX computer using Hewlett Packard ScanJet. The graphics were first obtained using SCAN GALLERY 5.0 and then edited using Microsoft Windows Paintbrush.

a. control animals; **b.** 139H-infected animals.

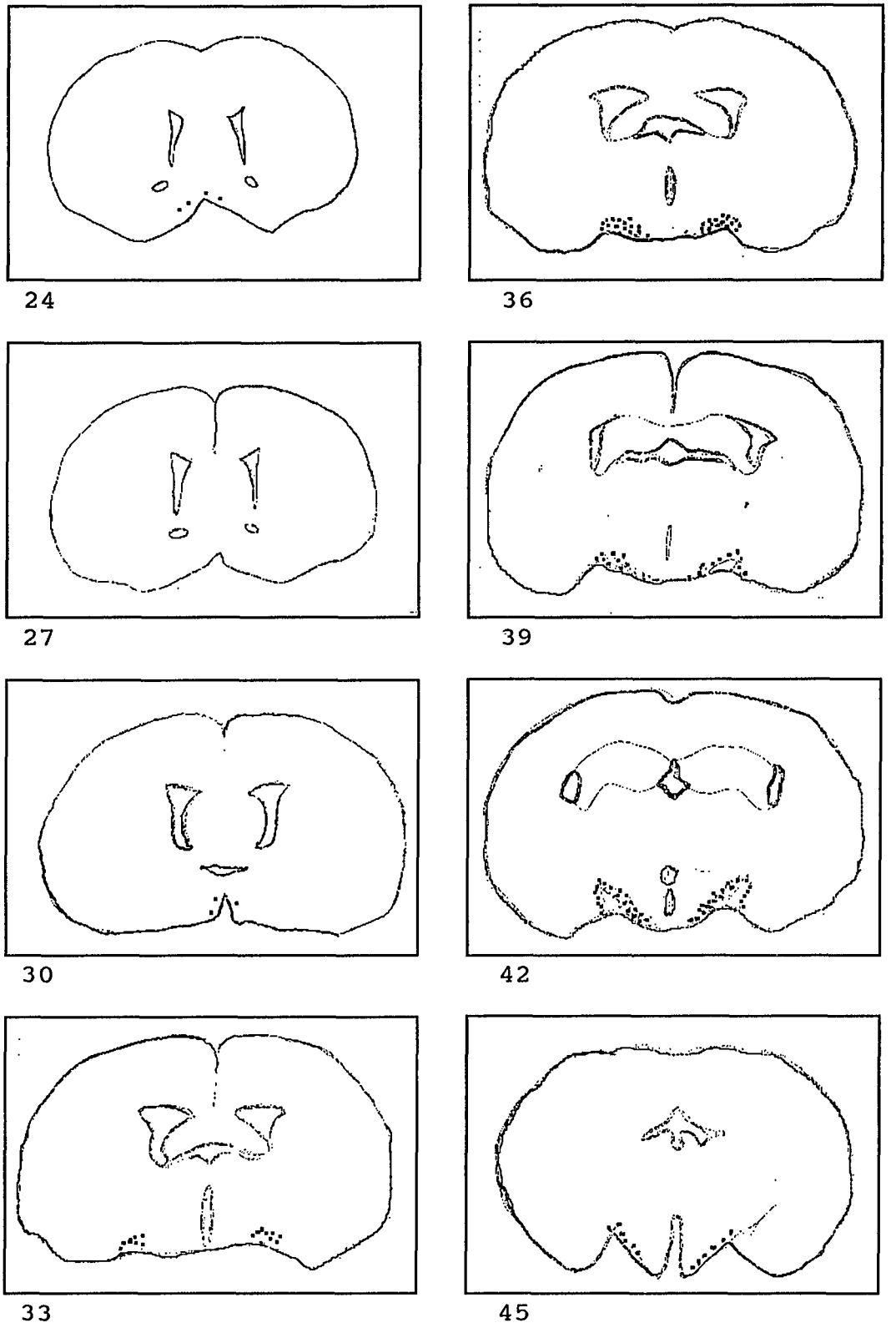

a. Ir-VP in the SON of Control Hamsters.

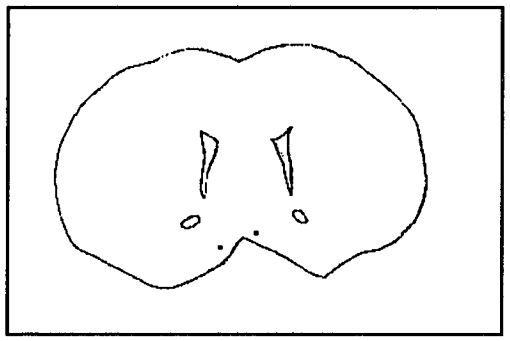

24

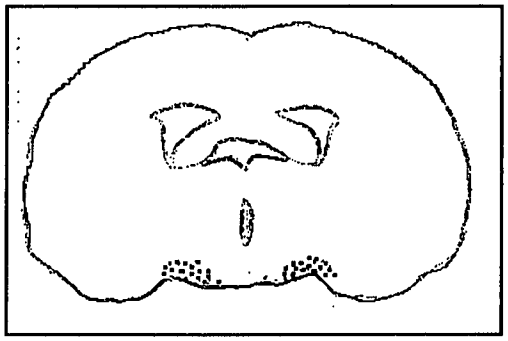

36

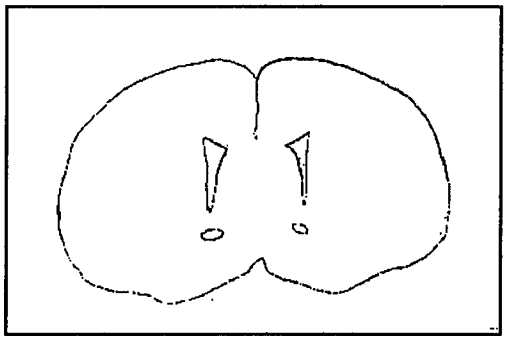

27

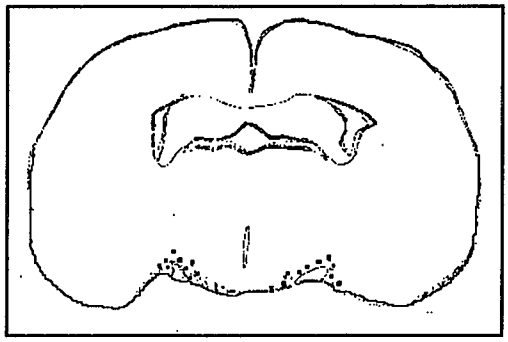

39

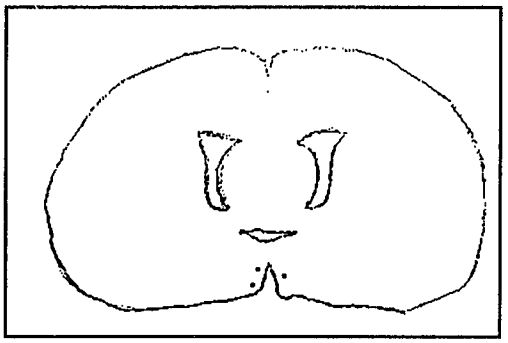

30

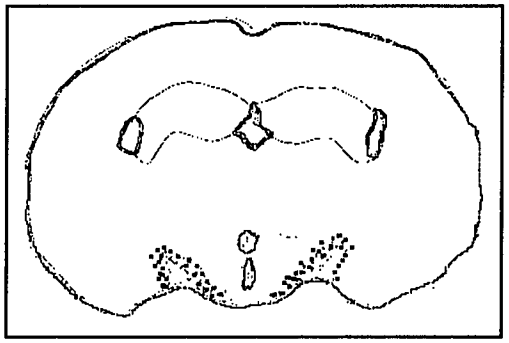

42

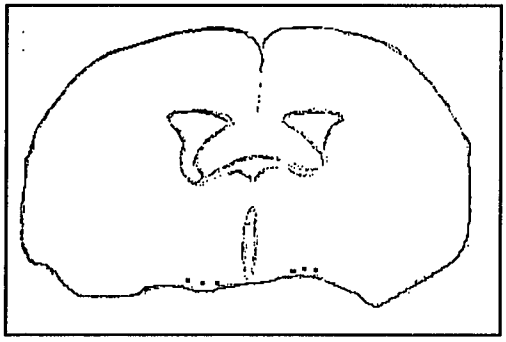

33

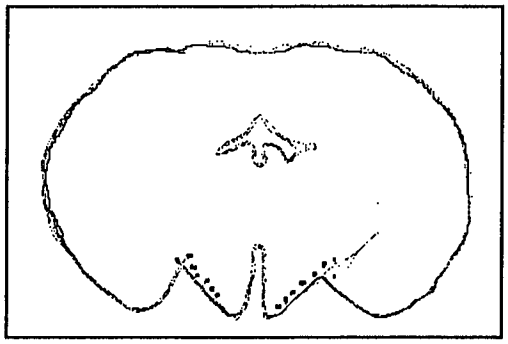

45

b. Ir-VP in the SON of 139H-infected Hamsters.

Figure 39. Immunostained VP Cells in the LHy, DMH and SON Regions.

The immunostained VP cells in hypothalamus in a control hamster. **a.** (20.5x), **c.** (41x), **e.** (41x), and **g.** (82x)

The immunostained VP cells in hypothalamus in a 139H-infected hamster. **b.** (20.5x), **d.** (41x), **f.** (41x) and **h.** (82x).

Note abbreviations and symbols: III-V: third ventricle; DMH: dorsomedial hypothalamus; LHy: lateral hypothalamus; OT: optic tract; PVH: paraventricular hypothalamus; SON: nucleus of supraopticus; SCN: nucleus of suprachiasmaticus, Arrowhead shows ir-VP cells, Small arrow shows the ir-VP fibers projection. Medium arrow shows that the ir-VP fibers project to the wall of the third ventricle.

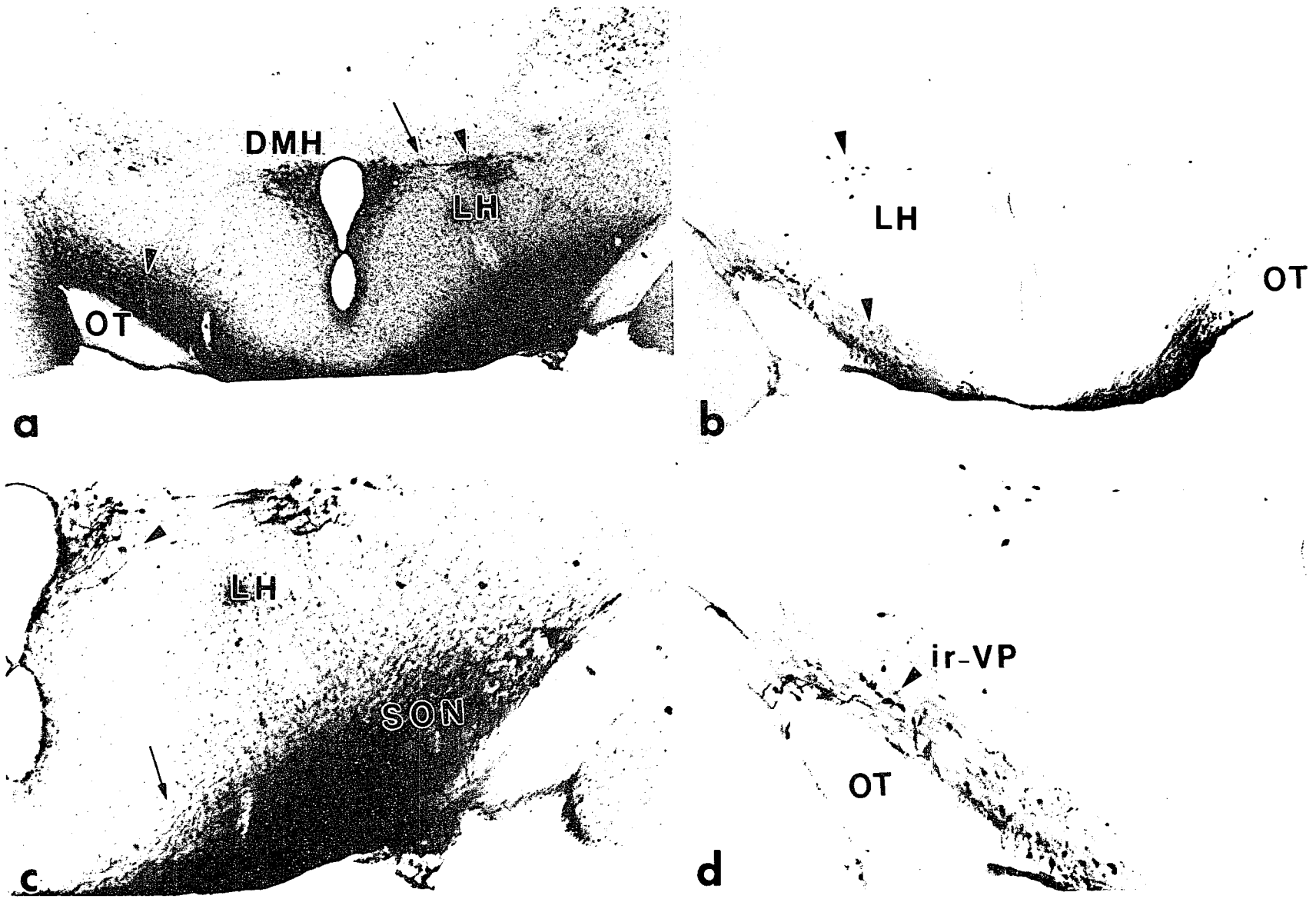
DMH
LH
OT
a
LH
OT
b
LH
SON
c
ir-VP
OT
d

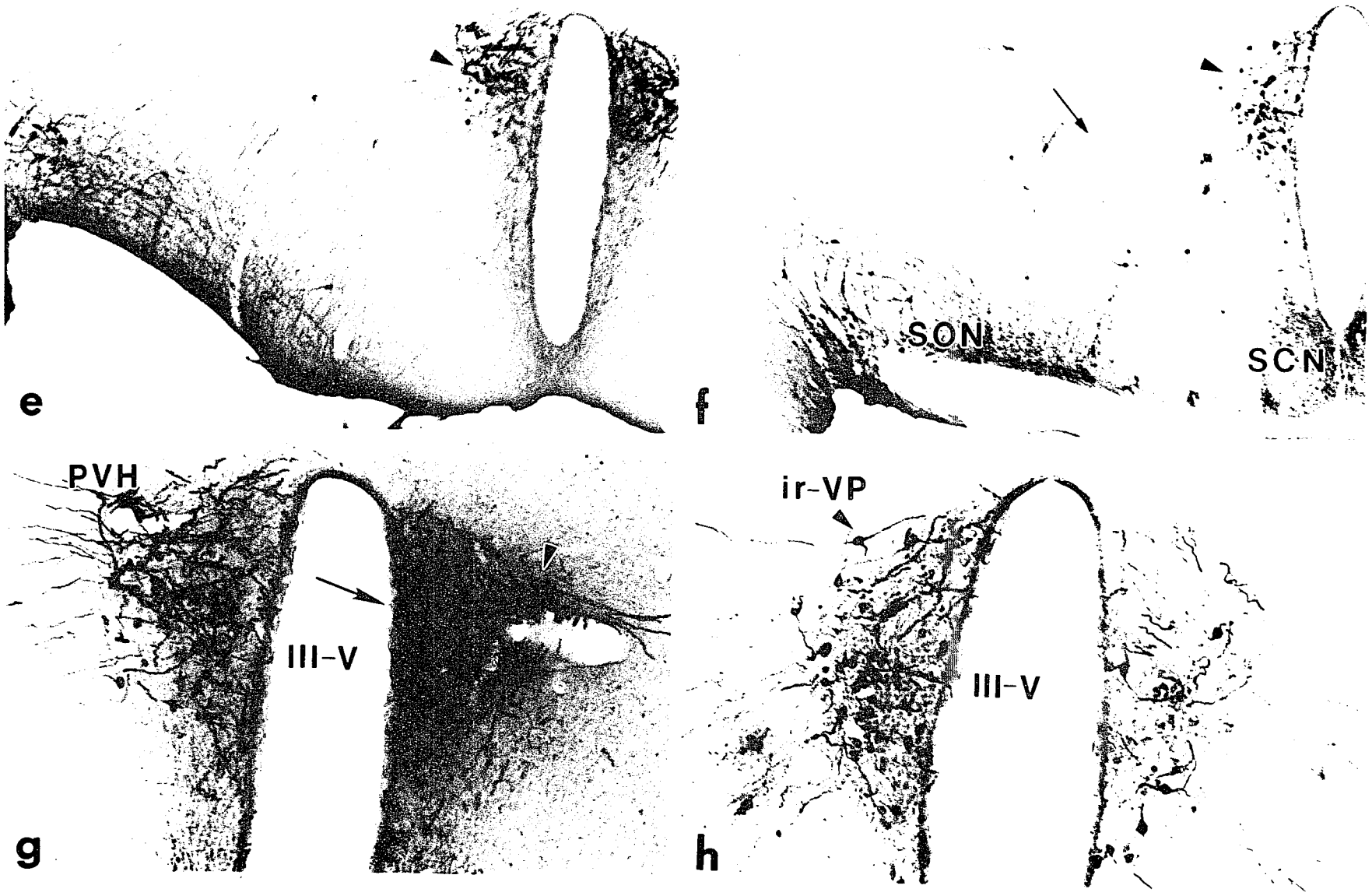
e
f
SON
SCN
PVH
III-V
g
ir-VP
III-V
h

Figure 40. Three-dimensional Reconstruction of Lateral Hypothalamic VP Immunostained Neurons in the Brain.

The three-dimensional models of VP immunostained neurons in the brains of control an 139H-infected hamsters were reconstructed from eight outlines of coronal sections. The models are viewed from a 60 degree rotation about the y axis; rostral, (left); caudal, (right). The cortexes are transparent so that interior structures and the VP immunostained neurons can be viewed. The right side of the cortex is colored white. The left side of the cortex is colored blue. The average population of lateral hypothalamic VP immunostained neurons in the whole group animals (N=10) is colored yellow. **a.** control. **b.** 139H-infected. Note: the population of VP immunostained neurons has decreased in the 139H-infected hamsters.

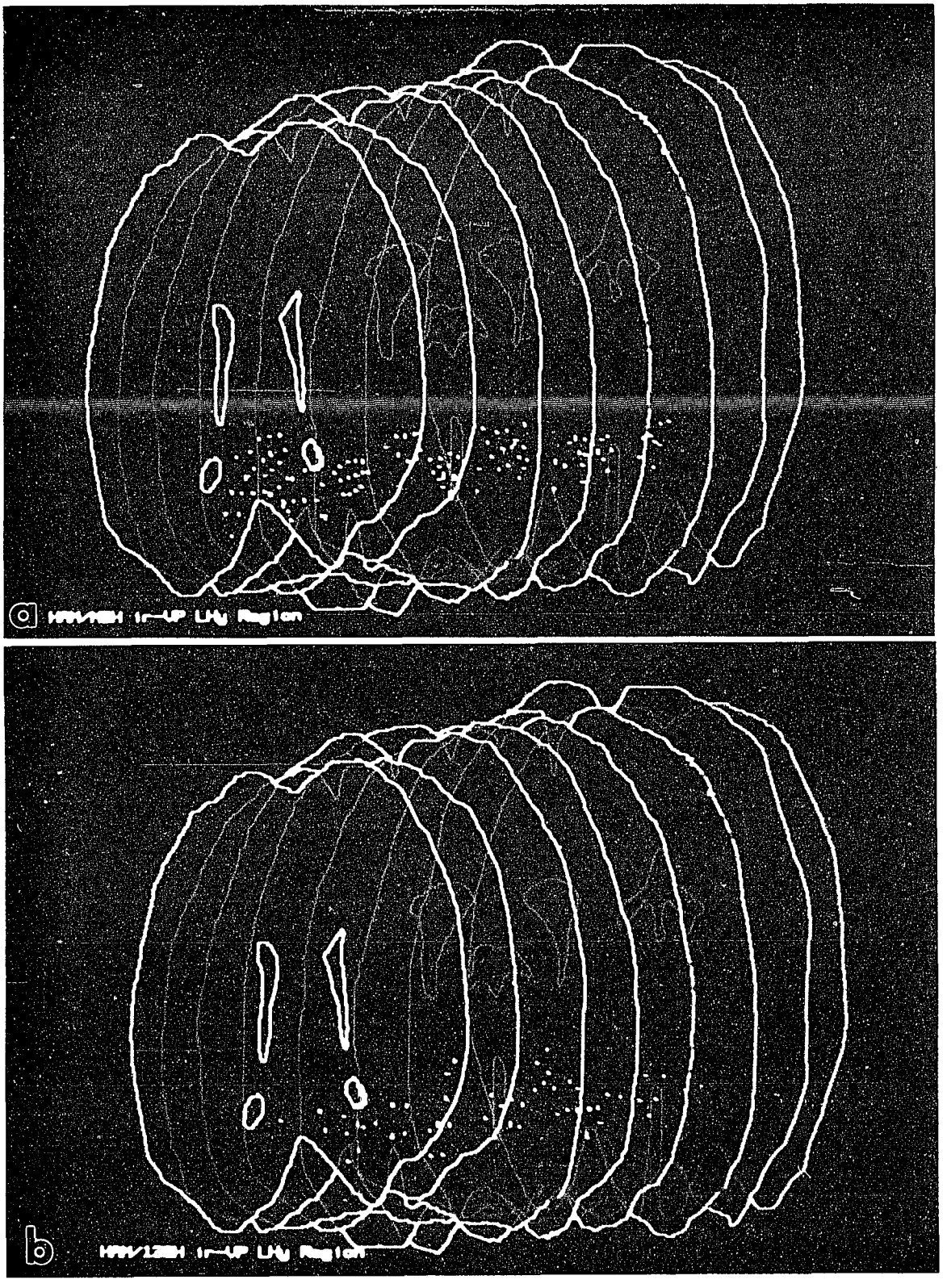
a
b

Figure 41. Three-dimensional Reconstruction of Dorsomedial Hypothalamic VP Immunostained Neurons.

Three-dimensional views of VP immunostained neurons in the brains of control and 139H-infected hamsters. The models of the brain are viewed from a 60 degree rotation about the y axis; rostral, (left); caudal, (right). The cortexes are transparent so that interior structures and the VP immunostained neurons can be viewed. The right edge of the cortex is colored white. The left edge of the cortex is colored blue. Parts of the ventricles and of the commissura anterior, pars anterior are also colored blue or white to provide a frame of reference. The average population of dorsomedial hypothalamic VP immunostained neurons in the group of animals (N=10) is colored yellow. **a.** control. **b.** 139H-infected. Note: the population of VP immunostained neurons was almost the same in both group, but the population of VP immunostained neurons shifted to the anterior part of hypothalamus in 139H-infected hamsters.

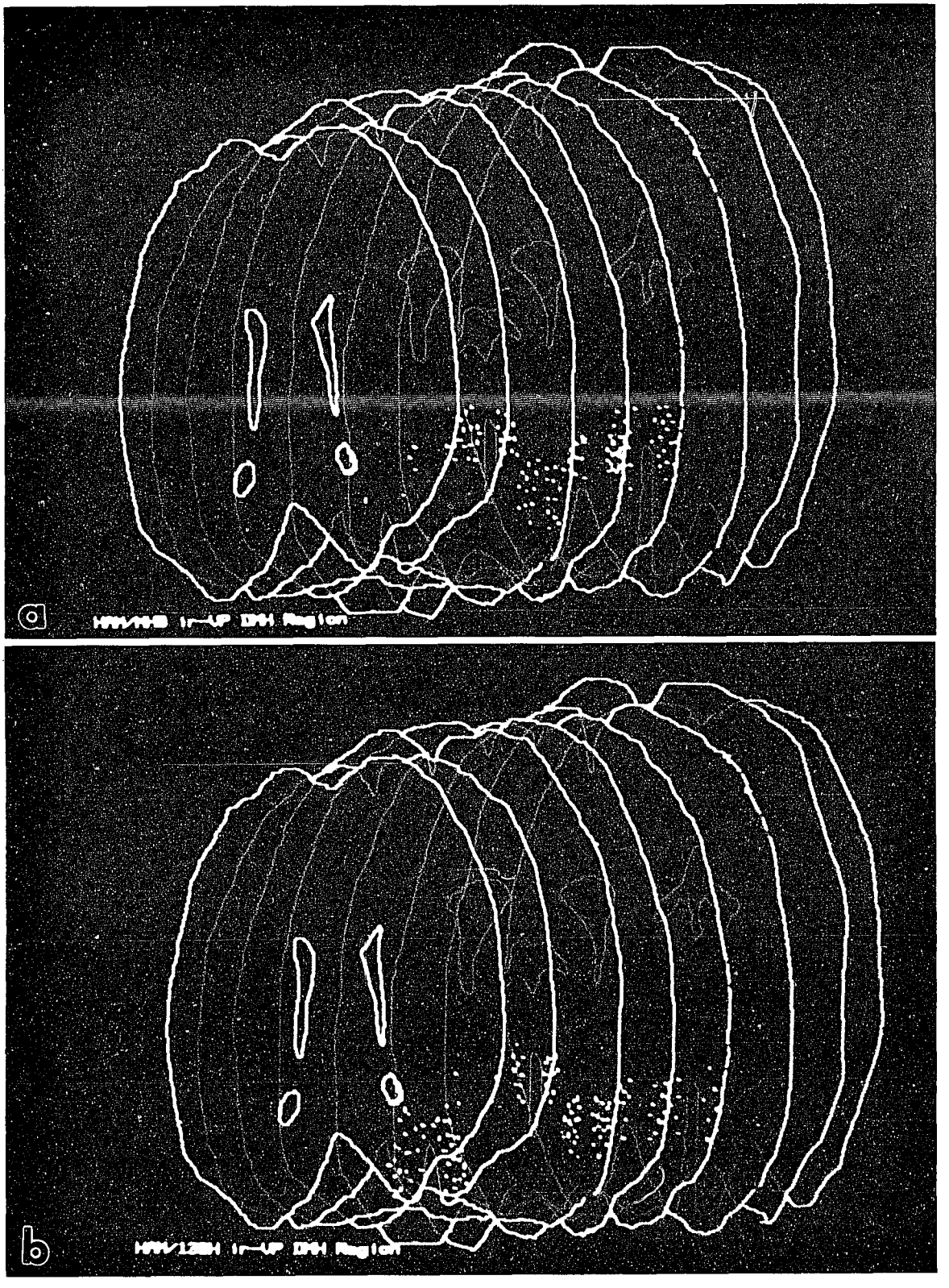
a
b

Figure 42. Three-dimensional Reconstruction of Supraoptic Hypothalamic VP Immunostained Neurons.

Three-dimensional views of VP immunostained neurons in the brains of control and 139H-infected hamsters. The models of the brain are viewed from a 60 degree rotation about the y axis; rostral, (left); caudal, (right). The cortexes are transparent so that interior structures and the VP immunostained neurons can be viewed. The right edge of the cortex is colored white. The left edge of the cortex is colored blue. Parts of the ventricles and of the commissura anterior, pars anterior are also colored blue or white to provide a frame of reference. The average population of supraoptic hypothalamic VP immunostained neurons in the group of animals (N=10) is colored yellow. **a.** control. **b.** 139H-infected. Note: the population of VP immunostained neurons was almost the same in both group.

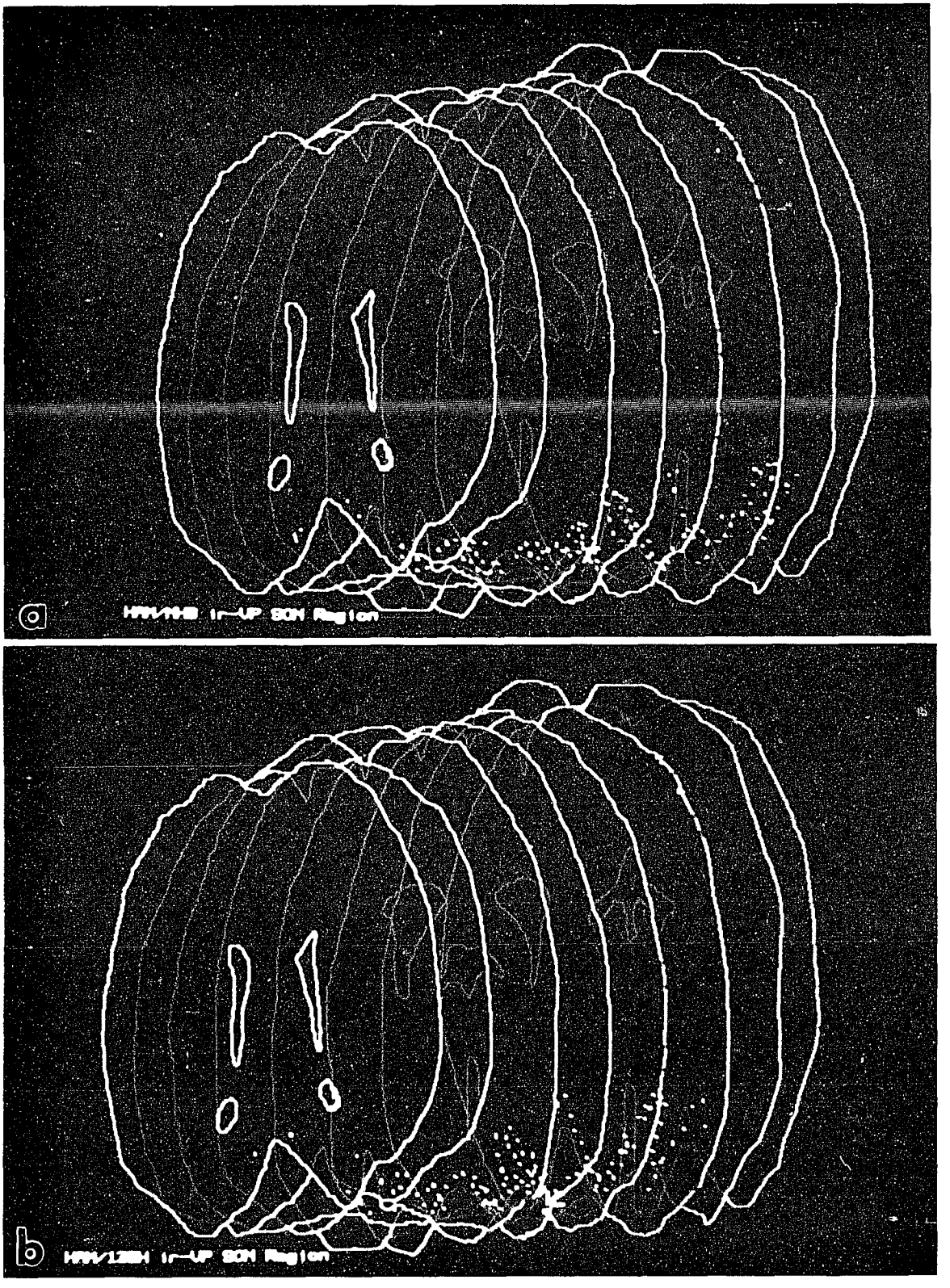
a
b

Figure 43. Comparison of CRF or VP Immunostained Neurons in Control and 139H-infected Hamsters with Three-dimensional Reconstruction Models.

Three-dimensional views of CRF and VP immunostained neurons in the brains of control and 139H-infected hamsters. The models of the brain are viewed from a 60 degree rotation about the y axis; rostral, (left); caudal, (right). The cortexes are transparent so that interior structures and immunostained neurons can be viewed. The right edge of the cortex is colored white. The left edge of the cortex is colored blue. Parts of the ventricles and of the commissura anterior, pars anterior are also colored blue or white to provide a frame of reference. The average population of immunostained neurons in the group of animals (N=10) in both control and 139H-infected hamsters is expressed simultaneously in the same model.

a. CRF immunostained neurons in brain, green: control, blue: 139H-infected.

b. VP immunostained neurons in the LHy region, blue: control, green: 139H-infected.

c. VP immunostained neurons in the DMH region, blue: control, green: 139H-infected.

d. VP immunostained neurons in the SON region, blue: control, green: 139H-infected.

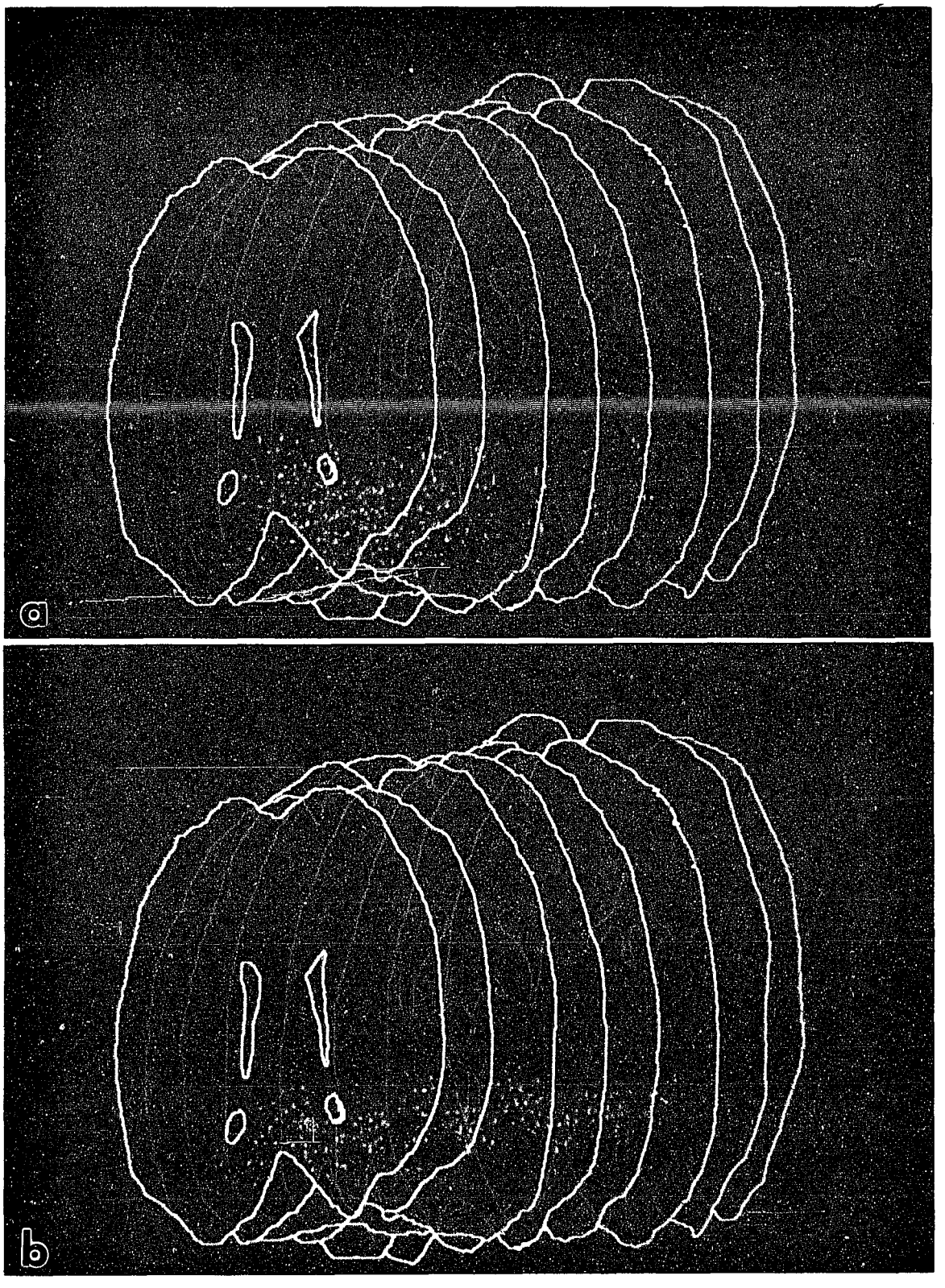
a
b

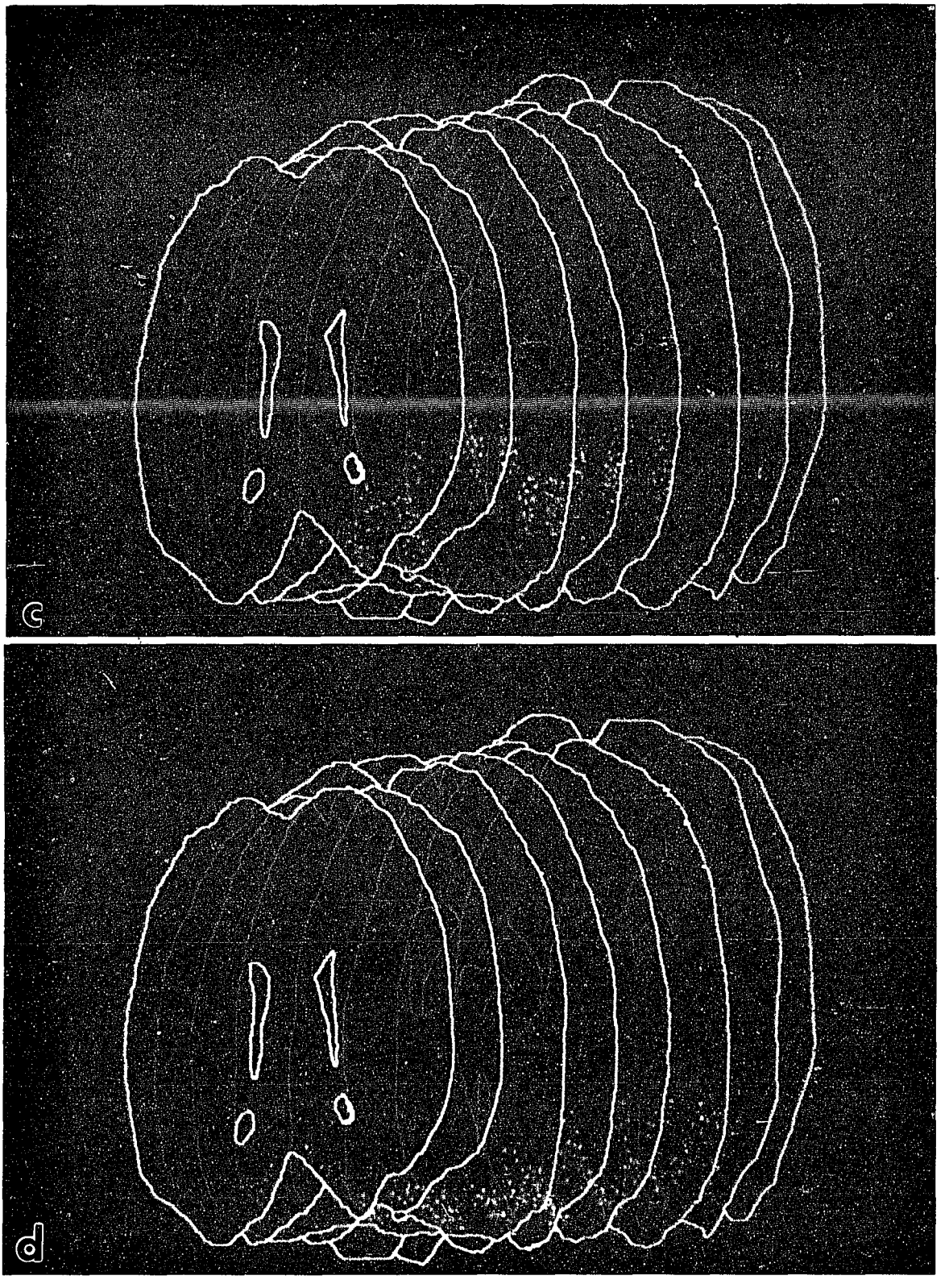
c
d

Figure 44. Comparison of VP Immunostained Neurons in the LHy, DMH and SON Regions in both Control and 139H-infected Hamsters with Three-dimensional Reconstruction Models.

The three-dimensional views of VP immunostained neurons in the LHy, DMH and SON regions in the brains of control and 139H-infected hamsters. The average population of immunostained neurons in the whole group animals (N=10) in the LHy, DMH and SON regions is expressed simultaneous in the same model. The VP immunostained neurons in different region are colored differently, LHy: blue, DMH: green, SON: red.

a. control.

b. 139H-infected.

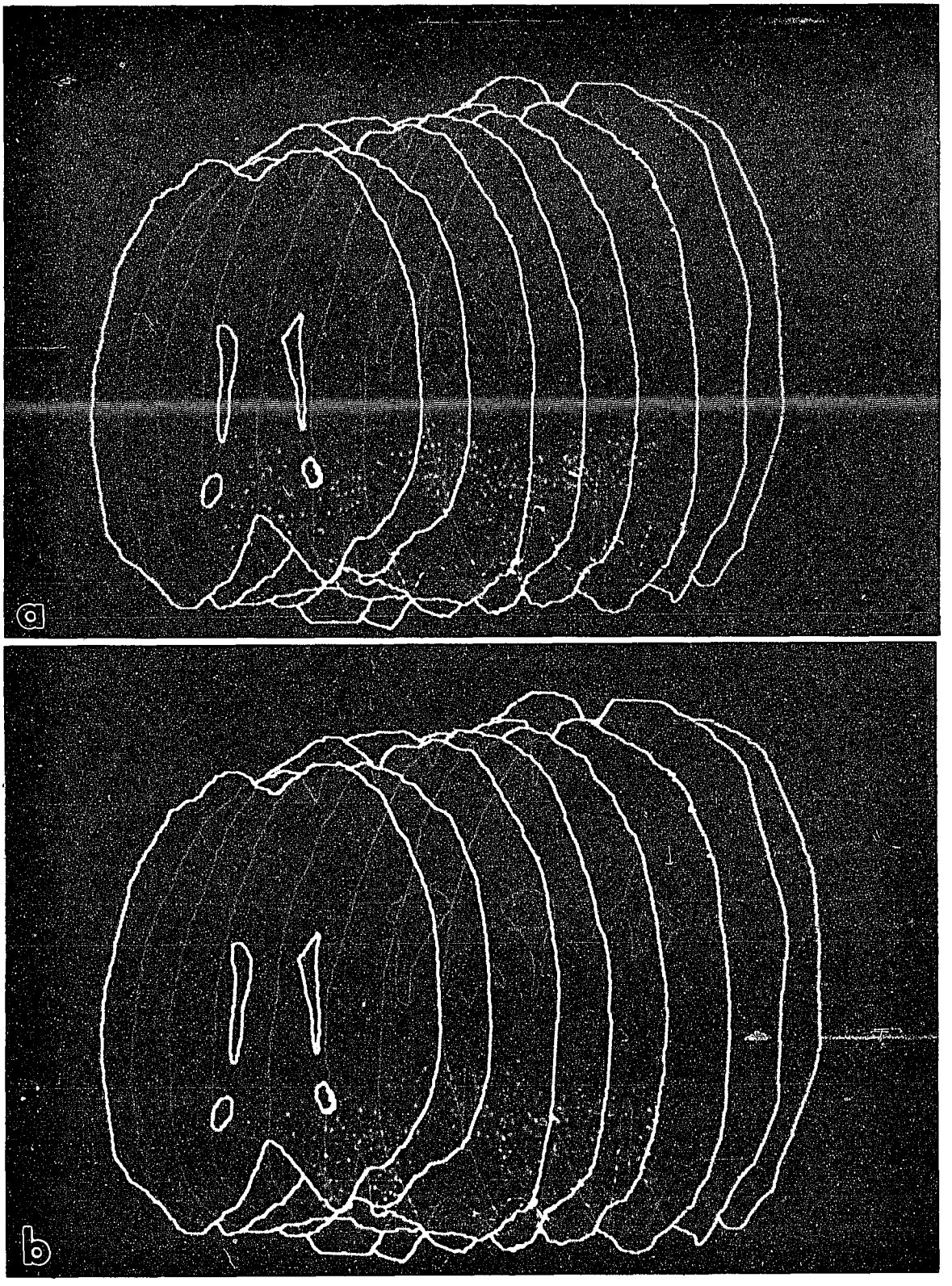
a
b

IV. DISCUSSION

A. Quantitative Changes in the Number and Size of the Islets of Langerhans

The pancreas has two different organs contained within one structure. The acinar portion has an exocrine function, secreting into the duodenal lumen the enzymes and ions used for the digestive process. The endocrine portion consists of the islets of Langerhans (described by Langerhans in 1869).

As reported by Carp et al. (1990), histopathologic examinations show that islets from 139H-infected hamsters are markedly enlarged, showing both hyperplasia and hypertrophy of the islet cells. Dispersion of the endocrine tissue of the pancreas in the form of small islets within a much larger exocrine gland greatly complicates quantitative studies. However, with the help of the Quantimet 970 image analyzer, quantitative changes in the number and size of islet profiles in a given area of pancreatic tissue can be determined with confidence. These data will be very useful when we calculate the changes in the cytologic composition of pancreatic islets.

The islets of Langerhans are made up of four different cell types and comprise 1-2% of total pancreatic mass (see Granner, 1988). As shown in this study, the proportion of the area of pancreas covered by islet tissue was much greater in scrapie(4.21 ± 0.73 $mm^2/50$ mm^2 pan, that was 8.42 % of the islet

area) than that in normal animals(0.55 ± 0.08 $mm^2/50$ mm^2 pan, that was 1.1 % of the islet area). The total number and area of the pancreatic islet profiles are much greater in 139H-infected hamsters than in normal animals. These results are consistent with the findings by Carp and his colleagues (Carp et al., 1990).

B. Analysis of A, B, D, and F Cell Ratios; Changes in Potential Interactions between Islet Cells

It is clear that there is paracrine and autocrine regulation within the islets of Langerhans. That is to say, that the secretory product of each islet cell type can regulate the activities of neighboring cells of another cell type or regulate the cell itself. According to Samols et al. (1983), if the A, B, and D cells are visualized as the vertices of an equilateral triangle, the potential interactions, whether by short (intra-islet) or long (systemic circulation) loops are: (1) insulin may inhibit glucagon secretion; (2) glucagon may stimulate insulin and somatostatin secretion; (3) somatostatin may inhibit insulin and glucagon secretion. Thus, there is a potential positive-negative glucagon-insulin feedback, a potential positive-negative glucagon-somatostatin feedback, and a potential negative somatostatin-insulin feedback (Samols et al., 1983). These

systems are affected by many factors such as islet architecture, islet cell composition, blood flow, extracellular fluid flow, cellular shape and orientation, extracellular depositions, receptor domains, cell-to-cell contacts and islet microenvironment. The changes in the number and ratio of A, B, D, and F cells in the islets of 139H-infected hamsters would certainly affect the potential interactions between these cells within the islet. I am going to discuss this in the following sections.

1. Effect of B Cells on A and D Cells.

As mentioned above, insulin can directly inhibit the secretion of glucagon from A cells and somatostatin from D cells. In my studies, the immunostaining area of B cells was increased significantly from 0.46 $mm^2/50\ mm^2$ pan in control animals to 3.53 $mm^2/50\ mm^2$ pan in 139H-infected animals. The B cell area in the 139H-infected hamsters was 7.7 times greater than that area in the control hamsters. The ratio of B:A cells was 5.4:1 in control animals and 17.4:1 in 139H-infected animals. Since the ratio of B:A was much higher in 139H-infected animals than in control animals and 139H-infected hamsters showed marked hyperinsulinemia, one could speculate that the inhibiting effect of insulin on glucagon secretion by A cells would be increased.

The same would be true for the effect of B cells on somatostatin secretion by D cells. The ratio of B:D cells was 27:1 in control animals and 122:1 in 139H-infected animals. Again, since the 139H-infected hamsters showed marked hyperinsulinemia and a much higher B:D cell ratio than that in control animals, it is possible that the inhibiting effect of insulin on somatostatin secretion by D cells would also be increased.

2. Effect of A Cells on B and D Cells.

A and D cells are located on the outer rim of the islets, while B cells can be divided into two parts. One part can be called peripheral B cells. These are close to the outer rim of the islet and they have a close relationship, such as cell-to-cell contact, with the outer rim A, D, and F cells. The other part can be called central B cells. These are located in the central part of the islet. There are some differences between the peripheral B cells and the central B cells. They have different densities of various intracellular organelles (Orci, 1974) and they respond to some stimuli differently (Beigelman et al., 1977). There are more gap junctions in the peripheral B cells than in the central B cells (Meda et al., 1980b).

Glucagon can stimulate the secretion of insulin and

possibly can also stimulate somatostatin release. Glucagon can bind receptors which couple G_s protein, and stimulate the adenyl cyclase system. Glucagon can bind to receptors which stimulate the phospholipase C system. Glucagon can also bind to receptors which inhibit the Ca^{++} pump (Cooke et al., 1988).

In my studies, the immunostaining area of A cells was increased significantly from 0.09 $mm^2/50\ mm^2$ pan in control animals to 0.20 $mm^2/50\ mm^2$ pan in 139H-infected animals. The effect of glucagon on insulin secretion by B-cells is complicated. The stimulative effect of glucagon on B cells is higher in the systemic circulatory loop than in the intra-islet loop.

In addition, the peripheral B cells are stimulated directly by glucagon produced from neighboring A cells, so that the stimulating effects of glucagon on peripheral B cells is higher than that on the central B cells within the same islet (the mechanisms of these stimulating effects will be discussed later in the dissertation). However, unless we measure the concentration of glucagon in the plasma, it is hard to say whether the stimulative effects of glucagon on insulin secretion by B cells would be changed in the islets of 139H-infected hamsters.

In my studies, the ratio of A:D was 5:1 in control animals and 7:1 in 139H-infected hamsters. Since both A and D cells are located in the outer rim of the islet and the ratio of A:D cells was almost the same in control and as it

was in 139H-infected animals, the effect of A cells on D cells might not change significantly in 139H-infected hamsters.

3. Effect of D Cells on B and A Cells.

The major portion of pancreatic islet somatostatin appears to be identical to hypothalamic somatostatin 14 (SS_{14}) (Samols et al., 1981). Somatostatin can very rapidly and potently inhibit secretion of A and B cells in vivo (Alberti et al., 1973) and in vitro (Iversen, 1974). For instance, in the isolated perfused canine pancreas, one can observe the inhibitory effect within 60 seconds with a concentration of >= 10 pg/ml (Samols and Harrison, 1976).

Somatostatin is probably equipotent as an inhibitor of A cell and B cell secretion, with weaker effects on the F cells (Hermansen And Schwartz, 1979). Increases in secretion of insulin and glucagon by virtually all known stimulants (including glucose, glucagon, arginine, B-adrenergic or cholinergic agonist, phosphodiesterase inhibitors or CAMP, tolbutamide and divalent cations) have been inhibited by appropriate concentrations of somatostatin in mammals (Gerich, 1981).

There is also a minor portion of somatostatin 28 (SS_{28}) in pancreatic islets. SS_{28} is about 10-100 times more potent than SS_{14} as an inhibitor of arginine-stimulated B cells

(Benoit et al., 1981), but equipotent with SS_{14} with respect to the arginine-stimulated A cells (Samols et al., 1981). It is thought that SS_{28} would selectively inhibit the B cell. The dissociation of biologic activity of synthetic somatostatin analogs on the A cells and B cells suggests that the somatostatin receptors on A cells are different from those on B cells (Weir et al., 1980). Alternatively there might be different second messenger systems in A cells from those in B cells. Somatostatin can bind to receptors which couple G_i protein and inhibit the adenyl cyclase system. On the other hand, it can bind to receptors which couple with G_k (or G_i) protein and open K^+ channels. Somatostatin can also bind to receptors which can close Ca^{++} channels (Cooke et al., 1988).

In the studies reported in this dissertation, the immunostaining area of D cells was not changed significantly in 139H-infected hamsters. However, the ratio of D:B cells was decreased significantly from 1:27 in control animals to 1:122 in 139H-infected hamsters. These changes would decrease the inhibitory effect of somatostatin on B cell insulin secretion in 139H-infected hamsters, a subject which I will discuss at greater length later in this dissertation.

The effect of D cells on A cells might not change significantly in 139H-infected hamsters. Based on the facts that they are all in the outer rim of the islets and that the ratio of D:A was almost the same in control animals as in 139H-infected animals, it is probable that the inhibitory

effect of somatostatin on secretion of glucagon by A cells does not change significantly in 139H-infected hamsters.

4. Effect of F Cells on B Cells.

Pancreatic polypeptide mainly affects gastrointestinal secretion (see Granner, 1988). The effect of pancreatic polypeptide on insulin secretion by B cells is controversial. While Samols et al. (1977) showed that infused pancreatic polypeptide did not influence insulin and glucagon secretion in the isolated, perfused pancreas, Murphy et al. (1981), demonstrated that human pancreatic polypeptide inhibited insulin release in the rat when administered intravenously.

The population of F cells might be different in different parts of the pancreas. The head or duodenal portion of the human pancreas, which is derived from the ventral pancreatic anlage, and is supplied by the inferior pancreaticoduodenal artery, contains islets whose mantle contains about 74% B cells, 20% F cell, 5% D cells and very few A cells (Bencosme and Liepa, 1955; Orci et al., 1976a). The tail and body, or splenic portion of the pancreas receives its blood supply from the gastroduodenal and splenic arteries, and has its embryonic origin in the dorsal pancreatic anlage. This part of the pancreas has almost the same proportion of B and D cells, but has 20% A cells and very few F cells (Orci et al., 1976).

Based on this fact, one can speculate that the effect of F cells on B and A cells and also the effect of A cells on B and D cells might be different between these two parts of the pancreas.

In my studies, I used the splenic portion of the pancreas. There were very few F cells, with an area of about 0.0006 mm^2/50 mm^2 pan. There was no significant difference between the F cell staining area in control animals and that of the 139H-infected animals. Since B cells were increased significantly in 139H-infected hamsters, the ratio of F:B was reduced significantly in these animals. If it is true that pancreatic polypeptide can inhibit insulin secretion, then the inhibiting effect of F cells on insulin secretion by B cells would be decreased in 139H-infected hamsters.

5. Effects of Autocrine Regulation within the Islets.

A secreted mediator might influence the cell from which it was secreted so that there might be a feedback relationship. Cell types which could be influenced by autocrine mechanisms include B cells which can be inhibited by insulin (Frerichs et al., 1965), D cells which can be inhibited by somatostatin analogs (Ipp et al., 1979) and A cells which can be suppressed by glucagon (Kawai and Rouiller, 1981).

In the studies noted in this dissertation, the immunostaining area of B cells was increased significantly in 139H-infected hamsters, about 7.7 times greater than that in control animals. It has also been shown that there was marked hyperinsulinemia in 139H-infected hamsters, the concentration of immunoreactive insulin in the plasma was as much as 49 times higher in 139H-infected hamsters than that in control hamsters (Carp et al., 1990). It is possible that the effect of autocrine regulation of insulin on B cells might be decreased in 139H-infected hamsters. The reasons for this may be explained by down regulation of receptors. Down regulation of receptors is a general response to a high level of circulating hormone. Prolonged exposure of tissues to a high concentration of insulin would decrease insulin receptors on the cell membranes and, therefore, the autocrine effect of insulin might be decreased.

C. Pathological Changes in the Islets

Pathological changes in islet architecture and at the cellular, subcellular and molecular levels in the cells of pancreatic islets in 139H-infected hamsters will be discussed in the following sections.

1. Pathological Changes in Islet Architecture.

The most pronounced changes in the pancreatic islets of 139H-infected hamsters were islet size changes and vascular system changes. As observed by Carp et al. (1990), the pancreas showed small brown and red-brown nodules scattered over the surface. Also some of the islets in 139H-infected hamsters contained hemorrhages. There was marked hyperplasia and hypertrophy of the cells of the islets in 139H-infected hamsters. Immunostaining studies showed that: (1) the increase in B cells serves as a major component for the enlargement of the pancreatic islets; (2) there was almost no variation in the arrangement of islet cells: i.e., normal islets contain a core of B cells and an outer rim of A, D and F cells. The same was true in the islets of 139H-infected animals. This finding suggests that the increased B cell population was due to increased B cell mitosis rather than the transformation of exocrine cells.

As is seen for all endocrine organs, the pancreatic islets have a rich blood supply. The arterial supply of the pancreas arises from the splenic, hepatic and mesenteric arteries and the venous drainage is into the splenic and mesenteric veins. The vascular system in the pancreatic islets plays an important functional role in supplying oxygen, nutrition, hormonal signals and removing carbon dioxide, metabolic wastes and biologically active secretory products

from these endocrine cells.

In rat islets, the afferent vessel enters the islet at a gap of the non-B cell mantle, thus directly entering the B cell core, whereupon it branches into numerous capillaries that form the glomerular structure within the B cell core. As the capillaries leave the core, they pass through the mantle of non-B cells and either coalesce at the edge of the mantle forming an overlying network of collecting venules, or _ depending upon the size of the islet _ they pass through exocrine tissue before coalescing (Bonner-Weir and Orci, 1982).

In my studies, it seems that this vascular pattern appears in the pancreatic islets of normal hamsters. However, in the islets of 139H-infected hamsters, this vascular pattern is disturbed significantly, in which there is a large mass of blood cells which is not surrounded by traditional arterial, venous or capillary wall cells. I refer to this structure as "blood vessel core" (BVC). These structures were almost always centrally located within the islets and surrounded by normal appearing or elongated B cells.

Carp et al. (1990) had already shown that some of the islets in 139H-infected hamsters contained hemorrhages. However, the mechanisms of genesis of hemorrhage and/or BVC formation in the islets are still not clear.

There are two possibilities for the fate of the blood within the BVC. One possibility is hemorrhage; which means

that the blood within the BVC escapes from capillaries inside the islet. The blood oozing from the capillary will leave the circulation and be trapped in the BVC. The blood cells will eventually die and will be cleared by macrophages. In this case the BVC is not a part of the circulatory system. The other possibility I will refer to as "pseudo-hemorrhage"; which means that the blood within the BVC is from one or more capillaries, and sooner or later the blood cells will re-enter the circulation through other capillaries inside the islet. In this case the BVC is a part of the circulatory system. In assessing these two possibilities, the following points are relevant: (1) The endocrine pancreas is richly vascularized by an extensive labyrinth of capillaries. (2) It has been estimated that islets receive 13%-20% of the entire pancreatic blood flow, in spite of the fact that islets comprise only 1.5% of pancreatic volume (Lifson et al., 1980). (3) In my studies, I observed that rather than clear up the blood cells in the BVC, many macrophages migrate from the BVC into the islets. In my opinion, the possibility of pseudo-hemorrhage is much higher than that of hemorrhage.

In my studies, the numbers and areas of these large BVCs increased significantly from zero in number and area in control animals to 13.0 /50 mm^2 pan in number and 0.67 mm^2/50 mm^2 pan in area in 139H-infected animals. The average diameter of the BVC is 0.13 mm. These changes would affect both blood flow within the islets affecting blood volume and

blood velocity. For example, blood volume would increase and blood velocity would decrease in the large BVC.

(The mechanism of these changes will not be discussed in detail in this dissertation).

Another aspect for consideration is that arterial blood flow regulation and interstitial fluid flow-direction and velocity would affect the islet microenvironment. Small vessels are well known to be able to constrict and dilate and this capability might exert some control over islet secretion. Because islet cells and islet vascular systems are innervated by the autonomic nervous system, the enlargement of islets in 139H-infected hamsters would affect the autonomic nervous terminal system within the islets.

We know that the vessel tone within islets is affected by the local release of acetylcholine from the vagus nerve, norepinephrine from sympathetic nerves, and vasoactive intestinal polypeptide (VIP) and a number of other vasoactive mediators which presently have an unspecified source. The opening and closing of certain capillaries would change the interstitial fluid flow within the islet thus changing the microenvironment. Together with the changing cell size, shape, orientation and receptor domains, the activities of islet cells would change.

2. Effects of Pathological Changes at the Cellular Level on Islet Cell-to-cell Communications.

In addition to the cellular changes already described, there are other pathocytological changes in the islets of scrapie hamsters such as vacuolization, cellular atrophy, necrosis, changes in cell shape and in cell orientation. These cytological changes can provide useful information for analysis of functional activities since structure and function are closely related.

As mentioned above, the islets of Langerhans contain cords and irregular clumps of cells and capillaries. There are experimental data which indicate that there is spatial restriction and compartmentalization of islet secretory products. It is known that very low concentrations of somatostatin or glucagon introduced into the arterial supply of islets can profoundly alter the secretion of other islet hormones (Samols and Harrison, 1976). To be specific, when the somatostatin concentration in the venous effluent is over 100 pg/ml, an arterial infusion of less than 100 pg/ml can inhibit insulin and glucagon secretion (Samols et al., 1983).

Because these concentrations are lower than those leaving pancreatic draining veins they must be far lower than concentrations found in certain parts of the islet interstitial space. It is thought that the concentration of somatostatin in that portion of interstitial space into which

D cells release somatostatin must be extremely high, almost certainly more than 1,000-fold higher than those quantities which can influence A and B cell functions (Samols et al., 1983). If there is not some sort of physiologic and anatomic compartmentalization, the concentration of somatostatin released by D cells would be high enough to inhibit all of the A and B cell functions within the islets (Samols et al., 1983).

I will discuss the significance of this physiologic and anatomic compartmentalization and also analyze how this physiologic and anatomic compartmentalization might be disturbed in the islets of 139H-infected hamsters.

a. Islet Vasculature and Starling's Hypothesis.

The microanatomical relationships between the endocrine cells of the islet of Langerhans, namely the existence of fixed location of insulin-, glucagon-, and somatostatin-containing cells, which have been discussed above, are the most important physiologic and anatomic compartmentalization.

In addition to that, the first major considerations are of islet vasculature and Starling's equilibrium hypothesis. As mention above, according to Bonner-Weir and Orci (1982), in rat islets short arterioles enter the islets at discontinuities of the non-B cell mantle and branch into

capillaries that form the glomerular structure occupying the area of the B cell core. After traversing the B cell mass, capillaries penetrate the mantle as the blood leaves the islets. In small islets, efferent capillaries often pass through exocrine tissue before coalescing into collecting venules. However, in large islets, capillaries coalesce at the edge of the islet and run along the mantle as collecting venules before reaching a vein.

As the authors pointed out, blood first reaches the B cells of the rat and then carries insulin in high concentrations to A and D cells. The B cells are exposed to low titer of systemic glucagon and somatostatin. This microportal vascular system provides for a negative feedback mechanism. It seems likely that insulin can be carried vascularly to the mantle where A, D, and F cells are located. It is also possible that glucagon and somatostatin can be carried via vessels to other parts of the mantle (by short or intra-islet loop). It is also possible that glucagon and somatostatin can be carried thorough portal vascular systems (and/or the systemic circulatory loop) to the B cells in other islets. However, the concentrations of systemic glucagon and somatostatin are diluted a great deal. It is unlikely that glucagon and somatostatin can be carried to central B cells by intra-islet loops (Samols et al., 1983).

According to Starling's hypothesis, the quantity of fluid filtering outward through arterial capillaries will return to

the circulation by reabsorption at the venous ends of the capillaries. In view of the direction of interstitial fluid flow, it is likely that insulin can be carried by interstitial fluid to the mantle. It is also possible that glucagon and somatostatin can be carried via interstitial fluid to peripheral B cells. It seems unlikely, however, that glucagon and somatostatin can reach the central B cell core via interstitial fluid. Although it does not preclude a local diffusion whereby secreted glucagon and somatostatin could create a concentration gradient to influence a deeper layer of B cells via the interstitial fluid.

My studies have shown that the increased number of B cells result in the enlargement of the central B cell core in the islets of 139H-infected hamsters. The distance between D cells in the outer rim and B cells in the central area would be increased. Thus, it might be more difficult for somatostatin (and/or pancreatic polypeptide) to influence B cells in the central area by diffusion in the islets of 139H-infected hamsters. As a result, B cells in the central area would release more insulin to the blood stream due to a decrease in somatostatin inhibition.

Another interesting point is that somatostatin can reduce splanchnic blood flow (Wahren and Felig, 1976). It is possible that somatostatin, either secreted locally or circulating systemically, could regulate islet vasculature thereby influencing islet cell activities.

b. The Roles of Tight Junctions.

Another kind of compartmentalization could be created by tight junctions, which are narrow areas of fusion between homogeneous and heterogenous islet cell types (Orci, 1976). These tight junctions could create barriers within the interstitial spaces such that secretory products could be shunted through specific channels between the cells. By freeze-fracture replica study, Orci (1976) had shown that the islet cell membrane face contained a network of short ridges or fibrils, which are characteristic of tight junctions. These ridges are plastic structures amenable to profound modification under different functional conditions.

My studies have shown that the islet cells undergo a process of cytopathological changes in 139H-infected hamsters, such as cellular hypertrophy, changes in cellular shape and orientation, cellular atrophy and vacuolization. These changes certainly could affect the tight junctions between islet cells.

In my semi-thin section studies, in spite of many dilations of the extracellular spaces between cells, islet cells maintained intimate contacts with each other at several points in both control and 139H-infected hamsters (see Figures 14 and 15). The contact points consisted of a close relationship of the respective islet cell plasma membranes with no intervening extracellular space. Such a zone might

correspond to a tight junction (for reference see Orci, 1976). In my study, these contact points were changed significantly in 139H-infected hamsters compared with control hamsters, such that the zones corresponding to tight junctions were sometimes elongated or did not exist (see Figures 14 and 15).

The effects of cellular hypertrophy and cellular atrophy on tight junctions between cells might be totally different. These effects might be examined in more detail under the electron microscope. Different changes in tight junctions might happen at different stages of the incubation period. The physiologic significance of these changes is not clear.

c. The Roles of Gap Junctions.

The role of gap junctions is another point that should be addressed. Islet cells might communicate with one another through interstitial and vascular spaces, important communication may also occur by direct contact of cells via gap junctions (Meda et al., 1982). These specialized junctions are known to occur not only between homogeneous cell types, but also between heterogeneous cells in the islets (Orci et al., 1975). They occupy a relatively small area of the surface of islet cells compared to other secretory tissues (Meda et al., 1980a). They are not randomly distributed among B cells in that they are less frequent in the center of the

islet B cell core and more frequent in B cells adjacent to the non-B cell mantle (Meda et al., 1980b).

Gap junctions are thought to allow the passage between cells of electrical impulses, ions, cAMP and small molecules of molecular weight 1,200 daltons or less (Simpson et al., 1977). Because many small mediators would transfer through gap junctions and because gap junctions are found not only between homogeneous islet cell types, but also between heterogeneous islet cell types, it is possible that these junctions play an important role in coordinating the function of an entire islet. The fact that cAMP and Ca^{++} can pass through gap junctions means that hormonal stimulation of one or a few cells will initiate a metabolic reaction in many islet cells. It will ensure a synchronized secretory response (Darnell et al., 1986).

In the islets of normal animals, these gap junctions would not only coordinate islet secretion, but also play an important role in islet growth and development or other intra-islet metabolic interrelationships. However, in the islets of 139H-infected hamsters, one can speculate that these gap junctions would transfer signals to stimulate B and A cell proliferation or mitosis, and might transfer pathogenic molecules or other warning signals to the other cells within the islets. I will discuss this later in more detail.

One important aspect of gap junctions is that the channels can be regulated by the concentration of Ca^{++} ion.

Thus, islet cells may modulate the degree of coupling with their neighbor (Darnell et al., 1986). The opening and closing of the gap junctions and the different density of the gap junctions within islet cells might create functional compartmentalization.

Another important fact is that gap junctions may coordinate the electrical activity of the B cells. It is well known that this activity of B cells changes after islets are exposed to insulin secretagogues (Dean and Matthews, 1970). There is evidence that B cells are heterogeneous with regard to granularity and also to the different thresholds which are required for glucose to stimulate electrical activity (Beigelman et al., 1977). Therefore, one can postulate that there are B pacemaker cells which respond to particular glucose concentrations and, in turn, recruit other B cells which otherwise might not have responded to glucose (Meda et al., 1980c). In the studies reported here, B cells were increased significantly in 139H-infected hamsters. The granularity and electrical stimulating threshold of these B cells is unknown. It is also not known what changes happen in gap junctions when the islet cells are changed in 139H-infected hamsters. The potential contributions of gap junctions to the functions and interrelationships among A, B, D, and F cells in the islets of normal and 139H-infected hamsters are unclear. Further insight into these questions awaits future studies with electron microscopy.

d. The Roles of Extracellular Spaces.

Earlier studies have shown that pronase treatment of isolated islets led to an augmentation of glucose-induced insulin release associated with a striking proliferation of tight junctional elements, thus trapping secretory material in pockets of extracellular space (Orci, 1976). These pockets of extracellular space might exist not only between homogeneous cell types, but also between heterogeneous cells. They can store secretion products of the islet cells. In my semi-thin section study, there were many necklace-like chains between islet cells; they were the extracellular spaces. It has been suggested that:

(1) The activity of B cells changes after islets are exposed to insulin secretagogues (Dean and Matthews, 1970).

(2) There are B pacemaker cells which respond to particular glucose concentrations and, in turn, recruit other B cells which otherwise might not have responded to glucose (Meda et al., 1980c).

(3) cAMP and Ca^{++} can pass through gap junctions in B cells which will ensure a synchronized secretory response (Darnell et al., 1986).

(4) There are numerous excytotic stomata in B cell membranes, most of which are situated within the tight junctional domain and are released into the extracellular spaces (Orci, 1976).

(5) After stimulation, the intercellular space is expanded at several places so that large masses of released secretory products may be accommodated. The B cells associated with dense masses appear strongly degranulated (Orci, 1976).

In order to explain the role of the extracellular spaces, my hypothesis is: under normal physiological conditions, as the synthesis of insulin increases in B cells, the volume of B cells would increase and the volume of extracellular spaces would decrease. After a synchronized secretory response from the stimulated B cells, the secretory product would move from the intracellular spaces into the extracellular spaces, the volume of the B cells would be decreased and the volume of the extracellular spaces would be increased. Some of the secretory products might be released into the blood stream, the rest might remain in the enlarged extracellular spaces. The cycle would then repeat starting with increasing synthesis of insulin by B-cells, the volume of B cells would increase and this would squeeze the remaining secretory products out of the extracellular spaces. That is to say, the enlarged extracellular space would serve as a buffer system and a reservoir to collect and store some secretory products for future use. I will refer to this concept as "the accordion effect".

In my study employing semi-thin sections, I saw two types of vacuolization. One type of vacuolization I have called

localized vacuolization (LV). LV is similar to or the same as the intracellular vacuolization seen in the stained paraffin sections. The other type of vacuolization I have called diffuse vacuolization (DV). DV is related to the extracellular vacuolization seen in the stained paraffin sections. DV may span intracellular and extracellular regions of the tissues. DV and extracellular vacuolization might be the result of cell death.

My studies showed that the extracellular spaces were enlarged in the islets of 139H-infected hamsters compared to control hamsters. The islet cell-to-cell contacts were reduced in DV or EV regions. The extracellular spaces in DV region in 139H-infected hamsters were also enlarged. These findings suggest that the synchronized secretory response of B-cells in DV or EV regions is damaged and the accordion effect of the extracellular spaces might not function normally.

These findings should be examined more closely in the electron microscope. These findings also suggest that the islet cells were hyperactive and that, therefore, there were more secretion products trapped in the enlarged extracellular spaces. This, in turn, might affect islet cell functions by autocrine or paracrine effects.

e. The Effects of Blood Vessel Cores (BVCs).

The purpose of this section is to discuss the exchange of substances between the blood and the islet cells and especially to compare the functioning of capillaries with that of the BVCs.

As we know, the pancreatic islets are vascularized by an extensive labyrinth of capillaries. Each islet is normally vascularized by 1-3 arterioles which abruptly terminate into capillaries and 1-6 veinules, depending upon the size of the islet. Morphological studies of the islets indicate that their endocrine cells are arranged in cords or short bands of cells, with each islet cell being adjacent to a capillary. The capillaries present in the pancreatic islets are comprised of fenestrated endothelial cells and the basement membrane (see Norman and Litwack, 1987). The substances exchanged between the blood and the islet cells have to traverse the wall of the capillary. The most important way by which substances are transferred between the plasma and interstitial fluids is by diffusion. For water-soluble substances such as sodium ions, chloride ions, glucose and many hormones, the permeability of the capillary for different substances will depend upon their molecular diameters.

In my studies, I could not find endothelial cells or basement membranes around the BVCs. This indicates that the blood directly contacts the islet cells in BVCs. Furthermore,

I have shown that there are many dilated intercellular spaces between islet cells. Some of which might be as large as the diameter of a capillary (see Orci, 1976). I have also observed that there are channels connecting BVCs and other islet cells. Unless there are unexpected tight junctions that connect all islets cells around the BVCs, it is possible that the plasma would enter into the intercellular spaces and mix with interstitial fluids inside the islets. Many blood components, such as proteins and glucose, might stimulate islet cells directly without passing the capillary wall.

Blood usually does not flow at a continuous rate through the capillaries. Instead, it flows intermittently. The cause of this intermittency is the phenomenon called vasomotion, which means intermittent contraction of the metarteriols and precapillary sphincters (see Guyton, 1981). The blood flow to different areas of the islet is auto-regulated. The vasomotion in the islets might create some sort of physiologic and anatomic compartmentalization. However, in the presence of large BVCs, vasomotion can no longer regulate the large mass of blood in the BVCs.

Another consideration is that the blood volume would increase and blood velocity would decrease in the BVCs. In the normal islet, it can be predicted that there is rapid equilibration between plasma and interstitial fluid. It is difficult to see how modulation in regional islet blood flow in BVCs would create lasting gradients in the concentrations

of secretion products as well as secretagogues of islet cells. Unless there is unexpected re-uptake of secreted peptides by the islet cells, it is possible that the secretion products would accumulate within the islets if the blood flow velocity decreased in the large BVCs. On the other hand, it seems that physiological variations in blood flow could alter islet hormonal secretions. For instance, if there is a particular interstitial space in which a certain concentration of hormone exerted a paracrine, or even an autocrine effect, then a change in blood flow might cause this hormone concentration to either increase or decrease, thereby affecting islet hormonal secretions. In addition, these blood flow changes would also affect oxygen, nutrition, carbon dioxide and metabolic waste exchanges.

f. Cell Polarity and Orientation.

Since the islets of Langerhans contain cords and irregular clumps of cells arranged near capillaries, another consideration is the orientation and polarity of islet cells. Cell orientation and polarity are achieved by specialized contact sites of the plasma membranes of adjacent cells. These contact sites or cell junctions include adhering, impermeable and communicating varieties, which serve mechanical, barrier and transport functions, respectively.

In most epithelial tissues, cells have clear polarity in their orientation, with obvious basolateral and apical surfaces. Thus, it is not surprising that one can sometimes see a columnar-like arrangement of cells in some sections of mammalian islets (Like, 1977). Frequently mammalian D cells have been found to have dendritic-like cytoplasmic extensions extending from one side of the cell (Larsson et al., 1979). Thus, it will not be surprising to eventually demonstrate that islet cells have polarity in their orientation.

Polarity could facilitate compartmentalization in that hormones might be secreted from an apical surface almost directly into a capillary and have very little contact with neighboring cells. Not only secretion, but also receptors might be polar as seen in pancreatic acinar cells. Thus, there may be a domain of the cell surface which has a high receptor concentration and which is sensitive to endocrine, paracrine and autocrine regulation. Other areas of that cell plasma membrane could be deficient in receptors and thus unresponsive to stimulatory peptides in the interstitial space. In my studies, I have shown that the orientation and polarity of some B, A and D cells were changed. In addition, the islets of 139H-infected hamsters showed cellular pathological changes. These changes could disturb the normal receptor domain patterns and other functions such as barrier, transport and communication within the islets thereby disrupting the normal functional activities of islet cells.

3. Effects of Pathological Changes at the Subcellular Level.

Although the sequential gradation of our ability to examine the pathological changes are from higher order to lower order, such as from organ to tissue, from cell to subcellular organelles, pathological changes happen from lower order to higher order, such as from molecular level to subcellular level. The lower the order of changes we study, the more likely we will be able to understand the basis of pathological changes. I will discuss nuclear pathological changes and cell death, pathological pattern synchronism and possible sequential events of the pathological changes in the islets of Langerhans in 139H-infected hamsters.

a. Nuclear Pathological Changes and Cell Death.

The most positive indication that cells are dead is the appearance of their nuclei. The nuclear changes indicating cell death are of three general kinds. The commonest is called pyknosis which entails shrinkage of the nuclear material into a homogeneous and darkly stained mass. In other instances, cell death is indicated by nuclei breaking into fragments; this type of nuclear change is called karyorrhexis. Thus, instead of shrinking, nuclei may completely disintegrate with the ultimate formation of such tiny fragments of nuclear

material that they are sometimes referred to as nuclear "dust". The third appearance presented by nuclei in dead or dying cells is that they dissolve. This type of nuclear change is termed karyolysis (see Ham and Cormack, 1979).

With light microscopy, the islets of 139H-infected hamsters showed clearly some subcellular pathological changes including: cytoplasmic vesicles, and nuclear pathological changes such as swelling, vesicular changes, changes in shape and orientation, vacuolization (IV, EV, LV, and DV), irregular formation, pyknosis, karyorrhexis and karyolysis. These changes indicated that those islet cells were going to die. The reasons for islet cell death are very complicated. In normal conditions, the cell may have many functions including energy generation, homeostatic control, motility, uptake of materials, synthesis, secretion, cell communication, excitability, and reproduction. However, in the abnormal condition, the steady state of the cell would alter; if injury is sufficiently intense and protracted, the cell is unable to maintain its homeostasis at a level sufficient for functional compatibility with life, and cell death results.

b. Pathological Pattern Synchronism.

In my studies, I observed different pathological patterns, such as B-cell proliferation, BVC formation, PPS

formation, IV, EV, LV, DV, cellular hypertrophy, atrophy, changes in cell orientation and polarity, nuclear swelling, ring-form nuclei, pyknosis, karyorrhexis, and karyolysis. These pathological changes occur only in the islets of Langerhans and/or pituitaries of 139H-infected hamsters but not in those of 263K-infected hamsters. From these different patterns of pathological changes, we can find the following phenomena:

(1) Different pathological patterns happen in different tissues or different regions within the same tissue, such as BVCs in the islets of Langerhans (see Figure 10); vacuolization in pars distalis but not in pars intermedia or pars nervosa of the pituitary (see Figure 22); astrocytosis or amyloidosis in the brain of 139H-infected hamsters (see appendix).

(2) Different pathological patterns occur in the same tissue or the same region of the tissue at the same time, i.e. LV, DV, and cellular hypertrophy in the islet of Langerhans in the 139H-infected hamsters (see Figures 13, and 14).

(3) A similar pathological pattern is seen in different tissues or different regions in the same tissue. Some of the evidence is that: (a) EV, cellular atrophy and pyknosis are found in the islet of Langerhans as well as in the pituitary in 139H-infected hamsters (Figures 10 and 22). (b) PPS is seen in the islet of Langerhans, the adrenal medulla and the pituitary in 139H-infected hamsters (Figures 12, 20 and 21).

(4) A similar pathological pattern happens in the same tissue or the same region. As shown in Figure 14 and 15, if you see LV in one cell, you might also find other LVs in nearby cells. This is also true for many pathological changes such as DV (Figures 14 and 15) and cellular atrophy (Figures 11, 12 and 22). I have referred to this phenomenon as "pathological pattern synchronism".

Different pathological patterns can occur in the same tissue or the same region of the tissue at the same time. It is hard to say whether these different pathological patterns are a function of the sequence of events of cell injury or are caused by different pathologic agents. Due to differences in structure and function of the regions affected, it is also possible that different pathological patterns are caused by the same agent. This pathological agent might be (1) endogenous, produced by the cell itself, such as a toxic by-product or "free radicals"; or (2) exogenous, received from outside the cell. Although the agents causing cell injury are unknown, it is possible that the pathologic agents can transmit from one cell to another, thereby causing a domino or a cascade effect in a particular area. The transmission pathway can be gap junctions, endocytosis or other diffusions. If a specific pathological agent can cause a specific pathologic pattern and the agent is transmissible, it may explain the phenomenon termed pathological pattern synchronism.

In neuronal disease, different neurons can be affected by different infectious agents or neurotoxins. Classical examples of this include that paralysis occurs when the specific motor neurons are damaged by poliomyelitis virus, and the dopaminergic neurons are deficit in the substantia nigra in the instance of Parkinson's Disease (see Carp et al., 1992). This specific targeting has been referred to as pathoclisis which can be defined as the selective vulnerability of different neurons to a variety of noxious factors such as various viruses and toxins (see Carp et al., 1992). In my studies, a single scrapie strain 139H can induce different pathological patterns in different organs of a hamster. Since scrapie infectivity titer in these organs (pancreas and adrenals) are extremely low, it is unlikely that scrapie agent directly causes pathological changes in organs outside the central nervous system. The different pathological changes in different organs may be a function of the specific targeting effect of the 139H strain scrapie in the central nervous system (Carp et al., 1990).

c. Possible Sequential Events during Pathological Changes.

In the studies related in this dissertation, one could speculate that the following sequence of events would occur in the islets of 139H-infected hamsters: for some still-unknown

reason, the B cells are stimulated. It is possible that a B cell specific trophic factor is up-regulated within brain or elsewhere which stimulates B cell replication. B cells must have a unique receptor which is not found on A, D, and F cells. These receptors on B cells cause B cell activation and mitosis. Some specific genes in B cells would be activated to initiate DNA synthesis. The B cells entered the cell cycle from G_1 into the S phase, leading to B cell hyperplasia and enlargement of islet size. The increased number of B cells would disturb normal cell-to-cell communication. The cells within the islets would no longer be coordinated with each other. In another scenario, the insulin receptors in brain could be affected so that the brain would not recognize the quantity of insulin in the plasma (I will discuss more later). The work demand from brain to B cells would be increased which would result in the pathological changes of islet cells as follows:

(1) The transcription of specific genes for insulin synthesis would be increased. The transcription of other genes for ribosomes and other cytoplasmic components necessary for protein synthesis would also be increased. This would lead to increased insulin synthesis and release, and also might lead to nuclear swelling.

(2) The increase in insulin and other protein synthesis would increase energy consumption. As a result, the ADP/ATP ratio would increase, the functions of active ion pumps in the

cell membrane would decrease, and ion concentrations in the cytoplasm would increase. At the same time, glycolysis would increase, there would be lactate accumulation, and intracellular pH would decrease. All of these would increase intracellular osmolality, and increase water influx, resulting in islet cell hypertrophy. The islet cells might also change shape and orientation.

(3) Increases in B cell proliferation, increases in insulin and other protein synthesis would increase oxygen consumption. As a result, blood supply would have to be increased to meet increasing demand. Meanwhile, tissue histamine might be released as cell injury was initiated. Histamine can cause dilatation of capillaries and increase the permeability of blood vessels. Capillaries would be stimulated and enlarged, with some forming the BVCs that were observed.

(4) As injury progresses, the islet cells could no longer stand the severe damage. The swelling of lysosomes would cause the permeability of the lysosomal membranes to increase and release hydrolases. Most of the subcellular organelles would be destroyed, leading to cellular and nuclear vacuolization, cellular atrophy, clumping of nuclear chromatin, pyknosis, karyorrhexis, and karyolysis.

(5) The degenerative products from cell damage and death can cause chemotaxis of both neutrophils and macrophages. In these studies, I have seen increasing margination and

diapedesis of macrophages through the membrane of large BVC in the islets of 139H-infected hamsters. This study suggests that the neutrophils and macrophages are going into the islets to clean up the debris of cellular disintegration.

4. Margination and Diapedesis of Inflammatory Cells.

In addition to observations that a single lymphocyte or a single macrophage can migrate through the wall of postcapillary venules, it has been shown that a group of two or more lymphocytes or a group of mixed lymphocytes and macrophages or other inflammatory cells can migrate through the wall of postcapillary venules (Castenholz, 1990; Simon, 1979). The intimate contact between inflammatory cells and the wall of postcapillary venules is not a simple process. One obstacle to intimate contact of membranes is that the surface of normal mammalian cell membranes, including peripheral blood cells, possess a uniform negative membrane charge (Weiss, 1985). It is also known that the surface of the endothelial cells possess a uniform negative charge (Danon et al., 1972; Nagy et al., 1983; Skutelsky et al., 1976). Several studies have suggested that sialic acid groups (Simionescu and Simionescu, 1986) and sulfated glycosaminoglycans rich in heparin sulfate (Simionescu et al., 1981) represent the most common constituents which contribute

to membrane anionicity. Another obstacle to cell-to-cell contact is the high negative surface charge of the phosphate groups on phospholipids and on sialic acid residues found in cell surface glycolipids. Therefore, the mechanism of interaction between inflammatory cells and the walls of postcapillary venules is still not clear.

It has been shown that lymphocytes can come into close contact with one another and also with reticulum cells and macrophages (Castenholz, 1990; Shelton and Rice, 1959; Sundberg and Downey, 1955; Sundberg, 1960). Groups of lymphocytes can surround a macrophage, attaching to it intimately (Shelton, 1962). This phenomenon has been described as "peripolesis" in lymph nodes and spleen (Sharp and Burwell, 1960). This phenomenon can be interpreted as a sign of an exchange of information between both types of cell.

In earlier studies, by means of time-lapse cinemicrography of tissue cultures, an association between lymphocytes and cells in mitosis, megakaryocytes and malignant cells, had been recorded by Humble, Pulvertaft and their colleagues (Humble et al., 1956). This process has been termed "emperipolesis" _ "inside round-about-wandering". A functional significance for this was not proposed.

In the present studies, I have observed another phenomenon: the interaction between groups of macrophages and/or other inflammatory cells with B-cells at the wall of BVCs. I referred to this phenomenon as "linkage reaction";

this group of macrophages or inflammatory cells as "linkage-macrophages" or "linkage-inflammatory cells".

The significance of the linkage reaction is not clear at this time. It may be suggested that:

(1) During touching or fusing of cellular membranes a very intense exchange of information occurs that is necessary for a specific defense response in the immune system as in peripolesis and emperipolesis (see Castenholz, 1990).

(2) The intimate contact between inflammatory cells and B-cells at the wall of BVCs means that surface receptors were activated or surface charges were changed or both.

(3) When leukocytes and monocytes reach the basement membrane, the membrane is lysed by collagenase-type enzymes (Cochrane and Aikin, 1966). The migration of macrophages into islet tissues can be considered an energy-consuming process. If one macrophage opens a pathway from BVC into islet tissues, other linkage-macrophages can follow the same pathway into the islet. In addition, macrophages may act like a multi-locomotive and have a push-pull effect. Therefore, they may save a great deal of energy.

(4) The ultimate function of a macrophage is phagocytosis, clearing inflamed territory of all necrotic debris and foreign particles. If a group of macrophages work together to clean up the debris, they may increase their survival rate by decreasing the possibility of over-phagocytosis.

5. Pathological Changes at the Molecular Level.

First of all, abnormal depositions in the islets are regarded as important features of pathological phenomena. They provide an image of the interrelationship between those abnormal molecular products and the pathological changes at the molecular level. There are several different kinds of pathological changes associated with depositions in the pancreatic islets.

a. Hyaline Change and Amylin.

Hyalinization of the pancreatic islets has been described for many years and is now generally considered the most typical pancreatic lesion in diabetes mellitus. Gellerstedt (1938), chiefly on the basis of studies with the methyl violet reaction, concluded that hyaline is actually amyloid and the condition should be called "insular para-amyloidosis". Schwartz (1965) using fluorescent dyes such as thioflavin-T confirmed that hyaline deposits in islets represent a manifestation of senile amyloidosis which was also found in the brain and heart. Under electron microscopy, the amyloid appears as tightly packed fibrillar bundles which extend into deep recesses in the cells, formed by infolding of the cell

plasma membrane. Lacy (1964) had found the same type of fine fibrillar structures in hyaline material in islets.

Although the presence of hyaline (amyloid-like material) was first noted in the specimens of human pancreas as early as 1901 by the pathologist Opie, it was not until 1986 that efforts to solubilize this material were successful (see Nishi et al., 1990). This amyloid is neither the same as the amyloid found in Alzheimer Disease (AD), nor the amyloid found in scrapie-like diseases. It is related to the 37-amino acid neuroendocrine peptides, calcitonin gene-related peptides (CGRP) 1 and 2 (see Cooper et al., 1987). It is called islet amyloid polypeptide (IAPP) or amylin.

Amylin is synthesized in and co-released with insulin from the B-cells of the islets of Langerhans (see Banks, 1990). Amylin is a novel hormone which may control carbohydrate metabolism in partnership with insulin and other glucoregulatory factors (see Cooper et al., 1990). Amylin inhibits insulin-stimulated glycogen synthesis in skeletal muscle, while leaving insulin-stimulated carbohydrate metabolism in adipose tissue unchanged (Cooper et al., 1990).

In well-nourished mammals, the body requires nutrients sufficient to provide energy and substance for immediate requirements and storage. Usually, the excess dietary carbohydrate is converted to glucose and then either initially stored as glycogen for later use or converted to fatty acids for longer-term storage as triacylglycerol in adipose tissue.

The major sites of glycogen storage in the body are liver and skeletal muscle. Skeletal muscle accounts for 40% of the total body mass, therefore, it has the greater capacity for glycogen storage. After feeding, if the rate of glycogen synthesis in skeletal muscle is decreased by amylin, glucose will either be diverted into triacylglycerol storage in adipose tissue, which in pathological situations may lead to obesity, or will remain in the blood and result in hyperglycemia, as in non-insulin-dependent diabetes mellitus (NIDDM) (see Cooper et al., 1990).

It is interesting to point out that 139H-infected hamsters show hyperinsulinemia and obesity (Carp et al., 1990) (in these studies, the body weight was increased significantly from 205.8±9.9 g in control animals to 262.4±4.9 g in 139H-infected hamsters). In my studies, I did not find amyloid formation in the islets of 139H-infected hamsters by Congo red or thioflavin-S staining. Based on the fact that their amino acid sequences are different, only some mammals such as cats, raccoons and humans form amyloids in islets. Neither rat amylin, nor any of the CGRPs are known to form amyloids in vivo (see Cooper et al., 1990). It is not surprising that we can not find amyloid formation in the islets of 139H-infected hamsters. However, since (1) 139H-infected hamsters show hyperinsulinemia, and a significant increase in B-cells and (2) amylin is co-localized and co-released with insulin in B-cells, it is possible that the synthesis and release of amylin

from B-cells is also increased in 139H-infected hamsters. It would be interesting to determine comparative amylin concentrations in 139H-infected and control hamsters and to assess its role in induction of obesity in 139H-infected animals.

b. PAS-positive Substance (PPS).

Using PAS and Orange G stain, I found deposits of PPS in the islets of Langerhans, the adrenal medulla, the pituitary and the blood stream of 139H-infected hamsters. I did not see PPS deposits in control hamsters. This substance is located both inside and outside cells in the endocrine organs. At this time we cannot definitely say whether or not PPS is amylin. At present, amylin is only found in B-cells in islets, however, PPS is found in the islets, adrenal medullas and pituitaries in 139H-infected hamsters. Unless amylin can also be produced and/or taken up from blood by cells of the adrenal medulla and of the pituitary, there is no reason to presume that PPS is amylin. The significance of PPS in the pathological changes found in these organs is still not clear. Further experiments should be done to identify the nature of PPS and the occurrence of PPS in different organs in various stages of the scrapie incubation period.

c. Fibrosis.

Next to hyalinization, the most frequent pathological change in islets is fibrosis. It is present primarily in the atrophic type of islet. In the present study, when pancreatic sections were stained with Gomori's one step trichrome, which yields a blue-green color with collagen fibers, a few of the islets of Langerhans in 139H-infected hamsters showed fibrosis. The areas of fibrosis are located around the elongated islet cells. Fibrosis might help to change islet cell shape and orientation. Fibrosis might also impede cell-to-cell communication within the islets. The cause of fibrosis in the islets is difficult to explain. It could be partly due to islet inflammation and to a collapse of the framework of the islets after the disappearance of B cells.

d. Insulin Bioactivity.

Another interesting question concerns the optical density of insulin immunostaining. I used two very useful tools in our immunostaining studies: (1) the immunostains were done with the Histomatic Slide Stainer-Code On Series (Fisher Scientific) technique, which can standardize the immunostaining intensity. (2) since our human visual system can not accurately quantitate optical density of immunostains

and the background density of the slides, the Quantimet 970 image analyzer was used to accurately quantitate the optical density of objects. These studies showed that the optical density of insulin immunostaining cells was decreased in 139H-infected hamsters compared to that of control animals. It suggested that either the concentration of insulin in B granules was decreased or the number of B granules was decreased, or both.

Based on the fact that hamsters infected with the 139H scrapie strain were only moderately hypoglycemic but showed marked hyperinsulinemia (values of immunoreactive insulin (IRI) as much as 49X higher than those seen in control animals, Carp et al., 1990), it is possible that B cells release insulin molecules more quickly in 139H-infected hamsters than in control animals. Those insulin molecules might not have enough time for post-translational modification. That is to say, B cells may be releasing insulin molecules prematurely in 139H-infected hamsters and therefore the bioactivities of these insulin molecules would be affected.

Usually, proinsulin (PIn) levels are 5-15% of IRI in normal individuals. The levels of PIn can be substantially elevated in patients with NIDDM, islet cell tumors, or chronic renal failure. Recently, Saad et al. (1990) reported PIn accounted for 50% of the total IRI in some NIDDM patients with severe hyperglycemia. Current insulin RIAs possess high

cross-reactivity to PIn and thus over-estimate insulin values. A specific assay for the measurement of true insulin levels is now available (Linco Research, Inc. St. Louis). The results of my studies suggest that:

(1) Either the optical density of B granules will be decreased or the number of B granules will be decreased (B cells degranulation) or both. This can be investigated in detail under the electron microscope.

(2) The percentage of true insulin in total IRI will be decreased in 139H-infected hamsters compared to control animals. Total IRI can be measured with insulin RIAs and true insulin can be measured with specific insulin assays, or other methods, such as Western blot.

D. Interrelationship between Pathological Changes in Islets and in the Central Nervous System

Compared with other endocrine organs, the regulation of islets of Langerhans by the central nervous system is most complex. The purpose of this section is to discuss the possibilities of the interrelationships between Pathological Changes in the Islets and the Central Nervous System.

1. The Pituitary.

The pituitary is generally considered to be structurally and functionally the most complex organ of the endocrine system. It controls many endocrine glands in the body. In these studies, coronal sections of the pituitary were stained with hematoxylin and eosin, and were examined with light microscopy. The scrapie strain 139H-infected hamsters showed extensive vacuolization in the pituitary. Most vacuoles were located on the ventral and/or ventrolateral parts of the pars distalis. The pituitaries of 139H-infected hamsters also showed cellular hypertrophy, cellular atrophy, and cytoplasmic vesicles. There were nuclear pathological changes such as swelling, vesicular changes, pyknosis, karyorrhexis and karyolysis. The cellular and nuclear pathological changes were most pronounced in the regions with vacuolation. The pathological changes found in the pituitary in 139H-infected hamsters were not seen in 263K-infected hamsters. These data suggest that the pathological changes found in the pituitary in 139H-infected hamsters might play an important role in the severe generalized endocrinopathy seen in these animals.

Using PAS and orange G stain, we noted PPS in grape-like or plaque-like forms located in the pituitary in 139H-infected hamsters but not in control hamsters. This substance is located both inside and outside the cells in the pituitary. The significance of PPS in the pathological changes in the

pituitaries of 139H-infected hamsters is still not clear. We also found PPS in the islets of Langerhans of 139H-infected hamsters. The relationship of PPS in the pituitary to PPS in the islets is not clear at this time.

In the present studies, the number of cells immunostained with antibodies to different hormones noted below (except GH) were decreased in the vacuolated areas in 139H-infected hamsters. This indicates that the pituitary in 139H-infected hamsters can no longer function normally. This might affect a number of endocrine organs including the islets of Langerhans in these animals.

The synthesis and secretion of many pituitary hormones such as PRL, FSH, LH, ACTH, and GH are influenced by a variety of stimuli (eg. sleep, stress) and, are episodic and pulsatile. Plasma levels of many pituitary hormones such as LH, FSH, PRL, and GH levels can be changed very large degree within a few minutes. This is especially true in female hamsters because of the estrus cycle. This may explain the high levels of variation seen in immunostaining patterns within the same group of animals in these studies.

2. The Hypothalamus.

The hypothalamus is a very important control organ for the neuroendocrine system. Hypothalamic hormones are released

from the hypothalamic nerve fiber endings around the capillaries of the hypothalamic-pituitary system in the pituitary stalk and reach the anterior lobe through the special portal system. In addition, hypothalamic-releasing factors can stimulate the synthesis and release of pituitary tropic hormones, which can regulate the activities and functions of other endocrine target organs.

a. The CRF and VP Systems.

We know that CRF produced in the hypothalamus has a hormonal function which stimulates production and release of ACTH in the pituitary. Several reports showed that CRF levels are decreased in regions other than the hypothalamus in AD. Using radioimmunoassay techniques, Whitehouse et al. (1987) showed that CRF levels were lower in frontal, temporal and occipital regions of the neocortex. In another study, CRF immunostaining was reduced in the amygdala and cortex of AD patients, while in these same patients there was an up-regulation of CRF receptors in the cerebral cortex. These same authors found a dramatic increase in CRF immunostaining of perikarya and axons located in the paraventricular nucleus of the hypothalamus.

In the present studies, there was a significant increase in the number of CRF immunostained neurons in the hypothalamus

(preoptic area) in 139H-infected hamsters compared with those in control animals. One possible explanation of the increase in ir-CRF neurons is a complementary effect related to the reduction in ir-ACTH cells in the vacuolization areas of the pituitary that has been seen in 139H-infected hamsters.

There was a significant decrease in the area of VP immunostained neurons in the lateral hypothalamus (LHy) of 139H-infected hamsters compared with control animals, but there was no significant difference in the DMH and SON. This study suggests that mineral metabolism might be disturbed in 139H-infected hamsters. All these studies indicate that the hypothalamus-pituitary system is affected by infection with the 139H scrapie strain.

b. The CLIP and Insulin-secretion-promoting Factor Systems.

It has been shown that in genetically obese mice (ob/ob) a hormone is located in the pars intermedia lobe of the pituitary which stimulates insulin release. It cross-reacts with an antiserum directed against the C-terminal portion of ACTH, suggesting that it may be related to corticotropin-like intermediate peptide (CLIP), the 18-39 amino acid fragment of ACTH. This hormone has been named B-cell tropin and is present in the plasma of ob/ob mice. It potentiates glucose-

induced insulin secretion. The intermediate lobe is poorly vascularized and is not reached by the portal system. Thus, it is not affected by CRF. This tissue also has no glucocorticoid receptors, thus glucocorticoids do not regulate POMC release in the intermediate lobe. CLIP is regulated by the hypothalamic-dopamine system.

It has also been found that there is hypothalamic origin of an insulin-secretion-promoting factor which stimulates insulin release. It is a thermostable polypeptide with a molecular weight of 1000 Daltons which is released from the ventral hypothalamus (Bobbini-Harsch and Jeanrenaud, 1989).

Recently, it has been shown that a significant decrease in tyrosine hydroxylase (dopaminergic) immunoreactive neurons in hypothalamus in mice infected with canine distemper virus. These mice are also induced obesity by the virus (Nagashima et al., 1992). It would be interesting to know whether the insulin secretion promoting factor systems and the hypothalamus-CLIP system are affected in 139H-infected hamsters.

c. The Insulin Receptor System in Brain.

It has been known for many years that a lesion in the ventromedial hypothalamus can cause obesity in rats, however, the mechanism of this hypothalamic obesity is still not clear.

Recent studies showed that in the central nervous system there are two types of insulin receptors: one type is on neurons, the other is on glial cells. The neuronal receptors are slightly smaller than both the glial cell insulin receptors and insulin receptors on other insulin target tissues, such as fat cells or liver (see Lattemann, 1989). In muscle, fat, and other target tissues, receptors detect tiny amounts of insulin and then send the signal that causes "doors" to open for glucose. In brain, nerve cells do not have insulin-regulated plasma membrane "barriers". They are permeable to glucose without the intermediation of insulin. The neuronal insulin receptors do not help glucose to enter nerve cells, instead, they help send signals to control eating behavior. It has also been shown that there are insulin receptors in an area of hypothalamus that help regulate food intake (see Lattemann, 1989).

Although the central nervous system is protected by "blood-brain-barrier" against moment-to-moment fluctuations of insulin levels, circulating insulin does reach the brain by way of the cerebrospinal fluid. There is evidence that when insulin reaches the brain in rat, it can actually provide a signal that says, "Stop eating" (Lattemann, 1989). If the evidence does turn out to be applicable to hamsters, the extremely hyperinsulinemia and the obesity in 139H-infected hamsters suggests that:

(1) The insulin has trouble to enter into the brain or

the bioactivity of the insulin decrease.

(2) The insulin receptor system is damaged by 139H scrapie infection.

My study suggests that the lesion in the hypothalamus might also contribute to the obesity in the 139H-infected hamsters. It is also possible that the insulin receptor system in the hypothalamus is affected by scrapie infection.

3. Innervation of the Islets of Langerhans.

The major neural connection between the central nervous system and the endocrine pancreas is from the ventral hypothalamus via the autonomic nervous system. The efferent output of the autonomic nervous system from the hypothalamus is via the dorsal motor nucleus of the vagus and the sympathetic system in the spinal cord.

Parasympathetic neurons were found in the medial two-thirds of the dorsal motor nucleus and in the rostral pole of the nucleus ambiguous. Preganglionic sympathetic fibers in the splanchnic nerves have synapses with postganglionic neurons in the celiac ganglion. Axons from these neurons travel to the pancreas in the mixed pancreatic nerve which follows the arterial system. Nerve terminals end blindly 20-30 nm from islet cells. It suggests that neurotransmitters released from these nerve endings diffuse through the

extracellular space of the islet and may affect several types of endocrine cells simultaneously (Roy et al, 1981). This diffusion may in turn be regulated by tight junctions which have been shown to vary, depending upon the functional status of the islet (Miller and Horton 1979; Roy et al, 1981).

There are at least four basic types of axon terminals within the islet i.e., cholinergic, adrenergic, serotonergic and peptidergic terminals. The cholinergic, adrenergic and peptidergic axon terminals are all found in relation to A cells (Roy et al, 1981). The serotonergic nerve fibers are seen in islets (Kirchgessner and Gershon, 1990). The same axon can innervate more than one islet cell and even more than one islet secretory cell type, however, there may be preferential distribution of a given type of nerve terminal to a specific population of islet cells. Lundquist and Ericson (1978) have reported that, in the mouse, most adrenergic terminals innervate A cells. Stimulation of the sympathetic nervous system or application of epinephrine can likewise stimulate glucagon production and inhibit insulin secretion. Epinephrine can inhibit glucose induced secretion of insulin from the B islet cells by stimulating α_2 receptors. Nerves which contain cholecystokinin (CCK), VIP, substance P, somatostatin, and enkephalin were noted to be primarily associated with A cells and they can affect glucagon secretion (Larsson et al., 1978; Larsson, 1980; Smith and Madson, 1981).

It has been known that a lesion in the ventromedial

hypothalamus (the "satiety center") will increase the efferent parasympathetic activity (Bray et al., 1981). Acetylcholine released from vagus nerve can stimulate B-cell activity and lead to insulin secretion and inhibition of glucagon secretion. It is possible that the increased insulin and amylin synthesis and release from B-cells in the islets can induce hypothalamic obesity. I do not know whether this also occurs in scrapie-induced obesity in the hamsters. Furthermore, it is not known if there are pathological changes in nerve terminals; this issue will be resolved by use of the electron microscope to assess the ultrastructure of nerve endings.

4. The Galanin System.

Insulin secretion from B-cells is stimulated by glucose. After glucose application, a slow wave of depolarization, due to the closure of ATP-sensitive K^+ channels by elevated levels of intracellular ATP, evokes a cyclical pattern of electrical activity. Calcium, which then enters the B-cell through voltage-dependent calcium channels during depolarization, triggers insulin release (see Beigelman et al., 1977; Weille et al., 1988).

Recently, it has also been shown that galanin, a 29-amino acid hormone, known to inhibit insulin secretion and to cause

hyperglycemia, activates ATP-sensitive K^+ channels in a rat insulin-secreting cell line (Weille et al., 1988). Galanin-like immunoreactivity (ir-Gal) is widely distributed in central and peripheral neurons of several mammalian species including humans, nonhuman primates, dogs, cats, cows, and various rodents (Rokaeus, 1987). In addition, it has been found that: (1) Ir-Gal is a secreted product of rat anterior pituitary cells (Kaplan et al., 1988). (2) A dense network of ir-Gal nerve fibers has recently been demonstrated in association with the islets of Langerhans (Dunning et al., 1986). (3) A 53- to 55-kDa peptide has been isolated from the cell membrane fraction of rat brain and a hamster pancreatic B-cell tumor that selectively binds radio-labeled galanin with high affinity. These results are consistent with a role as a galanin receptor protein (Servin et al., 1987; Amiranoff et al., 1987). All these suggest that galanin may function as a neurotransmitter and as an additional anterior pituitary hormone. In future studies it will be important to determine whether there are defects in galanin receptors in the brain and islet B-cells of 139H-infected hamsters. Since there are extensive vacuolization in the pars distalis of the pituitary and enlargement of the islets in 139H-infected hamsters, it will also be interesting to investigate whether the synthesis and release of galanin are decreased in the anterior pituitary and/or in the neurons with fibers associated with the islets of Langerhans in 139H-infected hamsters.

E. Summary

(1) In these studies, using the Quantimet 970 image analyzer system, I quantitated the changes in size and number of the pancreatic islet profiles.

(2) I determined the immunostaining area, the ratio and the percentage changes of A, B, D and F cells in the pancreatic islet profiles in 139H-infected hamsters. The results indicated that the increase in B cells could serve as a major component in the enlargement of pancreatic islets and play an important role in the hypoglycemia-hyperinsulinemia seen in hamsters infected with the 139H scrapie strain.

(3) The optical density of insulin immunostaining cells was less in 139H-infected hamsters than in control animals. It suggested that either the concentration of insulin in B granules was decreased or the number of B granules was decreased, or both.

(4) I observed histopathological changes in the islets of Langerhans in hamsters infected with the 139H scrapie strain; the changes included fibrosis, vacuolization (IV, EV, LV and DV), cellular atrophy, cellular elongation, changes in cell shape and orientation. There were also nuclear pathological changes such as swelling, changes in shape, pyknosis, karyorrhexis and karyolysis.

(5) The vascular pattern was disturbed significantly in the islets of 139H-infected hamsters. There was a large mass

of blood cells which did not appear to be surrounded by traditional arterial, venous or capillary wall cells. I refer to this structure as "blood vessel core" (BVC). These structures were almost always centrally located within islets and were surrounded by B cells, some of which were elongated abnormally.

(6) Using semi-thin sections stained with toluidine blue, I observed cytoplasmic vesicles and nuclear vacuolization in 139H-infected hamsters. I also observed margination and diapedesis of inflammatory cells (macrophages or lymphocytes) through the membranes of B cells surrounding the BVCs in 139H-infected hamsters. I observed another phenomenon: the interaction between a group of macrophages and/or other inflammatory cells with the B-cells at the wall of BVCs. Some of these inflammatory cells form a ball shape like structure inside the islets. I refer to this phenomenon as "linkage reaction"; this group of macrophages or inflammatory cells as "linkage-macrophages" or "linkage-inflammatory cells".

(7) I observed histopathological changes in the pituitaries of hamsters infected with the 139H scrapie strain. The pituitaries of 139H-infected hamsters showed extensive vacuolization, with most vacuoles located in the ventral and/or ventrolateral parts of the pars distalis. The pituitaries of 139H-infected hamsters also showed cellular hypertrophy, cellular atrophy, and cytoplasmic vesicles. There were nuclear pathological changes such as swelling,

vesicular changes, pyknosis, karyorrhexis and karyolysis. The cellular and nuclear pathological changes were most pronounced in regions with vacuolation. Some of these changes were also seen in hamsters infected with the 263K strain of scrapie, but at a much reduced incidence.

(8) Using PAS and orange G stain, I noted an abnormal PAS positive substance in grape-like or plaque-like forms located in the pituitary, islets of Langerhans, adrenal medulla, and blood stream in 139H-infected hamsters but not in control hamsters. This substance is located both inside and outside cells in the endocrine organs. I refer to this PAS positive substance as "PPS". Using Congo red and thioflavin-S stain, I could not find evidence of amyloid formation in islets and pituitaries of 139H-infected hamsters.

(9) I observed that the immunostaining patterns of different hormones were changed in the pituitaries of hamsters infected with the 139H scrapie strain. Using antibodies to a number of hormones, I noted a marked decrease in the number of immunostained cells in the areas showing vacuolation in 139H-infected hamsters. This indicated that the pituitaries in 139H-infected hamsters can no longer function normally. This might affect a number of endocrine organs including the islets of Langerhans in these animals.

(10) There was a significant increase in the number of CRF immunostained neurons in 139H-infected hamsters compared to control animals. There was a significant decrease in the

area of VP immunostained neurons in the LHy of 139H-infected hamsters compared to that of control animals, but there was no significant difference in the DMH and SON region.

The islets of Langerhans in 139H-infected hamsters undergo extensive histopathological changes. I have discussed:

(1) The changes in the potential interactions between islet cells; pathological changes in the islet architecture.

(2) The effects of pathological changes at the cellular level; the islet vasculature pattern and Starling's hypothesis; the potential roles of tight junctions, gap junctions, extracellular spaces, BVCs, and cell polarity and orientation.

(3) Possible effects of the pathological changes at the subcellular level, nuclear pathological changes and cell death, pathological pattern synchronism, possible sequential events during pathological changes.

(4) Margination and diapedesis of inflammatory cells; pathological changes at the molecular level, hyaline change and amylin, PPS, fibrosis, insulin bioactivity.

(6) The interrelationship between pathological changes in islets and changes occurring in the central nervous system, the pituitary, the hypothalamus, the CRF and VP system, the CLIP and insulin-secretion-promoting factor systems, the insulin receptor system in brain; innervation of the islets of Langerhans and the galanin system.

F. Conclusion

I have learned a great deal from the study of the pathological changes in the islets of Langerhans in hamsters infected with the 139H strain of scrapie. Although the pancreatic islet is a tiny organ, it comprises a very complicated system with regard to architecture, vascular system, and cell-to-cell communications.

The study of the islets of Langerhans in 139H-infected hamsters can allow us to use knowledge of physiology, histology, pathology, molecular cell biology, and neuroendocrinology to explain the pathological changes in the islets of Langerhans.

These studies will help us relate the pathological changes to the aberration in insulin biosynthetic pathways and will enlarge our knowledge of the causes and pathogenesis of human diseases involving insulin dysfunction such as diabetes, obesity, and nesidiodysplasia and/or nesidioblastosis of infancy. Further studies of the pathological changes of the islets of Langerhans and the interrelationship with pathological changes in the central nervous system in 139H-infected hamsters can enlarge our understanding of the mechanisms of scrapie-induced changes in the periphery, particularly in endocrine organs.

APPENDIX

Scrapie-infected animals can be used as a unique model to study human diseases such as Alzheimer disease (AD), non-insulin dependent diabetes mellitus (NIDDM), obesity, and nesidiodysplasia and nesidioblastosis of infancy. Scrapie-infected animals show astrocytosis, microgliosis, amyloid formation, neuronal death, and neurite degeneration in the brain. Many of these pathological changes are also seen in AD. Hamsters infected with the 139H scrapie strain also show obesity, hyperinsulinemia, and pathological changes in the islet of Langerhans, which are characteristics shared with NIDDM. If we can understand the mechanisms of the pathological changes shared by these human diseases and scrapie, it will certainly help us to elucidate the pathogenesis of these human diseases and perhaps to devise therapeutic strategies for them.

In order to use animals as a model to study human diseases, I have proposed two research projects: the first one **"The Electron Microscopy Study of Pathological Changes in the Islets of Langerhans in Hamsters Injected with the 139H Strain of Scrapie"** to New York State Department of Health Diabetes Program, Health Research Council Postdoctoral Fellowship Program; the second one **"Effects of NGF and bFGF on Brain Pathology in Scrapie"** to American Health Assistance Foundation, Alzheimer's Disease Research.

The hypotheses of my first project are that:

(1) The electron optical density of B granules will be decreased or the number of B granules will be decreased (B cells degranulation) or both. This can be investigated in detail under the electron microscope.

(2) The percentage of true insulin in total IRI will be decreased in 139H-infected hamsters compared to control animals. Total IRI can be measured with insulin RIAs and true insulin can be measured with a specific insulin immunoassay, or other methods such as Western blot can be used.

The long term objective of my second project is to use scrapie animals as a model system to investigate the interrelationship between trophic factors and pathological changes such as gliosis, amyloid formation, and neuronal and neurite degeneration in the brain.

In both AD and scrapie, astrocytosis, microgliosis, neuronal and neurite degeneration and neuritic amyloid plaques are found in the brain. In addition, there is a pronounced loss of cholinergic neurons of the basal forebrain in AD. These neurons are located in specific areas. Their axons project to the hippocampus and cortex. This population of neurons is trophically affected by nerve growth factor (NGF) and basic fibroblast growth factor (bFGF). A large body of evidence supports the view that these cholinergic neurons are involved in functions related to cognition and memory. In rodents and primates, lesions of cholinergic neurons in the

septum and nucleus basalis or of their respective projections to the hippocampus and cortex result in deficits in learning and memory. However, the relationship among trophic factors, astrocytosis, microgliosis, plaque formation, and neuronal and neuritic degeneration in AD and scrapie is still uncertain. There are still arguments with regard to the importance of amyloid plaques in AD and scrapie pathogenesis.

Amyloid formation is a common pathological hallmark in many neurodegenerative diseases in humans and animals. In AD and in Down's syndrome, degeneration of certain nerve cells is accompanied by the formation of amyloid plaque cores in the brain, and amyloid deposits in blood vessels. The amyloid protein called A4 is derived from three large precursor proteins called b-amyloid precursor protein(s) (APP). In slow infectious diseases, such as scrapie of sheep, bovine and rodents, and Creutzfeldt-Jakob disease (CJD), Gerstmann-Straussler-Sheinker syndrome (GSS) and Kuru in humans, neurodegeneration is also accompanied by the amyloid-like filaments composed of proteinase K resistant protein called PrP^{Sc}. PrP^{Sc} is not the same as amyloid A4 in AD; it is from a precursor protein called PrP^{c}, but both APP and PrP^{c} are membrane-associated proteins. The physiological functions of APP and PrP^{c} are not known. The reasons for the increase in amyloid plaque formation in these neurodegenerative diseases remains unclear. The roles of abnormal amyloid protein A4 and PrP^{Sc} in neurodegeneration in AD and scrapie disease,

respectively, are still being debated. In both AD and scrapie, the contribution of bFGF and interleukin-1 (IL-1) to gliosis, and the potential contribution of gliosis to amyloid plaque formation are not known. It is also not clear if there is an effect of amyloid protein on neuronal and neuritic degeneration during neurodegenerative changes in these two diseases. The relationships between gliosis, vacuolation, plaque formation, neuronal and neurite degeneration during scrapie infection are not known. NGF and other trophic factors such as bFGF, acidic fibroblast growth factor (aFGF), and IL-1 are trophic factors for neurons and/or glial cells. Recent evidence suggests that AD and its hallmark, amyloid plaques, may involve an imbalance of trophic support. My hypotheses are:

(1) bFGF and IL-1 levels are increased in some astrocytes and/or microglia in brain during scrapie infection.

(2) Increased levels of bFGF could have effects on astrocytes and microglia cells, thereby causing astrocytosis and microgliosis.

(3) Neurons, astrocytes and/or microglia can produce amyloid protein during scrapie infection. However, gliosis plays an important role in amyloidosis during scrapie infection.

(4) Amyloid protein has a trophic effect on astrocytes and microglia which in turn induces more BFGF, thereby inducing more glial cells, and thus more amyloid, altogether

producing a "snowball effect". Amyloid protein (PrP^{Sc}) also has a neurotoxic effect on neurons and neurites, thereby causing neuronal and neurite degeneration and vacuolization.

(5) Experimental modulation of trophic factors (e.g. NGF, BFGF) in scrapie infected animals should affect PrP^{Sc} levels, histopathological changes, incubation periods and perhaps survival rates.

My preliminary studies outlined below support these hypotheses:

(1) Histopathological changes were found in the brain in hamsters infected with 139H- and 263K- and in mice infected with ME7. The changes include vacuolization, gliosis, neuronal and neurite degeneration, especially in cortex and hippocampus.

(2) By using Holzer stain and GFAP immunostain, I found extensive astrocytosis in both 139H- and 263K- infected hamsters.

(3) By using thioflavin-S stain, which has been used clinically for diagnosis of amyloidosis, I found that there were many thioflavin-S positive cells, both neurons and glial cells, in the brains of 139H-infected hamsters and in ME7-, 139A-, and 22L-infected mice. In 263K-infected hamsters, there were few thioflavin-S positive cells; however, there were many thioflavin-S positive plaques around the pia mater, the corpus callosum, fimbria, ventricles and blood vessels. There was no positive staining in control animals.

(4) More recently, by using antibodies to PrP ($ME7^{\#3}$, and 3F4, these antibodies were developed by Dr. Kascsak in our Department), I found that PrP immunoreaction was increased in nuclei of some neurons and glial cells, and around pia mater, the corpus callosum, fimbria, ventricles and blood vessels in 263K infected hamsters. In 139H-infected hamsters, PrP immunoreaction was increased in plaques around the pia mater, the corpus callosum, fimbria, ventricles, and blood vessels, but not in cells. In control hamsters, there was no PrP immunoreaction. These studies suggest that there are different isoforms of PrP.

(5) By using antibodies to NGF or bFGF, I found that compared to control hamsters, NGF and bFGF immunoreactivity was increased in some neurons and glial cells in 263K- and 139H- infected hamsters, especially in the cortex and hippocampus.

Scrapie infected animals can be used as a model to study AD because these animals also show astrocytosis, microgliosis, amyloid formation, neuronal death, and neurite degeneration in the brain. If we can understand the relationship between trophic factors and the pathological changes shared by AD and scrapie, it will certainly help us to understand the pathogenesis of AD and perhaps to devise therapeutic strategies for AD.

BIBLIOGRAPHY

Alberti K.G.M.M., Christensen N.J., Christensen S.E., Hansen A.A.P., Iversen J., Lundbaek K., Seyer-Hansen K., and Orskov H. (1973) Inhibition of insulin secretion by somatostatin. Lancet 2:1299-1301.

Asplin C.M., Paquette T.L., Palmer J.P. (1981) In vivo inhibition of glucagon secretion by paracrine beta cell activity in man. J. Clin. Invest. 68:314-318.

Bank P. (1990) Amyloid deposits of diabetes spark new interest. J. NIH. Reseach Vol.2 34-35

Beigelman P.M., Ribolet R., Atwater I. (1977) Electrical activity of mouse pancreatic beta cells. J. Physiol. (Paris) 73:201-217.

Bencosme S.A., Liepa E. (1955) Regional differences of the pancreatic islets. Endocrinology 57:588-593.

Benoit R, Bohlen P, Brazeau P, Ling N, Guillemin R. (1980) Isolation and characterization of rat pancreatic somatostatin. Endocrinology 107 (6): 2127-1529.

Bobbioni-Harsch E. and Jeanrenaud B. (1989) The hypothalamic origin of an insulin secretion promoting factor present in the plasma of normal rats. J. of Neuroendocrinology, vol.1, No.2

Bolander F. F. (1989) Molecular Endocrinology. Academic Press, Inc.

Bonner-Weir S., and Orci L. (1982) New perspectives on the microvasculature of the islets of Langerhans in the rat. Diabetes 31:883-889.

Bray G.A., Inoue S., and Nishizawa Y. (1981) Hypothalamic obesity. Diabetologia 20:366-377.

Brigati D.J., Budgeon L.R., Unger E.R. (1988) The capillary action system for immunocytochemistry. prepared in the Dept of Pathology, Pennn State's Milton S. Hershey Medical Center At Hershey.

Carp R.I., Kim Y.S., and Callahan S.M. (1990) Pancreatic lesions and hypoglycemia-hyperinsulinemia in scrapie-injected hamsters. J. Infectious Diseases. 161:462-466.

Carp R.I., Merz P.A., Kascsak R.J., Merz G.S. & Wisniewski H.M. (1985) Nature of the scrapie agent: current status of facts and hypotheses. Journal of General Virology 66, 1357-

1368.

Carp R.I., Kascsak R.J., Wisniewski H.M., Merz P.A., Rubenstein R., Bendheim P. and Bolton D. (1989) The nature of the unconventional slow infection agents remains a puzzle. Alzheimer Disease and Associated Disorders, 3(1/2):79-99.

Carp R.I., Kascsak R.J. and Rubenstein R. (1992) Pathogenesis of unconventional slow infections. (in press).

Castenholz A. (1990) Architecture of the Lymph Node with Regard to Its Function. In: Current Topic in Pathology. 84/1 Reaction Patterns of the Lymph Node. Eds. E. Grundmann and E. Vollmer. Springer-Verlag. pp. 1-32

Chandler R.L.(1963) Experimental scrapie in the mouse. Res. Vet. Sci. 4:276-85.

Cochrane C.G., Aikin B.S. (1966) Polymorphonuclear leukocytes in immunologic reactions. The destruction of vascular basement membrane in vivo and in vitro. J. Exp. Med. 124, 733-745.

Cooke B.A., King R.J.B. and van der Molen H.J. (1988) Hormones and their Actions Part I, New Comprehensive Biochemistry. Volume 18A, general editors: Neuberger, A., and van Deenen, L.L.M., Elsevier.

Cooke B.A., King R.J.B. and van der Molen H.J., (1988) Hormones and their Actions Part II, new Comprehensive Biochmistry Volume 18B, general editors: Neuberger, A., and van Deenen, L.L.M., Elsevier.

Cooper G.J.S., Day A.J., Willis A.C., Roberts A.N., Reid K.B.M., and Leighton B. (1989) Amylin and the amylin gene: structure, function and relationship to islet amyloid and to diabetes mellitus. Biochimica et Biophysica Acta 1014:247-258

Danon D, Goldstein L, Marikovsky Y, Skutelsky E. (1972). Use of cationized ferritin as a label of negative changes on cell surfaces. J. Ultrastruct Res. 38: 500-510.

Darnell J., Lodish H., and Baltimore D., (1986) Molecular Cell Biology. Scientific American Books, Inc.

Dean P.M., Matthews E.K. (1970) Glucagon-induced electrical activity in pancreatic islet cells. J. Physiol. (Lond) 210:255-264.

Dickinson A.G. (1976) Scrapie in sheep and goats. Pages 210-243 in R.H. Kimberlin, Ed., Slow Virus Diseases in Animals and Man. North-Holland, Amsterdam.

Dickinson A.G. & Fraser H. (1979) An assessment of the genetics of scrapie in sheep and mice. In: Slow transmissible diseases of the nervous system. vol. 1, pp. 367-385, Edited by S.B. Prusiner & W.J. Hadlow. New York: Academic Press.

Frerichs H., Reich V., Creutzfeldt W. (1965) Insulin secretion in vitro. Klin Wochenschr 43:136-141.

Gajdusek D.C., (1977). Unconventional viruses and the origin and disappearance of Kuru. Science 197, 943-960.

Gavin J.R., Roth J, Neville D.M., De Meyts P., Buell D.N., (1974) Insulin-dependent regulation of insulin receptor concentrations: a direct demonstration in cell culture. Proc Natl Acad Sci USA 71:84-88.

Gerich J.E. (1981) Somatostatin. In: Brownlee M (ed) Handbook of diabetes mellitus, vol 1. Garland STPM Press, New York, pp 297-354.

Gellerstedt, N. (1938) Beitr. Z. Pathol. Anat. Allg. Pathol., 41:623.

Gould V.E., Memoli V.A., Dardi L.E., and Gould N.S. (1983) Nesidiodysplasia and nesidioblastosis of infancy: structural and functional correlations with the syndrome of hyperinsulinemic hypoglycemia. Pediatric Pathology. Vol;1 pp.7-31.

Granner D.K. (1988) Hormones of the pancreas. In: Harper's Biochemistry. 21st Edition, Murray R.K., Granner D.K., Mayes P.A. and Rodwell V.W. (eds) Appleton and Lange.

Guyton A.C. (1981). Textbook of medical physiology. sixth edition. W.B. Saunders Company.

Hermansen K. and Schwartz T.W., (1979) Differenttial sensitivity to somatostatin of pancreatic polypeptide, glucagon and insulin secretion from the isolated perfused canine pancreas. Metabolism 28:1229-1233.

Humble J.G., Jayne W.H.W. and Pulvertaft R.J.V. (1956) Biological interaction between lymphocytes and other cells. Br. J. Haematol 2:283-294.

Ipp E., Rivier J., Dobbs R.I., Brown M, Vale W, and Unger R.H., (1979) Somatostatin analogs inhibit somatostatin release. Endocrinology 104:1270-1273.

Iversen J. (1974) Inhibition of pancreatic glucagon release by somatostatin:in vitro. Scand. J. Clin. Lab. Invest. 33:125-129.

Kaplan L.M., Gabriel S.M., Koenig J.I., Sunday M.E., Spindel E.R., Martin J.B., and Chin W.W. (1988) Galanin is an estrogen-inducible, secretory product of the rat anterior pituitary. Proc. Natl. Acad. Sci. USA, Vol. 85, pp 7408-7412.

Kascsak R.J., Rubenstein R., and Carp R.I. (1991) Evidence for biological and structural diversity among scrapie strains. Current Topic in Microbiology and Immunology, Vol. 172: 139-152.

Kawai K. and Rouiller D. (1981) Evidence that the islet interstitium contains functionally separate "arterial" and "venous" compartments. Diabetes [Suppl 1] 30:14A.

Kimberlin R.H. and Walker C.A. (1986) Pathogenesis of scrapie (strain 263K) in hamsters infected intracerebrally, intraperitoneally or intraocularly. J. Gen. Virol. 67:255-63.

Kirchgessner A.L. and Gershon M.D. (1990) Innervation of the pancreas by neurons in the gut. J. Neurosci. Vol. 10(5): 1626-1642.

Kissane J.M., (1990) Anderson's Pathology. Vol I and II. The C.V. Mosby Company.

Kolod E., Meda P., Perrelet A., and Orci L. (1981) Influence of intra-islet environment on B cell function. Experimentia 37:650.

Lacy, P.E. (1964) In: Aetiology of Diabetes and Its Complications. Edited by M.P.Cameron and M.O'Connor. Ciba Foundation Coloquia on Endocrinology. Little, Brown, Vol.15:84.

Larsson L-I. (1980) New aspects on the neural, paracrine and endocrine regulation of islet function. Front Horm. Res. 7:14-29.

Larsson L-I., Fahrenkrug J., Schaffalitzky De Muckadell OB (1978) Innervation of the pancreas by vasoactive intestinal polypeptide (VIP) immunoreactive nerves. Life Sci 22:773-780.

Larsson L-I, Goltermann N, de Magistris L., Rehfeld J.F., and Schwartz T.W. (1979) Somatostatin cell processes as pathways for paracrine secretion. Science 205:1393-1395.

Lattemann D.F. (1989) How the brain reads insulin may be tomorrow's weight loss secret. Diabetes Forecast January 1989. pp 54-57.

Lifson N., Kraming K.G., Mayrand R.R., Lander E.J. (1980)

Blood flow to the rabbit pancreas with special reference to the islets of Langerhans. Gastroenterology 79:466-473.

Like A.A. (1977) Spontaneous diabetes in animals . In: Volk B.W., Wellmwn K.F. (eds) The diabetic pancreas. Plenum, New York, pp. 381-423.

Mandarino L., Stenner D., Blanchard W., Nissen S., Gerich J., Ling N., Brazeau P., Bohlen P., Esch F., and Guillemin R. (1981) Selective effects of somatostatin-14, -25, and -28 on in vitro insulin and glucagon secretion. Nature 291:76-77.

Lundquist I. and Ericson L.E. (1978) B-adrenergic isulin release and adrenergic innervation of mouse pancreatic islets. Cell Tissue Res. 193:73-85.

Meda P., Pettrelet A., and Orci L. (1979) Increase of gap junction between pancreatic B cells during stimulation of insulin secretion. J. Cell Biol. 82:441-448.

Meta P., Halban P., Perrelet A., Renold A.E., and Orci L. (1980a) Gap junction development is correlated with insulin content in the pancreatic B cell. Science 209:1026-1028.

Meta P., Denef J.F., Perrelet A., and Orci L., (1980b) Non-random distribution of gap junctions between pancreatic B cells. Am. J. Physiol. 238:C114-C119.

Meta P., Perrelet A., Orci L. (1980c) Gap junctions and B cell function. In Malaisse W.J., Taljedal I.B. (Eds) Biochemistry and biophysics of the pancreatic B cell. Thieme, Stuttgart, pp 157-162.

Meta P., Amherdt M., Perrelet A., and Orci L. (1981) Matebolic coupling between cultured pancreatic B cells. Exp. Cell Res. 133(2):421-430.

Meta P., Perrelet A., and Orci L. (1982) Endocrine cell interactions within the islets of Langerhans In: Pitts J.D.(ed) Functional integration of cells in animal tissues. Cambridge University Press, Cambridge, pp 113-131.

Meissner H.P. (1976) Electrophysiological evidence for coupling between beta cells of pancreatic B cells. Nature 262: 502-504.

Miller R.E., Horton E.S., (1979) Neural release of glucagon is inhibited by hyperglycemia and enhanced by phentolamine. Diabetes 28:762-768.

Nagashima K., Zabriskie J.B., and Lyons M.J. (1992) Virus-induced obesity in mice: Association with a hypothalamic

lesion. J. of Neuropathology and Experimental Neurology. Vol. 51, No.1, pp. 101-109.

Nagy Z., Peters H., and Huttner I. (1983) Charge-related alterations of the cerebral endothelium. Lab. Invest. 49:662-671.

Newman G.R., Jasani B., and Williams E.D., (1986) Multiple hormone storage by 'polycrine' cells in the pancreas (from a case of nesidioblastosis). Histochemical Journal 18, 67-79.

Nishi M., Sanke T., Nagamatsu S., Bell G.I., and Steiner D.F. (1990) Islet amyloid polypeptide. A new B cell secretory product related to islet amyloid deposit. J. Biol Chem. Vol. 265, No.8 pp 4173-4176.

Norman A.W., and Litwack G. (1987). Hormones. Academic press, Inc.

Orci L. (1974) A portrait of the pancreatic B-cell. Diabetologia 10:163-187.

Orci L. (1976) The microanatomy of the islets of Langerhans. Metabolism 25:1303-1313.

Orci L. and Unger R.H. (1975) Functional subdivision of islets of Langerhans and possible role of D cells. Lancet 2: 1243.

Orci L., Unger R.H., Renold A.E. (1973) Structural coupling between pancreatic islet cells. Experientia 29:1015-1018.

Orci L., Malaisse-Lagae F., Rouiller D., Renold A.E., Perrelet A., Unger R.H., (1975) A morphological basis for intercellular communication between alpha and beta cells in the endocrine pancreas. J. clin. Invest. 56:1066-1070.

Orci L., Baetens D., Ravazzola M., Stefan Y., and Malaisse-Lagae F. (1976a) Pancreatic polypeptide and glucagon: non-random distribution in pancreatic islets. Life Sci. 19:1811-1816.

Orci L., Baetens D., Rufenfer C., Amherdt N., Ravazzola M., Studer P., Malaisse-Lagae F., and Unger R.H. (1976b) Hypertrophy and hyperplasia of somatostatin-containing D cells in diabetes. Proc Natl Acad Sci USA 73:1338-1342.

Orci L., Baetens D., Ravazzola M., Malaisse-Lagae F., Amherdt M., and Rufener C., (1976c) Somatostatin in the pancreas and the gastrointestinal tract. In: Fujita T (ed) Endocrine gut and pancreas. Elsevier, Amsterdam New York, pp 73-88.

Orci L., Stefan Y., Bonner-Weir S., Perrelet A., and Unger

R.H. (1981) "Obligatory" association between A and D cells demonstrated by bipolar islets in neonatal pancreas. Diabetologia 21:73-74.

Outram G.W. (1976) In R.H. Kimberlin (ed.) Slow Virus Diseases of Animals and Man. Amsterdam: North-Holland. pp. 325-357.

Palkovits M., Leranth C., Gorcs T., and Scoott Young III W. (1987) Corticotropin-releasing factor in the olivocerebellar trace of rats: Demonstration by light- and electron-microscopic immunohistochemistry and in situ hybridization histochemistry. Proc. Natl. Acad. Sci. USA Vol.84. pp 3911-3915.

Pang P.K.T. and Schreibman M.P. (1986) Vertebrate endocrinology: Fundamentals and Biomedical Implications, Volume 1 Morphological Considerations. Academic Press, Ins.

Patton G.S., Dobbs R.E., Orci L., Vale W., and Unger R.H. (1976) Stimulation of pancreatic immunoreactive somatostatin (IRS) release by glucagon. Metabolism [Suppl 1] 25:1499.

Patton G.S., Ipp E., Dobbs R.E., Orci L., Vale W., and Unger R.H. (1977) Pancreatic immunoreactive somatostatin release. Proc Natl Acad Sci USA 74:2140-2143.

Pohl M.N., Swartz F.J., and Carstens P.H.B. (1981) Polyploidy in islets of normal and diabetic humans. Human Pathology, Vol 12:184

Roth K.A., Weber E., and Barchas J.D. (1982). Immunoreactive CRF and vasopressin are co-localized in a subpopuration of the immunoreactive vasopressin cells in the paraventricular nucleus of the hypothalamus. Life Sci. 31, 1857-1860.

Roy M.W., Jones M.S., Lee K.C., Miller R.E., (1981) Splanchnic neural stimulation suppresses secretion of pancreatic somatostatin by $alpha_2$, insulin by $alpha_2$, post synaptic receptors. Endocrinology [Suppl] 108:105.

Saad M.F., Kahn S.E., Nelson R.G., Pettitt D.J., Knowler W.C., Schwartz M.W., Kowalyk S., Bennett P.I. and Porte D.J. (1990) Disproportionately elevated proinsulin in Pima Indians with noninsulin-dependent diabetes mellitus. J. Clin. Endocrinol. Met. 70(5) 1247-53.

Samols E. (1983) Glucagon and insulin secretion. In: Lefebvre P.J. (ed) Glucagon I. (Handbook of experimental pharmacology, 66-) Springer-Verlag (Berlin). pp 485-518.

Samols E. and Harrison J. (1976) Remarkable potency of somatostatin as a glucagon suppressant. Metabolism [Suppl 1]

25:1495-1497.

Samols E. and Harrison J. (1977) Tolbutamide: stimulator and suppressor of glucagon secretion. In: Foa P.P., Bajaj J.S. Foa N.L. (eds) Glucagon. Its role in physiology and clinical medicine. Springer, Berlin Heidelberg New York, pp 699-710.

Samols E. and Stragner J. (1981) Modulation of insulin: local presynaptic α_2 but postsynaptic α_2 adrenoreceptors. Diabetes [Suppl 1] 30:44A.

Samols E. and Weir G.C. (1979) Adrenergic modulation of pancreatic A,B, and D cells: alpha-adrenergic suppression and beta-adrenergic stimulation of somatostatin secretion, alpha-adrenergic stimulation of glucagon secretion in the perfused dog pancreas. J. Chin Invest. 63:230-238.

Samols E., Marri G., and Marks V. (1965) Promotion of insulin secretion by glucagon. Lancet 2:415-416.

Samols E., Marri G. and Marks V. (1966) The interrelationship of glucagon, insulin and glucose. Diabetes 15:855-866.

Samols E., Tyler J., Marks V. and Mialhe P. (1969) The physiologic role of glucagon in different species. In Gual C, Ebling F.J.G. (eds) Progress in endocrinology. Excerpta Medica, Amsterdam, pp 206-219.

Samols E., Tyler J. and Kajinuma H. (1970) Influence of the sulfonamides on pancreatic humoral secretion and evidence of an insulin-glucagon feedback system. In: Rodriguez R.R., Vallance-Owen I (eds) Proceedings Seventh International Diabetes Federation Congress. Excerpta Medica, Amsterdam,pp 636-655.

Samols E., Weir G.C. and Bonner-Weir S. (1983) Intraislet insulin-glucagon-somatostatin relationships. In: Lefebvre P.J. (ed) Glucagon II. (Handbook of experimental pharmacology, 66-) Springer-Verlag (Berlin). pp 133-173.

Samols E., Weir G.C., Patel Y.C., Loo S.W., and Gabbay K.H. (1977) Autonomic control of somatostatin and pancreatic peptide secretion by the isolated perfused canine pancreas. Clin Res. 25:499A.

Samols E., Stagner J.I., and Weir G.C. (1981) Autonomic function and control of pancreatic somatostatin. Diabetologia [Suppl] 20:388-392.

Schubert D., Jin L-W., Saitoh T., and Greg Cole. (1989) The regulation of amyloid B-protein precursor secretion and its modulatory role in cell adhesion. Neuron, Vol.3, pp. 689-694.

Schwartz, P. (1965) Senile cerebral pancreatic insular and cardia amyloidosis. trans. N.Y. Acad. Sci., 27:393.

Sharp J.A. and Burwell R.G. (1960) Interaction ("peripolesis") of macrophages and lymphocytes after skin homografting or challenge with soluble antigens. Nature 188:474-475.

Shelton E. (1962) Prolonged survival of rabbit thoracic duct lymphocytes in a diffusion chamber. J. Cell Biol. 12: 652-655.

Shelton E. and Rice M.E. (1959) Growth of normal peritoneal cells in diffusion chambers: a study in cell modulation. Am. J. Anat. 105:281-342.

Sidman R.l., Angevine Jr. J.B. and Pierce E.T. (1971) Atlas of the Mouse Brain and Spinal Cord. Cambridge, Harvard Univ. press.

Simionescu M. and Simionescu N. (1986) Functions of the endothelial cell surface. Annu. Rev. Physiol. 48:279-293

Simionescu N., Simionescu M. and Palade G.E. (1981). Differentiated microdomains on the luminal surface of the capillary endothelium. I. Preferential distribution of anionic sites. J. Cell Biol. 90:605-613.

Simpson I., Rose B. and Lowenstein W.R. (1977) Size limit of molecules permeating the junctional membrane channels. Science 195:294-296.

Simon G.T. (1979). Ultrastructure of Acute Inflammation. In: Current Topics in Pathology 68. Inflammatory Reaction Edited by H.Z. Movat. Springer-Verlag, Berlin Heidelberg New York. pp. 1-32.

Skutelsky E. and Danon D. (1976) Redistribution of surface anionic sites on the luminal front of blood vessel endothelium after interaction with polycationic ligand. J. Cell Biol. 71:232-241.

Smith P.H., Madson K.L. (1981) Interactions between autonomic nerves and endocrine cells of the gastroenteropancreatic system. Diabetologia 20:314-324.

Snyderman R. and Goetzl E.J. (1981) Molecular and cellular mechanisms of leukocyte chemotaxis Science. 213:830-837

Sundberg R.D. (1960) Lymphocytes: origin, structure and interrelationships. In: Rebuck J.W. (ed) The lymphocyte and lymphocytic tissue. Hoeber, New York, pp 1-21.

Sundberg R.D. and Downey H. (1955) Lymphocytes and plasma cells. Ann. NY. Acad. Sci. 59:671-684.

Wahren J. and Felig P. (1976) Influence of somatostatin on carbohydrate disposal and absorption in diabetes mellitus. Lancet 2:1213-1216.

Weille J.DE., Schmid-Antomarchi H., Fosset M., and Lazdunski M. (1988) ATP-sensitive K^+ channels that are blocked by hypoglycemia-inducing sulfonylureas in insulin-secreting cells are activated by galanin, a hyperglycemia-inducing hormone. Proc. Natl. Acad. Sci. USA, Vol. 85 pp. 1312-1316.

Weiss L. (1985) Cancer cell arrest. In: Principles of metastasis. Academic Press, Orlando, pp 65-95.

Weir G.C., Schwarz J.A. and Mathe C.J. (1980) Inhibition of glucagon and insulin secretion from the perfused rat pancreas by a B cell selective somatostatin analog. Metabolism 29(1):68-70.

Whitehouse P.J., Vale W.W., Zweig R.M., Singer H.S., Mayeux R., Price D.L., and DE Souza E.B. (1987) Reductions in corticotropin-releasing factor (CRF)-like immunoreactivity in cerebral cortex in Alzheimer's disease, Parkinson's Disease, and Progressive Supranuclear Palsy. Neurology 37: 905-909.

AUTOBIOGRAPHICAL STATEMENT

Xuemin Ye was born on October 29, 1958 in Guangdong, PRC. He received a B.Sc. degree in animal physiology at the Department of Biology, Zhongshan University, Guangzhow in 1982. From 1982 to 1984, he began graduate studies in animal physiology in the laboratory of Dr. H.R. Lin in Zhongshan University. From 1984 to 1987, he was selected for a scholarship to study animal physiology for M.Sc. degree in the laboratory of Dr. D.J. Randall in the Department of Zoology, University of British Columbia, Vancouver. From 1987 to 1989, he studied neuroendocrinology for a Ph.D. in the laboratory of Dr. M.P. Schreibman in the Department of Biology, Brooklyn College, City University of New York. In September, 1988, he was selected for a fellowship for Ph.D. study in the College of Staten Island/Institute for Basic Research in Developmental Disabilities Center for Developmental Neuroscience. During the past years, he has been doing his Ph.D. thesis research in Dr.Carp's laboratory at the Institute for Basic Research in Developmental Disabilities.

Publication and presentations:

Ye, X. (U.B.C.). The Effect of Water pH on Swimming Performance and Blood pH, Erythrocyte pH in Rainbow Trout. Presented at the Meeting of Canadian Society of Zoologists, May, 1986 in Saskatoon, Canada.

G.K.Iwama and X. Ye (U.B.C.) Transepithelial Potential Measurements in Rainbow Trout During Acid-base Disturbance. Poster presentation at the XXX International Union of Physiological Sciences, Banff satellite symposia, on July, 1986, Banff, Canada.

Ye,X., R.I.Carp, Y.Yu, R.Kozielski. (CSI/IBR Center for Developmental Neurosciences) Pathological Changes in the Islets of Langerhans in Hamsters Infected with 139H Strain of Scrapie.
Abstract at the Third IBRO World Congress of Neuroscience, August 4-9, 1991, Montreal, Canada. p338.

Ye, X., R.I.Carp, S.Callahan, J.Shek. 1991. (CSI/IBR Center for Developmental Neurosciences) Histopathological Changes in the Pituitary of Female Hamsters Infected with the 139H Strain of Scrapie.
Abstract at the 21st annual meeting of Society for Neuroscience, November 10-15, 1991, New Orleans, Louisiana, U.S.A. Vol.17, p1274.

Ye, X. and Randall, D.J. 1991. The Effect of Water pH on Swimming Performance in Rainbow Trout (Salmo gairdneri). Fish

Physio. Biochem. 9: 15-21.

Ye, X., Randall, D.J. and He, X. 1991. The Effect of Acid Water on Oxygen Consumption, Circulating Catecholamines and Blood Ionic and Acid-base Status in Rainbow Trout (Salmo gairdneri). Fish Physiol. Biochem. 9: 23-30.

Ye, X., Carp, R.I., Yu, Y., Kozielski, R., Kozlowski, P. 1992. Scrapie-induced Obesity in Hamsters: Association with Pituitary and Hypothalamic Lesions.
Abstract at Third International Conference on Alzheimer's Disease & Related Disorders, Abano Terme (Padova), Italy. July 12-17, 1992.

Ye, X., Carp, R.I., kascsak, R., Kozielski, R., Kozlowski, P. 1992. Astrocytosis and Amyloid Deposition in Scrapie-infected Hamsters.
Abstract at 2nd Altschul Symposium, May 20-23, 1992 University of Saskatchewan, Saskatoon, Sask. Canada.